UNIVERSIDAD DE CHILE
FACULTAD DE CIENCIAS FÍSICAS Y MATEMÁTICAS
DEPARTAMENTO DE INGENIERÍA ELÉCTRICA

ANALYSIS OF FAILURES AND DEGRADATION MODES OF SMALL SCALE DOMESTIC/FARM PHOTOVOLTAIC POWER PLANTS IN RURAL COMMUNITIES OF THE ATACAMA DESERT

TESIS PARA OPTAR AL GRADO DE
MAGÍSTER EN CIENCIAS DE LA INGENIERÍA, MENCIÓN ELÉCTRICA

PIA JAVIERA VASQUEZ RIVERA

PROFESOR GUÍA:
RODRIGO PALMA BEHNKE

MIEMBROS DE LA COMISIÓN:
PABLO FERRADA MARTÍNEZ
FAUSTO MENA MENA

SANTIAGO DE CHILE
2020

RESUMEN DE LA TESIS PARA OPTAR
AL TÍTULO DE MAGÍSTER EN CIENCIAS DE LA INGENIERÍA, MENCIÓN ELÉCTRICA
POR: PIA JAVIERA VASQUEZ RIVERA
FECHA: 2020
PROF. GUÍA: RODRIGO PALMA BEHNKE

ANALYSIS OF FAILURES AND DEGRADATION MODES OF SMALL SCALE DOMESTIC/FARM PHOTOVOLTAIC POWER PLANTS IN RURAL COMMUNITIES OF THE ATACAMA DESERT

The present work is the result of a detailed analysis of the occurrence of failure/degradation modes found in 95 solar photovoltaic modules operating in the Atacama Desert. The data was collected using an IDCTool (Inspection Data Collection Tool) designed for desert climate applicability. This tool gathers visual inspection, thermal imaging and the electrical measurements of each module. Additionally, statistical data derived from a previous field testing campaign is used as well, and results are supplemented with a theoretical analysis based on the fundamental materials properties and interactions, from a physics perspective. With this five dimensional approach (visual, thermal, electrical, statistical, materials), failure/degradation modes and possible mechanisms characterization was enabled, regarding three solar module components: front cover glass, EVA encapsulant and solar cells. As a result, seven different abnormalities were detected and analyzed: Soiling, discoloration of front cover glass, delamination of EVA encapsulant, hotspots, partial shading, cell fracture and defective soldering. The last two failures were inferred from thermal profiles and described on a qualitative basis - given it is not feasible to check these failures without a further, and more detailed visual inspection - giving cause to discussion for future works and more in-depth inspections. The most common issue detected was soiling; in different intensities and deposition patterns, showing a correlation between dust deposition and modules geographical location. Regarding electrical measurements, the relationship between the short circuit current and maximum power drops due to soiling becomes patent; and, for severely soiled modules voltage is also affected. However, both soiling and partial shading (i.e. bird drops, localized mud or dirt) cannot be correlated to excessive heating. Hotspots are also a common issue, being present in more than 50 percent of the total sample. Severe temperature rising in cells may relate to loss of glass transmittance, but also to internal cell failures such as shunt paths or reduced parallel resistance. Chemical interactions between environmental agents such as moisture, atmospheric particles or pollutants and modules can also be inferred, given that permanent changes in front cover composition have been observed. Finally, although there is not statistical evidence, the data analyzed in this and previous work suggest that the excess of UV radiation, typical of desert regions does not seem to play a primary role in modules degradation, however, it may contribute as a catalyst in presence of other environmental agents.

RESUMEN DE LA TESIS PARA OPTAR
AL TÍTULO DE MAGÍSTER EN CIENCIAS DE LA INGENIERÍA, MENCIÓN ELÉCTRICA
POR: PIA JAVIERA VASQUEZ RIVERA
FECHA: 2020
PROF. GUÍA: RODRIGO PALMA BEHNKE

ANALYSIS OF FAILURES AND DEGRADATION MODES OF SMALL SCALE DOMESTIC/FARM PHOTOVOLTAIC POWER PLANTS IN RURAL COMMUNITIES OF THE ATACAMA DESERT

En este trabajo, analizamos las ocurrencia de fallas/degradación en 95 módulos fotovoltaicos instalados en el desierto de Atacama. La información utilizada fue recopilada mediante un herramienta de inspección (Inspection Data Collection Tool, IDCTool en inglés) diseñada para aplicaciones en clima desértico. Esta herramienta considera la inspección visual, imágenes térmicas and mediciones eléctricas de los módulos. Adicionalmente, utilizamos información estadística derivada de una campaña previa, y los resultados son complementados con un análisis teórico basado en ciencia de los materiales. Con este enfoque de 5 aristas, ha sido posible caracterizar y analizar los modos de falla/degradación para tres componentes de los módulos: la cubierta frontal de vidrio, el encapsulante de EVA, y las celdas solares. Consideramos 7 anormalidades: *soiling*, decoloración de la cubierta de vidrio, delaminación del encapsulante, *hotspots*, sombreado parcial, fractura de celda y soldadura defectuosa. Las dos últimas fueron inferidas de los perfiles térmicos y descritos de manera cualitativa (dado que no es posible comprobar la falla sin una inspección visual adicional), dando pie a generar discusión para trabajo futuro e inspecciones más detalladas. El problema más común detectado fue el *soiling*, con diferentes intensidades y patrones de deposición, que muestran correlación entre éstos y la ubicación de los módulos. Se evidencia la relación entre la disminución de la corriente de cortocircuito y la potencia máxima, y en el caso de los módulos con capas de *soiling* muy espesas también el voltage de circuito abierto se ve afectado. Sin embargo, tanto el soiling como el sombreado parcial no causan excesivo calentamiento en las celdas. Los *hotspots* son también un problema común, presente en más del 50% de módulos de la muestra total. Aumentos severos en la temperatura de las celdas pueden estar relacionados a la pérdida de transmitancia del vidrio, pero también a fallas internas de las celdas como *shunts* o baja resistencia paralelo. Además, pueden inferirse reacciones químicas entre agentes ambientales como humedad, partículas atmosféricas o contaminantes y los módulos, dado que se observan cambios en la composición de la cubierta frontal de vidrio. Finalmente, aunque no existe evidencia estadística, el exceso de radiación UV, típico de regiones desérticas, no parece jugar un rol fundamental en la degradación de los módulos, aunque puede contribuir como agente catalizador en presencia de otros factores ambientales.

Contents

List of Tables

List of Figures

Chapter 1

Introduction

Electricity comprises one of the most important aspects of modern societies, since it supports the global technological advancements in all areas of knowledge, together with the industrial activities and basic human needs. However, in the last decades, along with the concern of generating enough electricity to supply humankind needs, very much of the attention has been placed on the nature of resources we are exploiting to produce it. Although there exists debate on whether the causes of global warming are due to natural variability of Earth's processes and Sun's activity or due to human activity [12], there is general agreement about human contribution to global warming. Moreover, a great part of global emission of green house gas (GHG) is due to the production of electricity and transport using fossil fuels [13]. Additionally, there is concern with the exhaustion of fossil fuel resources in the present century. While the "peak oil" predicted in numerous studies has been extended further in time by technological advancements, by now is placed in the first half of the century (2050 for coal, 2040 for gas and 2020 for oil) [14]. These are two main reasons for improving technologies based on renewable sources for generation of electricity and transport, which until now, face several challenges (technical and economic) to fully replace fuel-based technologies [15].

Solar energy represents a feasible alternative to conventional technologies, environmentally friendly, technologically mature and with decreasing costs over time. Nevertheless, and although there exist constant improvement in solar photovoltaic (PV) technologies, their performance in field, and after a long term exposure can be very different from the information supplied by the manufacturer. This can reduce modules lifetime and consequently negatively impact the economic projection of the investor. Moreover, the in-field performance of solar PV systems in different locations around the world is subjected to different external variables: climate, weather, UV exposure, soiling, snow loads, moisture, etc. Different external variables determine modules operation, but also their aging and their propensity to degrade or fail. In the last decade, many research works concerning the outdoor performance of PV systems around the world have been reported, allowing to characterize the behaviour of standard manufactured modules on different climatic conditions. Data acquired allows to relate the occurrence of certain failure/degradation modes with specific features of these locations. For the assessment of modules, there have been developed standard inspection procedures which can be adjusted according to the specific research needs.

1.1 Motivation

In Chile, the climatic conditions offered by the Atacama Desert (the most arid desert on the planet) make it an ideal place to boost the solar energy production: A large desert area of 105,000 km^2, the highest irradiation levels of the world, which can reach up to 1200 W/m^2 (Direct Normal Irradiance, DNI) in some locations and clear skies throughout the year are very promissory for the development of a solar market. On the other hand, the National Energy Policy and the National Energy Strategy 2012-2050 have as a primary objective that the renewable generation by 2050 reaches at least 70 percent of renewable generation [16]. Given the high potential present in the north of Chile, solar energy can play a major role for accomplishing this goal.

For an optimum exploitation of solar technologies, it is imperative to know the local needs for developing technologies specifically adapted to the environmental conditions. Hence, it is necessary to understand the operation of solar modules under these specific conditions, how they degrade over time and how they can fail. Within this framework, an inspection data collection tool (IDCTool) has been developed in previous work [3], which enables standard inspection procedures to collect the information required. The next step, addressed in this work, is to conduct a detailed characterization and analysis of this information, in order to understand the issues affecting modules operation in the Atacama Desert. Particularly, the focus is on small scale residential/farm PV power plants from urban and rural communities, given that, unlike commercial plants, these kind of facilities usually lack of operation and maintenance protocols oriented geared to maximize the service life of the equipment.

1.2 Research Hypothesis

With the data collected through in-field measurements, and a exstensive literature review about the detection and diagnosis of failure/degradation modes and mechanisms (in which more sophisticated detection tools and tests have been used), it is possible to find clues about the internal behaviour of PV modules operating in the Atacama Desert.

With the available information, a detailed description of failure/degradation modes and possible mechanisms is expected, using an integrated analysis based on statistical information from previous work, visual inspection, electrical measurements, thermal imaging and a physical analysis of materials. With this analysis, the actual impact of the Atacama Desert specific climate conditions on solar modules could be further inferred.

1.3 Objectives

1.3.1 General Objective

The main objective of this thesis is to identify the different failure/degradation modes found in solar photovoltaic modules operating in the Atacama Desert, considering a five dimensional analysis based on previously collected information: On site measurements and characterization (visual inspection, thermal imaging, I-V curve measurement), statistical data (average operating temperatures, degradation rates of electrical parameters, optical failures observed)

and a physical analysis of each solar photovoltaic module components, indicating the possible underlying physical phenomena involved in the failure/degradation modes found.

1.3.2 Specific Objectives

In order to accomplish the general objective of this thesis, another issues related to the analysis shall also be addressed as listed below:

1. Carry out a detailed literature review on the causes and mechanisms behind the failures found in the modules analyzed.
2. Assess the performance of the IDCTool developed in a previous study, considering the quality of the collected data and the main parameters used in the literature to analyse failures and degradation modes.
3. Identify of a correlation among the failures found in the modules analyzed using each of the three aspects of the tool (visual, electrical, thermal) in order to find a cause/-effect relationship between certain environmental/operating conditions as well as the degradation of the most affected components in the modules.
4. Determine whether or not it is possible to diagnose (at least on a qualitatively basis) the occurrence of failure/degradation with limited field data, enlightening the critical aspects to perform this task, and advising, if necessary, about the additional tools that may contribute in obtaining more accurate results.

1.4 Scope of the Thesis

This thesis work uses the information collected by a previous research, thus an independent data collection campaigned was not conducted. The major limitation is that, the quantity and quality of visual, thermal and electrical information does not allow to determine exactly, but only suggests the failure/degradation modes and mechanisms that are more probably to be causing certain electrical or thermal signatures. This is why the application of additional tests is advised, in order to check the diagnosis conducted in this work. Additionally, the analysis based on materials properties and behaviour is done in a purely theoretical basis. The purpose is to generate discussion and future research in materials science to establish interdisciplinary bonds that allow to understand the fundamental properties of underlying failure/degradation processes detected through in-field measurements. Finally, the analysis was conducted based in measurements of modules affected by multiple failure/degradation modes simultaneously, hence the conclusions about the behaviour of modules that demonstrate certain issues are not absolute.

Chapter 2

Theoretical Background

Solar photovoltaic modules are devices that allow to collect solar radiation and convert it to electrical energy. The fundamental mechanism of solar energy conversion lies on the generation and separation of charge carriers [17]. At present, for this aim a wide variety of technologies based in different materials have been developed through the last decades [18]. However, due to the multiple requirements for sustainable applications to large scale energy generation (based both on technical and economic criteria) [19], many of these technologies still remain under research with small niche application and minimal market share. In contrast, mono and multi-crystalline silicon based solar cells are the most mature technology and have achieved great stability in terms of production costs, lifetime and conversion efficiency [20]. This has allowed these technologies to concentrate more than 90% of global PV market share [21]. However, the challenges for photovoltaics to address the global energy supply issue still require intense research in multiple disciplines. The main topics related to improve the performance of solar photovoltaic systems are: efficiency, materials availability and processability, durability and aging, life cycle constraints and the integration of PV to the global energy system [22]. In particular, durability and aging issues are highly related to materials quality, manufacturing processes and operating environment [23].

In this thesis, the analysis of failure/degradation modes found in operating modules since 2005 to 2018 is performed. All the modules are located in the city of Arica and nearby rural zones, a coastal region of the Atacama Desert. The analysis contemplates the evaluation of the data collected using the IDCTool designed in [3] by means of visual inspection, thermal imaging and measurements of the I-V characteristics of 95 modules of 15 different locations. Additionally, analysis based on materials behaviour under external stress conditions (in particular those found in the Atacama Desert) is performed, with the aim of generating discussion and further investigation in the areas of materials physics. This Chapter is organized as follows: In section 2.1 the physical characterization of solar modules components is given, in order to understand the fundamental features, at materials level that lead to certain behaviours and the occurrence of failures/degradations in solar cells/modules. In section 2.2 the general electrical model that characterizes the behaviour of solar cells/modules is given. In Section 2.3 a general review of literature about the main tools and criteria to perform detection, diagnosis and analysis of failures on fielded solar modules is given. Finally, in Section 2.4, the main results found in previous work [3] are summarized.

2.1 Materials Characterization of Solar Photovoltaic Modules

A complete understanding of solar photovoltaic devices, their behaviour and failures involves both a physics and an electrical engineering approach. As the main purpose of the Chilean Solar Research program is the improvement of solar technologies to optimize their operation in desert conditions, where we have our best (and world's best) solar resource, it is necessary to consider device details together with their operating conditions. In order to find a way to correlate the macroscopic failures observed/measured in solar PV modules with the primary processes involved in them, we briefly review the fundamental features of the materials that make up the solar photovoltaic modules. Special attention is put on the specific features or defects that can lead them to fail.

2.1.1 The Solar Cell

The basic unit that allows to generate electricity from solar radiation is the solar cell, which, for the case of crystalline silicon solar cells (as studied in this work) consists on a p-n junction [24]. Joining p-doped (normally boron) and n-doped (normally phosphorous) semiconductors it is established a potential difference between the two sides. This allows to selectively conduct the charge carriers across the junction to an external circuit. Apart from the semiconductor, the solar cell is completed by adding printed metallic contacts on the top, which allow the evacuation and transport of electrons out of the absorber, as shown in Figure 2.1.

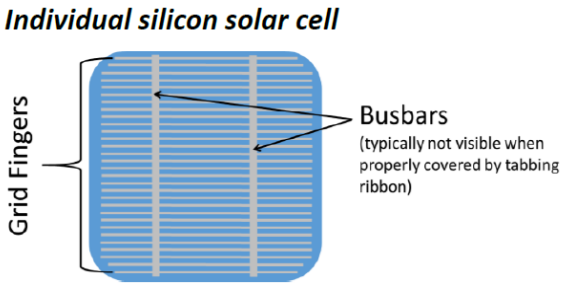

Figure 2.1: Basic structure of a solar cell [4].

In solar cell design, both the proper selection and adjustment of semiconductor and metallization properties are critical for technology improvements. This is mainly because, the high resistance of the emitter (usually the n+ front side) requires the existence of a metallic path to conduct the electrons [25]. This reduces the active area for charge carriers generation [26], and also establishes contact resistances between the semiconductor and metal materials [27].

The generation process begins with the arrival of photons into the solar cell. The incoming photons transfer their energy to the electrons in the solar cell, which can now move from the valence band to the conduction band of the crystal. In other words, this energy allows the electrons to break free from the attraction of atomic nuclei. However, for every excited electron in the conduction band, there remains a hole in the valence band (attached to the crystal), bounded with each other (electrons and holes) by the Coulomb attraction.

Physically, the separation of charge carriers occurs at the interface of the p-n junction, and then the separated electrons and holes are conducted to their respective contacts. A schematic of charge carriers generation and separation is shown in Figure 2.2

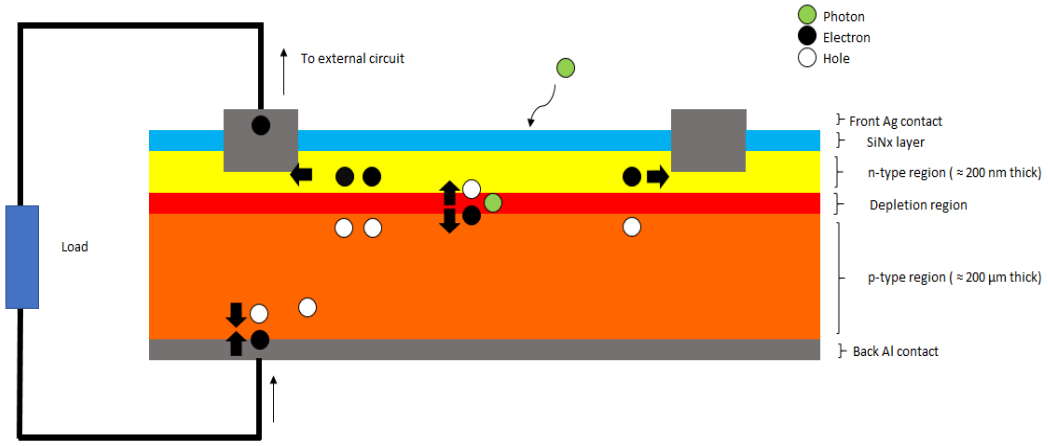

Figure 2.2: Schematic of charge carriers generation and separation within a solar cell .

One of the major challenges to improve solar cell performance is to improve their efficiency. Significant effort has been done to achieve this goal, which is directly related to the minimization of losses. There exist several mechanisms that lead to the loss of charge carriers, starting from theoretical limitations of solar energy conversion [28], optical losses (reflection, absorption, transmission), recombination mechanisms (radiative, Auger, SRH, among others) and electrical losses (series and shunt resistance) [29]. Some of these loss mechanisms are determined by the inherent features of the material. For example, the *bandgap* of single junction materials determines the minimum absorbable incident photon energy [30]. Other issues, such as recombination losses are highly dependent on impurities concentration derived from manufacturing processes [31].

Impurities concentration does not only determine the loss of efficiency of a solar cell [32], but also determines its behaviour under stress. According to [11], hotspots formation in solar cells is directly related to high impurity contaminants concentration, particularly of transition metals. Additionally, high impurity concentrations within the semiconductor generate large recombination regions which lead to the generation of shunt paths [33]. Shunts are basically internal short circuits at the p-n junction which degrade the solar cell performance [34], and are of major concern in solar cell design, because they can degrade the device performance in a large degree [35]. According to [36], the origin of shunts can be both processes induced (during manufacturing stages, like cracks, scratches, defective contacts, improper edge passivation or the presence of Al particles on the emitter surface, amongh other causes), or material induced (strong recombination sites at metal decorated grain boundaries, macroscopic Si_3N_4 inclusions, or microscopic SiC precipitates accross the wafer). These issues can be addressed by enhancing processes control during manufacturing, and by the use of better quality materials [37] which, of course, increases production costs.

As mentioned before, metallization is another main component in solar cells. Metallization contributes to losses as a small, but not negligible contact resistance [38]. In fact, there exist losses associated to each component of metallization (gridlines, busbar, back contact) and

transition regions between semiconductor and metallization [27], which gives rise to contact potentials [39]. In solar cells, front metallization contacts are usually based on screen-printed Ag pastes [40]. Al/Ag are used for rear contact [41]. These contacts can be considered as almost ohmic [27] due to the surface concentration of atoms in the semiconductor (10^{19} and 10^{17} atoms/cm^3 for n and p-type respectively), which is important for contact improvements although they are considered a small portion in the total power loss of the cell [42]. Silver pastes, the most used material for contacts, consist of heterogeneous mixtures containing silver powders, glass frits (which performs the adherence to the semiconductor surface and ensures the formation of contact [43]), organic binders, and optional metallic/metal oxide additives [44]. Recently, the role of glass frits on the formation of shunts by recombination in n-type solar cells, affecting the open circuit voltage has been investigated [45]. Finally, the interaction between silicon and metal compounds can lead to thermal stress derived from the difference in thermal expansion coefficients between both materials when they are subjected to temperature cycles [46]. This situation is relevant in a desert environment, for which in Atacama Desert thermal oscillations can reach 30°C.

2.1.2 Solar Modules Components

Solar cells are the generating units, however, they are very brittle by themselves. Additionally, individual commercial solar cells produce very low voltages, which are not suitable for large scale applications. In order to protect the cells from external hazards and to achieve higher voltages, they are series connected in groups of (usually) 60-72 cells and encapsulated between several materials into solar modules, as shown in Figure 2.3.

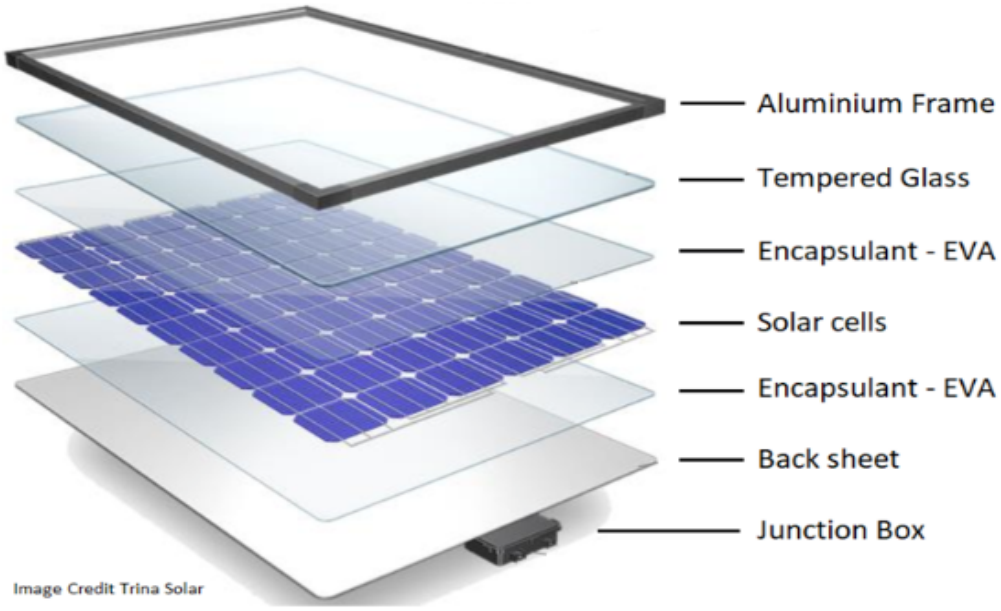

Figure 2.3: Solar photovoltaic module components [5].

The series connected solar cells are first sandwiched between two layers of an encapsulant, for which the most commonly used is based on etylene-vinil acetate (EVA). The advantages of EVA are mainly its good transmittance and adhesive properties, elasticity, low processing temperature, and low cost. However, it has been found that EVA degrades easily under severe environmental conditions [47]. The remaining components are the glass cover on

the front and the backsheet on the rear side of the solar module. Finally, all the components are attached within the aluminum frame, to isolate the internal structure and provide mechanical stability. For glass covers, commercial soda lime glass is normally used, while the backsheet is typically made of polymers like polyvinyl fluoride (PVF) or polyethylene therephthalate (PET) among others. In this thesis, the main materials considered for analysis of failures/degradations in solar modules are: the solar cell, the encapsulant and the glass cover. The reason for this is that these materials are involved in the main failures found in previous work [3]. Further, more information derived from the visual inspection, thermal imaging and electrical measurements is available for these components. In this section, the physical properties of front cover glass and EVA encapsulant are summarized.

Soda-lime Glass Front Cover

Soda-lime glass has been widely used as a coverage layer for solar modules because of its good structural, thermal and optical properties. It allows the passage of light at the same time that protects the underlying components against environmental and external mechanical stress. Glass lacks of a crystalline structure (belongs to amorphous materials), however, it is composed by a basic unit of one Si atom connected with four O atoms (SiO_4). To form the crystal, each O atom is bonded by two Si atoms, as shown in Figure 2.4. For soda-lime silica glass, the network shown in Figure 2.4 (b) is interrupted by the addition of impurities (Na^+, Mg^{2+}, Ca^{2+}, Mg^{3+}). These elements are added in order to modify some properties of glass, such as softening point (temperature), toughness and durability, without affecting the glass optical properties [48]. However, the inclusion of these network modifiers can contribute to negative issues, such as Potential Induced Degradation (PID). PID arises as the result of diffusion of ions through shunt paths accross the modules (cells, encapsulants and even through the frame). These shunt paths may appear due to environmental factors (such as humidity or temperature), the amount of network modifiers on the glass, and the quality of the polymer and semiconductor materials [49]. A schematic of a silica network is shown in Figure 2.5, where it can be seen that the addition of impurities (Na^+ in the image) alters the SiO_2 network arrangement, generating non-bridging oxygen sites (O atoms which do not bond between two Si atoms). Additionally, soda-lime glass is usually tempered to provide an improved mechanical strength.

Apart from its structural features, the optical properties of soda-lime glass make it suitable for photovoltaic applications. Its transmission spectrum ranges from the near UV (300 nm) to the infrared (IR), with more than 80% transmittance up to approximately 2500 nm [6]. It is also a good insulator [50]. Furthermore, transmission properties can be affected by the influence of environmental conditions, such as humidity and high room temperatures. Research on the response of soda-lime silica glass under damp-heat accelerated tests show that their transmittance spectrum is increased after 1000 hours exposure [51]. This can be a positive result in terms of the optical absorption in the solar cell, however, transmission in the UV range can be problematic since it contributes to degradation of encapsulant [52] and solar cells [53]. The role of impurities on the optical properties of soda-lime glass has also been studied. For example, the presence of Fe oxidation states, as a residue of raw silica, introduces absorption in the near UV and mainly a very broad absorption band in the near IR. This can decrease the power output of a finished module up to 10% [54].

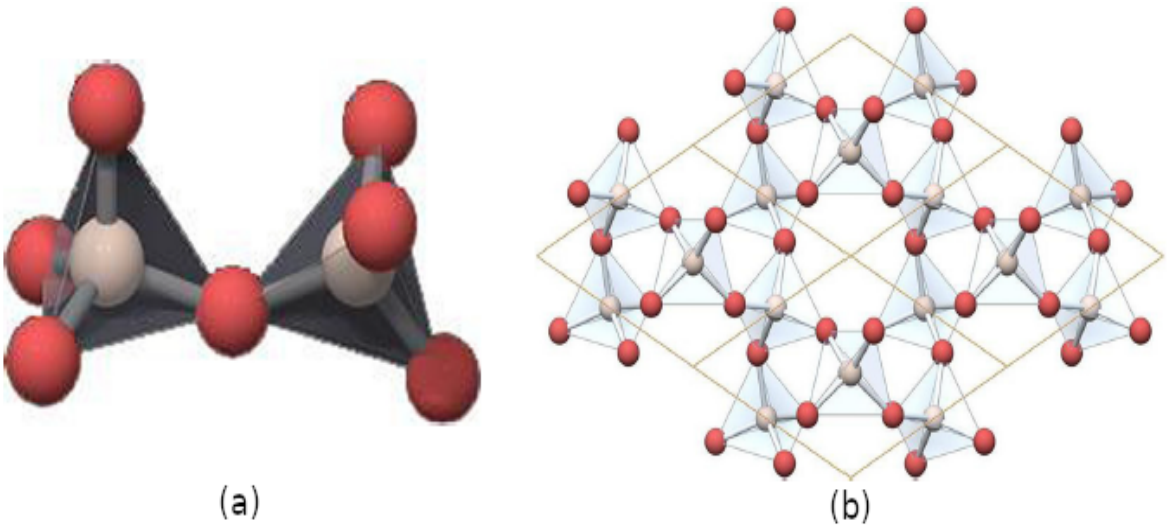

Figure 2.4: (a) Tetrahedral SiO_4 bond. (b) Crystal lattice composed by adjacent unit cells [6].

The comprehension of the interactions between the front cover glass and the environment are of great importance to characterize the degradation of glass, and also the other layers in the solar module. Although glass is chemically stable, damp heat tests and in-field inspections have shown that the mixture of water and contaminants over the glass surfaces of solar modules can lead to weathering in the presence of high temperatures [55]. In the process of weathering (atmospheric corrosion), several reactions can take place, triggered by the physical and/or chemical adsorption of molecular water on the surface, which reacts with the silica network cations or non-bridging oxygen [51]. In this process, cations are pulled apart from the glass network (leach) to the water layer which leads to corrosion and loss of transmittance.

EVA encapsulant

The current quality standards of solar photovoltaic systems ensure high reliability of modules up to 20 - 30 years of service. This depends directly on the performance of its components, which are selected considering a trade off between good quality and achievable cost. The encapsulant supplies the solar cells with protection against environmental effects: humidity, UV radiation, mechanical stress, among others. The main function of polymer encapsulants is to provide adhesion between the cells and the glass/backsheet, positioning the solar cells within the stack during manufacturing, installation processes and operation, while maintaining an optimum optical coupling between the glass and cells [52].

EVA is the most used polymer for encapsulation purposes, being used in about 80% of solar modules [47]. Although in general it exhibits good properties for photovoltaic applications (transmittance, low processing temperature, elasticity, high adhesion, etc), EVA is chosen amongst other polymers with better properties because of its cheap cost [56]. The polymer composition varies to improve its performance, but for PV applications typically contains 28 - 33 % by weight of vynil acetate (VA) compounded with additives like curing agents (to improve adhesion), UV absorbers, and photo-and-thermo antioxidants [57]. Examples of the chemical composition of these additives can be found in [52].

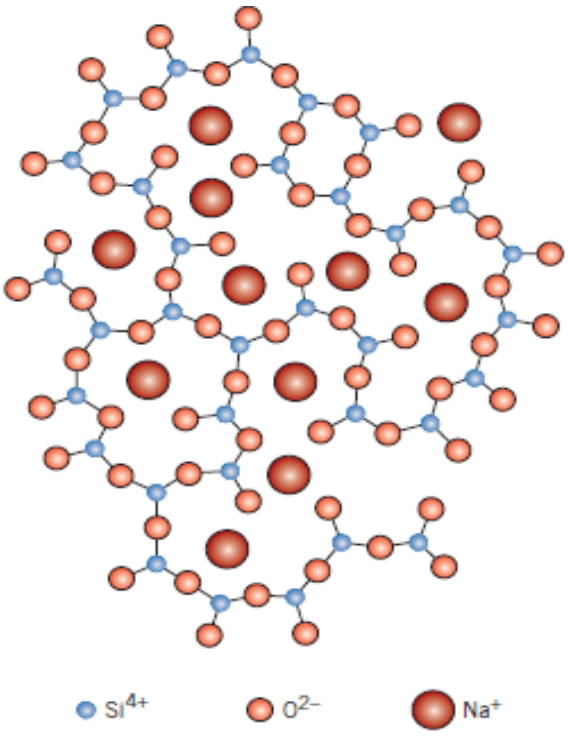

Figure 2.5: Schematic representation of a silica glass amorphous network [7].

The degradation modes that affect the EVA encapsulant are corrosion, delamination and discoloration [52]. The main triggers for these phenomena are humidity, high temperature and UV radiation. The data provided by [3] for the analysis performed in this thesis indicates that the only degradation mode observed in the EVA encapsulant was delamination, which will be briefly described in this section. Delamination is the loss of adhesion between the different interfaces that compose the solar module. In [58] it was shown that delamination is determined primarily by humidity, but temperature plays an accelerating role of degradation in time. Additionally, in [59] it was found that, when exposed to dry conditions, there was no significant loss of adhesion between the glass and the polymer, in a temperature range from 23 to 85 °C. Silanes (sillicon based coupling agents) which are compounds that enhance adhesion between interfaces [60] are sensitive to water ingress [61]. Furthermore, it is presumed that production of acetic acid (which is directly related to encapsulant discoloration [62]) enhances adhesion loss by acting as a catalyst for hydrolisis of bonds in the silane coupling agents [59]. Further, delamination induces corrosion of metallic components of the solar cells [63], as it propitiates the ingress of contaminants at the interfaces.

2.2 Electrical Characterization of Solar Photovoltaic Modules

2.2.1 The Diode Model

The separation and collection of charge carriers in a solar cell, as described previously in Section 2.1, can be represented as a diode. Several mechanisms can contribute to dissipate

certain amounts of the generated power. For example, the recombination of carriers, the establishment of shunt paths across the junction and other interfaces, the arising of contact resistances and material resistances . One simple but very complete description of the behaviour of the solar cell is the so called equivalent circuit representation, which is based in a single diode, and is shown in Figure 2.6. In this model, the light-generated current, which is proportional to the incident solar radiation, is represented as a current source I_L.

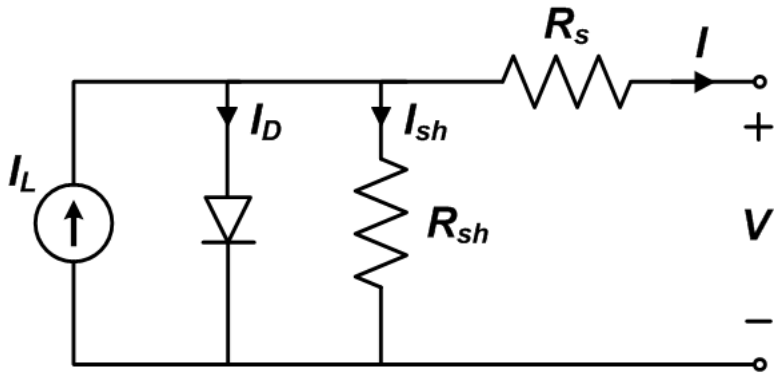

Figure 2.6: Representation of the solar cell with the equivalent circuit of one-diode . Image taken from [8]

.

The diode model allows to characterize the behaviour of the generated current as a function of voltage, and thus the power output of a cell. The diode-like behaviour arises from the depletion region established within the p-n junction. The reverse saturation current introduces the diode component to the circuit I_D, as shown in Figure 2.6. The series resistance component, R_s, comprises the losses caused by:

1. The movement of charge carriers through the semiconductor,
2. the resistance on the contact between metallization and semiconductor, and
3. the resistance of metallization components. As the current across the series resistance R_s is the same that the load current, this component should be as small as possible.

The shunt resistance R_{sh}, which comes from the recombination of charge carriers within the depletion region, gives rise to shunt currents, I_{sh}. In the ideal case no current should flow through the depletion region, therefore these currents are needed to be as negligible as possible. Considerably high values of R_s and low values for R_{sh} compromise the performance of the cell and lowers the output power. The diode model offers an accurate description of solar cells behaviour, which can be analysed through the current - voltage characteristic curve, as shown in Fig 2.7 (blue curve). The I-V characteristics, shows the variation of current at different voltages: The open-circuit voltage V_{oc}, which is the maximum voltage the cell can achieve at open terminals. The short circuit current I_{sc} is the maximum current the cell can deliver with its terminals shorted, and the maximum voltage V_{mpp} and current I_{mpp} which indicate the positions of the curve for which the maximum power $P_{mpp} = I_{mpp}V_{mpp}$ is delivered. Deviations in these parameters with respect to nominal values give information about the inner behaviour of the solar cell.

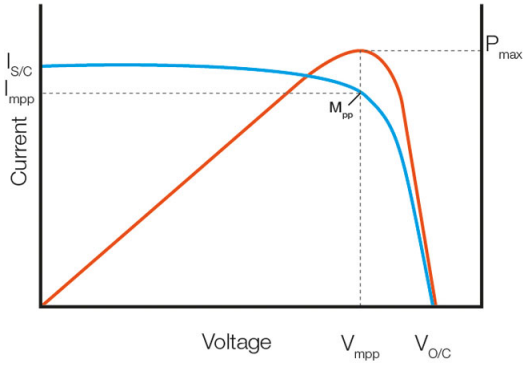

Figure 2.7: Current - Voltage characteristics of a solar cell. Image taken from *Seaward Solar*.

From this relationship between voltage and current, it is possible to characterize the power output of the cell through the P - V characteristics (red curve of Fig 2.7). The maximum power point P_{mpp} can be obtained by multiplying the maximum power point voltage V_{mpp} and maximum power point current I_{mpp}. Variations on the parameters R_s, R_{sh} cause variations on the shape of the curve. As in operative modules it is very difficult to measure the series or shunt resistance of the cells, these variations are used as indicators of changes in R_s, R_{sh}. This is graphically shown in Figure 2.8. Increasing values of R_s decrease the slope of the I - V curve near V_{oc}, while decresing values of R_{sh} increase the slope of the curve near I_{sc}. A considerable decrease in R_{sh} can also decrease V_{oc}. An interactive visualization of this situation can be found in [64].

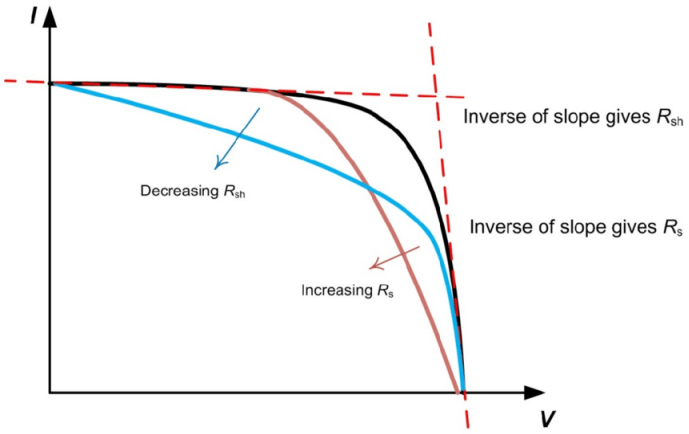

Figure 2.8: Effects of (a) R_s and (b) R_{sh} on the IV curve. Image taken from *pveducation.org*.

Photovoltaic modules are just aggregates of solar cells connected in series to fulfill the voltage requirements. Therefore, the I-V curve of a module is the same than that of a cell but with different voltage. Additionally, for safety reasons, modules also contain bypass diodes separating string of cells to limit the current dissipation in case of reverse biased cells, as will be discussed in the next section.

The equivalent circuit representation is a simple but a very powerful tool, widely used to model crystalline sillicon solar cell behaviour and power output with high accuracy [65]. As it can be constructed with the nominal parameters of solar cells/modules provided by

manufacturers, it is useful to compare the real performance of the system vs the expected performance in nominal STC operating conditions. This can help to quantify the degradation of the electrical parameters due to extensive outdoor operation, considering basic rules of the behaviour of the curve as enlisted below:

1. Less generation of charge carriers (either by poor irradiance, shading, loss of transmittance of solar modules components, etc) impacts directly the short circuit current.
2. Shunt paths across the p-n junction or other cell/module components, as well as temperature increases, contribute to decrease the open circuit voltage due to an increase in the recombination currents due to bandgap reduction [66].
3. Increased series resistance affects the slope of the I-V curve near the open circuit voltage [64], but does not modify its value since at V_{oc} there is no current flow out of the cell.
4. Decreased shunt resistance affects the slope near the short circuit current in the I-V curve, given that, the existence of alternative paths reduces the overall current that the solar cell can deliver and also the voltage from the cell [67].
5. Activation of the bypass diode creates a step in the I-V curve. The maximum current of each step corresponds to the current delivered by the bypassed string.
6. Isolation of part of a cell reduces the photocurrent that cell is capable of generate. This is evidenced on the I-V curve by small steps, proportional to the active area lost [68].

2.3 Detection and Diagnosis of Failures/degradation Modes in Solar PV Modules

The economic feasibility of solar PV installations shows an increasing trend given the reduction of the Levelized Cost of Energy (LCOE) for either domestic scale or utility scale PV power plants [69]. This makes of solar PV projects an attractive investment, in particular in regions with favourable irradiation conditions like Chile [70]. However, the long term performance of PV systems depends not only on the technology, but also in the environmental conditions where they operate [71], and the application of Operation and Maintenance (O&M) programs [72]. These factors can influence the reliability and durability of solar PV systems [2].

2.3.1 Failure/Degradation Modes in Solar PV Modules

Failures and degradations in solar modules have been widely defined in research works, reports and standards [1] [73]. According to [2], a failure can be considered as any issue which causes a power drop on the module beyond warranty limit, while a degradation causes loss of performance but the modules still meets the warranty requirements. In [74], a failure is defined as a mechanism that produces a sudden decrease in the device output, while degradation is a continuous output decay. Failures are directly related with reliability (probability of the device to maintain its operative state during a defined time interval). Therefore, a reliable PV system is the one that has high probability of perform its intended function during its warranty lifetime. In contrast, degradation is related to durability, which is concerned with long-term performance, rates of performance, property loss, etc. A considerable loss of material or product durability may lead to catastrophic failure (loss of reliability) [75].

Failures in solar PV systems are of major concern when safety risks of operation and handling are being considered, but also from an economic perspective due to the great amounts of power that can be lost as a consequence of faulty operation. Faults in PV devices can be studied using several approaches: According to the component affected by the failure (cell, metallization, encapsulation, glass, junction box, etc), type of failure (delamination, cracks, hot spots, arc faults, etc) lifetime related information (infant-failure, midlife or wear out failure), or underlying causes (manufacturing defects, mishandling, operation, environmental interactions, degradation). The visible or measurable effects of failures on the device performance are the footprints that allow us to infer the failure causes. An important difference exists between failure modes and failure mechanisms, within a purely conceptual plane. According to [76], on one hand, a failure mode is the recognizable electrical manifestation by which the failure is observed. For example, open or short circuit, increased current, etc. On the other hand, failure mechanisms are the specific microscopic physical, metallurgical, environmental phenomena or processes that cause the device degradation or malfunction.

According to literature, three categories of failure triggers can be distinguished, as shown in Table 2.1. Manufacturing defects can be referred to all these conditions found in cells/modules which arise from certain conditions at any stage in the production line of solar cells, that mainly contribute to reduce the final efficiency. For example, a relationship between reduced power output of high efficiency silicon solar cells after a few months before deployment, and the firing temperature (temperature for metallization printing on the solar cell) at the final stage of cells production [77] has been found. From these findings, researchers recommend that manufacturers use the lowest temperatures at firing to reduce certain impurities that can be related to the problem.

Another common manufacturing issue is related to the differences found in electrical characteristics of nominally identical solar cells packed in the same module, or series connected identical modules. This is important because the power output of the entire module or array is determined by the component with lowest output [78], and the excess of power produced by some cells is dissipated in lower performance cells in the form of heat. The uncertainty in the power output derived of current mismatch can be evidenced by looking at the power tolerance in module datasheets, which can range up to $\pm$ 5%. Cell mismatch in a finished module can be measured. Manufacturers have several sorting methods which categorize solar modules in different performance bins by, for example, maximum current (I_{max}), maximum power (P_{max}), current at fixed voltage or fixed P_{max}. Cells belonging to the same bins are encapsulated together to form a module [79], which can help decrease the mismatch. According to [80], several factors affect the power output of industrial solar cells. One example of this is the varying concentration and type of defects in a single Si column from which different wafers are extracted (for multi-Si based cells), or the tolerance on the diffusion processes, which is reflected on the fluctuation of emitter's sheet resistance up to 5%. Furthermore, the screen printing and firing back and front contacts can also affect the contact resistance.

Apart from manufacturing defects, there exist other possible causes of failures in modules associated to handling, and certain operating conditions of the modules. According to [1], defective clamping can cause glass breakage of frameless PV modules, allowing the passage of water vapour and oxygen into the PV module, enhancing corrosion and loss of performance. Additionally, glass breakage can facilitate the appearance of hotspots (warmer

Manufacturing defects	Handling/operation problems	Degradation modes
Cell defects due to high firing temperature [77]	Clamping	Corrosion
Electrical mismatch in cells [80]	Transport/installation	Discoloration
	Quick connector failure	Delamination
	Lightning	Cracks
	Shading mismatch	

Table 2.1: Different PV module failure triggers [1].

cells or warmer zones within cells). Transport and installation issues can lead to cracks and breakage of PV modules due to accidental falls, in-homogeneous stress distribution on PV stacks while transport, vibrations, residual stresses from prior processing [81], etc. Cracks in cells/modules are very difficult to detect, and in most cases they cannot be identified by simple visual inspection, being necessary the use of tools such as electroluminescence or lock-in thermography. Once detected, the cause of these defect is very difficult to infer, unless data from the modules prior and immediately after install are available. This is not usually achievable in PV plants that have been operating for several years, and even less probable to find in small scale plants with domestic or farm applications. For these reasons, cell/modules cracking due to mishandling or unexpected transport issues are not considered here as a failure. Another problem which arises from a poor planned installation is related to the location of the modules, which can be shaded by plants, trees or aerial power lines. This can permanently affect the performance of the PV systems, because shaded zones of a module or cell remain as inactive charge carriers generation zones. In the case of a considerable shaded area of a module the bypass diodes can activate, disconnecting the affected string with the subsequent reduction in power output. In partially shaded cells, the remaining active zones of the cell have to assume the entire string current, increasing the temperature and allowing the formation of hotspots [82]. An example of this is shown in Figure 2.9 where, (a) by visual inspection the presence of a plant shades the module in the upper corner. In (b), by performing IR Thermography an abnormal heat distribution in the affected cells is observed. An in-homogeneous thermal pattern is found on the shaded cells. The partial shading on cells/strings is considered as a current mismatch failure.

After assembled, transported and installed, the PV module will spend its entire life operating somewhere in the world, subject to the environmental and climatic conditions of that certain place. These conditions can vary widely in terms of atmospheric composition, wind, precipitations, dust, UV radiation, moisture, etc. Degradation appears as a gradual deterioration of the characteristics of a component or a system, which can affect its ability to operate within the limits of acceptability criteria. It is caused by the operating conditions [83], which can be related to temperature, humidity, UV irradiation, external mechanical stresses, etc.

Degradation modes can arise over the entire PV modules lifetime. Degradation causes reduction in the electrical output parameters of solar devices (I_{sc}, V_{oc}, P_{mpp}). Manufacturers provide a warranty of quality which ensures that PV modules will reduce their power up to 80% from the nominal power (P_{nom}) after 25 years, assuming a loss of efficiency of 0.5% each year [84]. Degradation is quantified by means of the electric power output reduction across time and the Fill Factor (ratio between the maximum obtainable power to the product

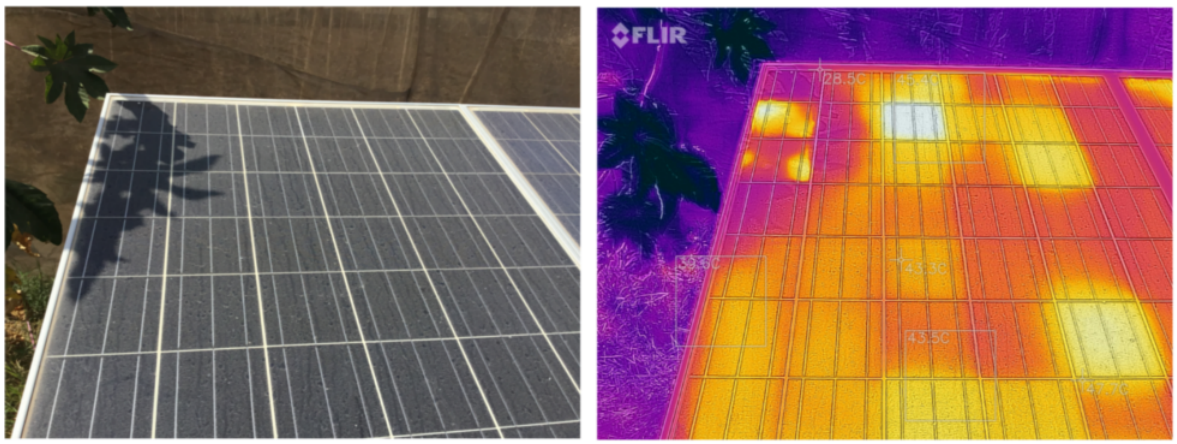

Figure 2.9: Partially shaded module by the presence of a plant: (a) Visual inspection, (b) Thermal image where the abnormal heat distribution can be observed.

of I_{sc} and V_{oc}), for which a value below 80% corresponds to a degraded module that needs to be replaced. Degradation and aging is highly conditioned to the geographical place and particular climatic features in which the modules operate [85]. Under extremely dry and arid conditions like the Atacama desert, one of the major challenges is the high amounts of UV radiation, which has been found to contribute to module degradation, affecting primarily the polymeric encapsulated [86]. Different failures/degradation modes may have a common cause. For example, gradual detachment of backsheet can be caused by moisture ingress through backsheet or laminate edges, due to poor adhesion or polymer disintegration, just like corrosion of cells and interconnections. Likewise, some failure/degradation modes can cause other failure/degradation modes. For example, glass breackage is a probable cause of hotspots, which can also can be caused by fragmentation of cells or interconnection failures, among others.

In order to differentiate the occurrence of a failure or degradation in solar modules, we consider that various degradation modes can lead to failure modes when are not properly addressed during long time intervals. For example, severe delamination can lead to PV modules fault for extensive loss of light transmittance and current mismatch between the affected cells or strings and the rest of the module. On the other hand, small/localized delamination may not cause great decrease in the electrical parameters and power output, neither hazardous temperature differences within the module. However, it can facilitate moisture and contaminants ingress which enhance corrosion and leads to further delamination issues. For this reason, in this work these issues that cause severe reduction in output parameters or temperature differences are considered as failure modes, on the contrary they are degradation modes. If detected a visual abnormality with no thermal or electrical abnormality associated, it is considered as a purely cosmetic issue. Nonetheless, considering that long term operation under any conditions different from those ensured by the manufacturer will possibly lead to further degradation and further faults.

The degradation/failure modes found in this work, which will be analysed in detail in the next chapter, are summarized in Table 2.2. Notice that soiling (accumulation of sand, dirt,

snow or any external drop deposited on the module components) and shading (projection of a massive object's shadow over the module surface) are not usually considered as failures or degradation [1], given that these are not an intrinsic issue of the system, but an environmental cause of modules degradation/failure. However, as found in this work, these are amongst the most common issues found in solar PV modules operating in the Atacama desert, hence they will be studied in detail in the next Chapter. The main failure modes found in the field test campaign are hotspots. Degradation modes found were encapsulant delamination, soiling, and gradual electrochemical corrosion (weathering). Milky discoloration of the front glass was also found, but for this issue has not been found a detailed description nor categorizing in literature except by its inclusion in visual inspection forms, as will be reviewed in the next section.

2.3.2 Analysis of Field Testing Data

To investigate on the primary causes of solar PV modules failures/degradations, as well as the physical, chemical or electrical mechanisms that lead its components to fail/degrade, an evaluation of the performance of modules in field is needed. In order to accomplish with the required standards and commercial warranties, manufacturers and researchers conduct accelerated testing under specific conditions of UV radiation, heat, humidity, electrical bias and white light. Accelerated tests provide a quick and useful tool to estimate the life characteristics of the product, by applying higher levels of stress than that of real operation but for a short period of time, in order to induce failures that would occur in the field [2]. However, improvements in accelerated tests need to be guided by in-field information, in order to match real measurements with laboratory induced degradations/failures [87]. For this reason, characterization of fielded PV modules and a detailed evaluation of failure/degradation modes that occur under different climatic conditions is of great importance. The level of detail on the evaluation and the quality of information collected are highly conditioned by increasing costs. The simplest tool to evaluate the current state of fielded modules, and also the cheapest is visual inspection, for which fillable forms and checklists based on international standards are available [88] [1]. With these tools, it is possible to detect issues as soiling, delamination and discoloration of encapsulant, junction box (j-box), wires, frame or other components abnormalities. However, other issues cannot be detected by bare eye, for example, thermal abnormalities derived from current-dissipating defective cells, shunts, overheating, current mismatch between cells, etc. For these issues, more sophisticated techniques are available, such as infrared thermal imaging (IRT), I-V curve measurement, ultrasonic inspection, electroluminiscence imaging (EL) and laser beam current (LBIC) [84]. The use of combined techniques allows to fully characterize fielded modules.

In this thesis, the data used for analysis were collected in a field test campaign performed by [3] in January 2018. The inspection was performed in three steps: 1. application of a fillable form to register information collected by visual inspection, 2. recording of thermal images using an infrared camera, and 3. measurement of the I-V characteristics for each of the 95 sample modules. All the modules are located in the western zone of the Atacama desert, near to the Pacific Ocean coast.

In desert climates the major attractive to install solar PV systems are mainly the high levels of global horizontal irradiation (GHI) and direct normal irradiation (DNI). Additionally,

Failure/degradation modes	Possible causes	Effects	Failure/degradation mechanisms
Encapsulant delamination	High temperature + humidity	Moisture ingress	Photochemical reactions
	Sensitivity of adhesive bonds to UV radiation	Enhanced corrosion	Chemical gradients at interfaces
	Poor adhesive bonds at the interfaces during processing	Transmission loss	Thermo-mechanical fatigue or severe electrical mismatch
	Contamination from other components (Excess Na in glass or acetic acid in encapsulant	Power drop beyond warranty limit due to optical decoupling and moisture ingress/corrosion	
Hotspots	Thermal expansion/contraction of interconnects of solder bonds	Backskin burns	
	Shadowing	Decrease in power	
	Faulty cell or cells in a string	Shattered glass	
	Low shunt resistance cells	Localized encapsulant bubbling	
	Failure of bypass diode	Localized encapsulant discoloration	
		Power drop beyond warranty limit	
Soiling	Low tilt angle of modules in soiling prone locations with infrequent rainfall	Slow transmission loss	Strongly adhesion and graduel hardening of soil layer on glass
	Defective cleaning protocols	Reduced current/power output but may not affect fill factor or warranty limit	
		Cosmetic/visual change	
Electrochemical corrosion	Moisture ingress through backsheet or laminate edges	Series resistance increase and/or shunt resistance decrease	Electrochemical corrosion or photoelectrochemical corrosion
	Higher ionic conductivity of encapsulant due to moisture	Potential induced degradation	
	Metallization sensitivity to moisture		
	Interconnect sensitivity to moisture		

Table 2.2: Failure/degradation modes studied in this work [2].

great extensions of free land (for large scale projects) and the absence of clouds contribute to maximize the energy yield. However, desert environments also present challenges, such as the absence of water supply for installations and cleaning. This depends on the cleaning technique used [89], however water based techniques are the prevalent cleaning mechanisms [90]. Another challenge arises from the high levels of thermal stress on PV modules due to

wide range thermal cycling [91]. Moreover, high levels of UV irradiation, which is particularly high in the Atacama desert [92] are related to EVA encapsulant degradation [93].

Soiling deposition on the surface of modules in dusty environments reduce drastically the economic feasibility of solar PV projects [94]. Several research have investigated the effects of soiling in different parameters of solar PV modules, such as optical transmittance, power output, energy yield or efficiency [95] [96]. As each individual research considers different measurement techniques, equipment and standards, it is difficult to perform a direct comparison between results of different studies [97]. However, all studies report energy yield losses due to soiling accumulation (which can vary with the PV plants specific location/climate) [9]. The net effect of soiling on the overall power output of solar modules is a reduction of the irradiance that reaches the cells, due to the blockage of particles on the glass surface.

Figure 2.10: Different degrees of soiling deposited on modules surfaces detected by visual inspection.

Soiling over PV modules can be detected by simple visual inspection. The effects of soiling deposition can range from a simple aesthetic issue (without affecting any output parameter) to a severe reduction in the energy output, so electrical measurements greatly influence the failure diagnosis. Moreover, the response of individual affected modules/cells depends on their inherent characteristics (materials quality, current mismatches, manufacturing issues), which affects the energy output, but also the thermal behaviour of modules. Therefore, it can be found that two soiled modules with similar soiling deposition patterns present very different thermal patterns and operating temperature. This can be characterized with high accuracy by IR Thermography. An important feature of soiling, treated as a failure/degradation mode, is that it is reversible as the module is cleaned. However, continuous operation under severe soiling conditions can lead to permanent degradation and damage of solar modules.

The most affected parameter on the I-V curve depends on the type of soiling deposition. According to [9], soft shading occurs when atmospheric particles deposit on the surface of the panels, decreasing the overall current, as shown in Figure 2.11(a). On the other hand, hard shading occurs when localized solid drops (like bird drops or accumulated dust or dirt) shade one or more cells in a clear and definable shape, which decreases the output voltage, as shown in Figure 2.11(b). Hard shade can also lead to hotspot generation [98].

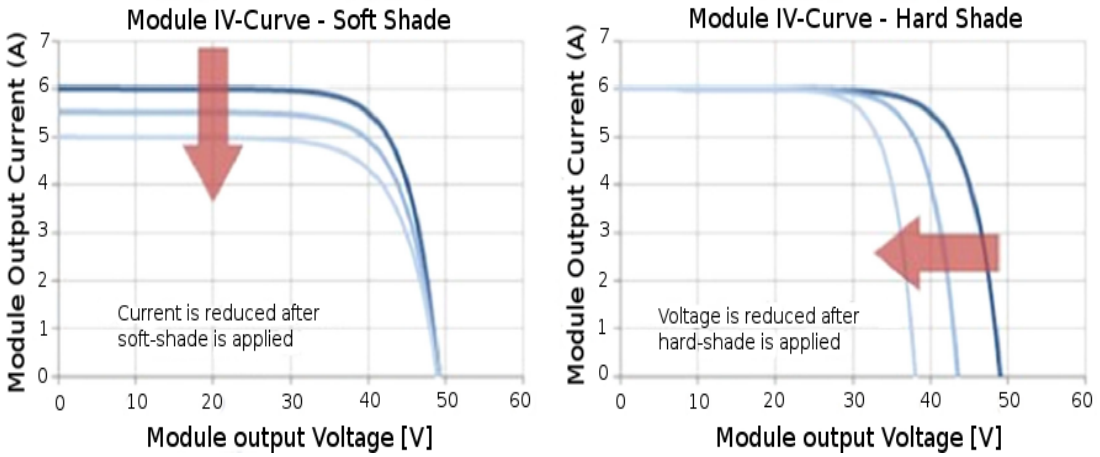

Figure 2.11: (a) Short circuit current reduction due to soft shading and (b) open circuit voltage reduction due to hard shading. Image taken from [9].

Among the different climates worldwide, in desert locations the highest degradation of short circuit current has been reported, affecting greatly the maximum power, but not the Fill Factor [99]. As it will be reviewed in the next Section, this is in accordance with the results obtained in previous work. In the Atacama desert, soiling rates depends on the geographical location, being the highest in Arica (0.6%/day) followed by Iquique (0.31%/day), while Calama and Copiapo exhibit less than 0.1%/day. However, the power loss depends also on rainfall, being again Arica the city with highest annual energy loss (39%) [100]. In [101], soiling composition and its effects on the transmittance of solar modules were studie. Results show that for different desert locations there can be found different mineral composition, influenced both by natural environment and the presence of mining industry. The transmittance losses have been found to reach 55% after four months of dust accumulation.

Another failure/degradation mode that can be detected by visual inspection is delamination. As shown in Figure 2.12, the visual manifestation of delamination is not unique, but shows a characteristic whitening over cells produced by the loss of adhesion of EVA [102]. As discussed in Section 2.1.2, the optical effect of delamination is the loss of transmittance across the EVA layer, thus decreasing the amount of light that reaches the cell in delaminated zones. This leads to heating and eventually to hotspot generation [103]. The decrease in transmittance also produces a drop in the short circuit current I_{sc} of the I-V characteristics [63].

Hotspot generation in solar cells depends not only on the causing failure, but also on the response of each individual cell to that failure. This concerns mainly the quality of the cell, but also the manufacturing defects or mishandling. A hotspot can be generated due to reverse bias operation by partial cell shading, cell fracture, defective interconnections or delamination of EVA. Despite the cause, the mechanism of generation of hotspots is a result of reverse biasing of one or more cells, when current mismatch between the string and the damaged cell occurs. By working at reverse voltage, the damaged cell(s) act as a power load, dissipating the power generated by the rest of the string, and consequently increasing their temperature. The schematic of Figure 2.13 shows the operating point of three PV devices connected in series, where PV3 is shaded. Therefore, this cell generates less current than

Figure 2.12: Delamination of EVA encapsulant detected by visual inspection.

its neighbors. If the string current is higher than the I_{sc} of the shaded cell, then it becomes reverse biased (the operating point turns to the reverse voltage region of the curve), sinking power instead of producing it, thus generating heat [10].

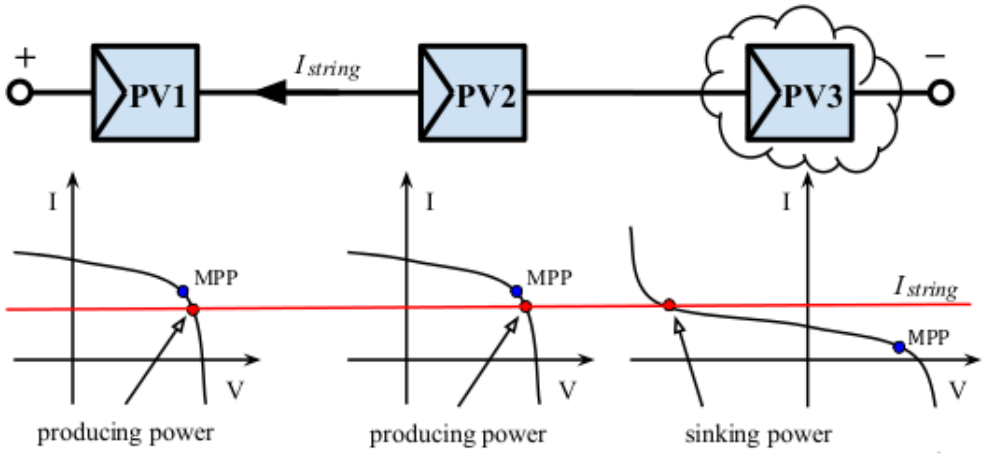

Figure 2.13: Current mismatch between three cells of a single string by shading of PV3 [10].

The shunt resistance R_{sh} is the parameter that determines the cells behaviour under reverse bias operation [104]. As shown in Figure 2.14, a high value of R_{sh} flattens the curve and shifts the breakdown region of the cell, while higher values contribute to steep the curve. This last results in a higher amount of dissipated power, causing breakdown and leading to hotspots. For operating voltages that exceed breakdown voltage of the cell, irreversible damage occur (solder melting, cell cracking) [11].

The reverse voltage at which the junction breaks down depends on the cell quality [105], and is of major concern for bypass diode design [106]. As shown in Figure 2.14, in forward bias the maximum voltage is very limited, but reverse voltages can be several times stronger. For commercial PV modules, manufacturers do not normally provide information about reverse bias characteristics of cells. It has been found that for the same module, individual cells can show wide variations in reverse operation conditions, possibly due to differences on material quality. In [106], mono and multi crystalline Si cells were measured individually, and poor cells were found to reach temperatures up to 150°C at a bias voltage of -10 V and a current

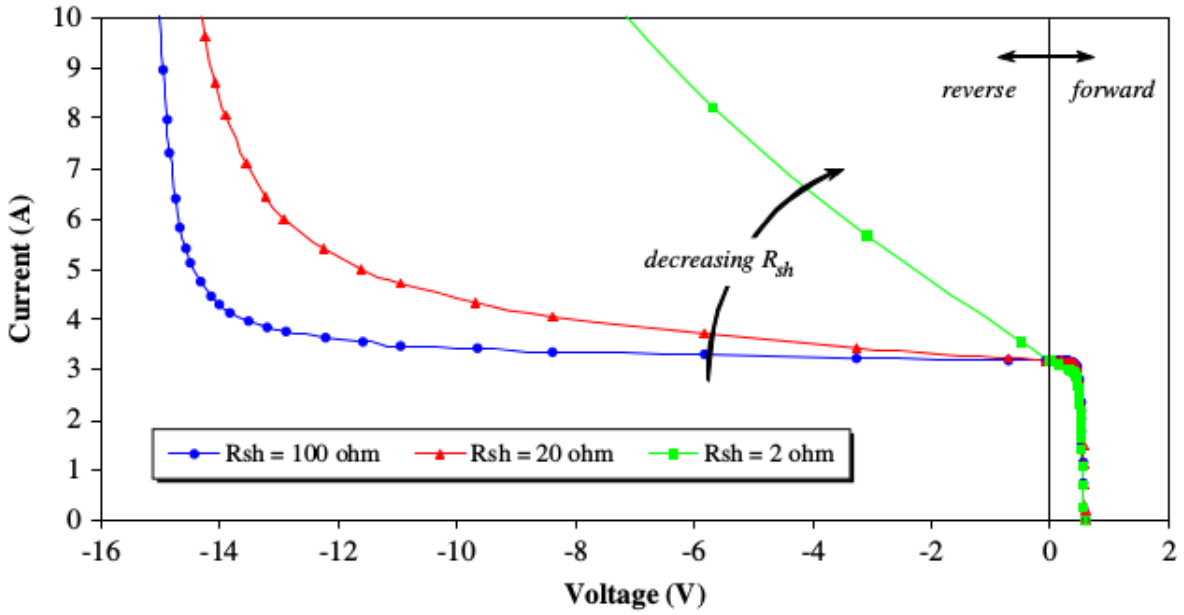

Figure 2.14: Reverse-bias I-V characteristics for three different shunt resistance values [11].

of 3 A. Usually, for multi crystalline solar cells the breakdown voltage is found to be around -13 V [107].

It results obvious that hotspots cannot be detected by simple visual inspection. Under operating conditions it is not possible to measure the reverse current of each cell to detect any abnormal electrical behaviour. For this issue, Infrared Thermography (IRT) is a popular non-destructive technique that allows to characterize thermal abnormalities in solar modules. Infrared cameras measure the IR radiation emmited by objects and then maps it to temperature distributions [108]. Measurements correspond to the apparent temperature of the object, and depends highly on the reflected radiation of the surroundings, transmission and emmisivity of the object [109].

2.4 Review of Field Test Campaign in the Atacama Desert

2.4.1 Summary of Results from Previous Work

In a previous work [3], visual, electrical and thermal information related to fielded PV modules operating in the Atacama desert was collected by means of a field test campaign. Results were analysed using a statistical approach, and were classified following three different approaches: by operating zone, manufacturer and deployment date.

From the collected information, 89.5% of the total amount of modules inspected showed some visual defect (including soiling that was the most common defect found) and 4.2% showed delamination of the EVA encapsulant, 79% showed cells with thermal abnormalities in the range of 10-20°C higher than modules average temperature, and 56.8% above 20°C. From electrical measurements, it was found that 95% of the inspected modules showed P_{mpp} degradation rates higher than 1.0%/year. Furthermore, it was found that the occurrence of

visual issues like soiling deposition, corrosion, chalking, can be related to location of the PV modules, being more present in the city and valley than in coastal zones. A summary of failures found in [3] is shown in Table 2.3. From the total of 18 failures analysed, for this thesis work they were only selected those that could be studied with all the tools used in the data collection campaign (visual, thermal, electrical). These were mainly those failures concerning the front glass, encapsulant, interconnection ribbons, cells, gridlines and busbars. Although soiling was the most dominant issue found, other visual failures like delamination of EVA encapsulant (4 modules) were also detected, but for these cases electrical measurements were taken under bad irradiance conditions (G$<$ 600 W/m^2) which does not allow to perform a reliable analysis of electrical parameters, and thermal images did not reveal temperature abnormalities related to delamination. This last can be possibly due to the presence of other failures in the same modules, of which thermal patterns predominate. A more detailed analysis is developed in section 3.2.1.

Component	Failure mode	Features	Number of cases
Glass	Soiling	Strong	39
		Light	52
		Weathered	2
	Crazing	Small	1
	Milky discoloration	Extensive	2
		Small/localized	6
Encapsulant	Delamination	Over cells	4
Gridlines	Discoloration	Dark	1
		Light	7
Interconnection ribbons	Discoloration	Dark	2
		Light	3

Table 2.3: Failures and degradation modes found in the field test campaign performed in [3].

Regarding to the measurement of electrical parameters, degradation rates seem to be congruent to other research conducted in desert climates [110]. In those studies, higher degradation rates for the short circuit current (I_{sc}) and maximum power point (P_{mpp}) than those for open circuit voltage (V_{oc}) and *Fill Factor* (FF) have been found. Short circuit current drops seems to be highly correlated to soiling deposition (which is directly related to irradiance). Maximum power point degradation rates seem to be related to the degradation of I_{sc}. The known relationship between operating temperature and reductions in the open circuit voltage [66] is not direct to infer in fielded modules because each of them can present many failures at the same time. For example, severely reverse biased cells can yield to an altered V_{oc} of the module in the I-V measurements. A summary of measured electrical parameters drop and degradation in % is shown in Table 2.4, where it can be seen that, in average, P_{mpp} values are above typical degradation rates normally guaranteed by manufacturers (0.7-1.0%). In fact, only five modules were found to be within this range.

It has also been found that modules which showed the highest drops of V_{oc} were affected by particular issues like activation of the bypass diode, presumably due to a complete inactive

	Deviation from nominal value (Drop)				Degradation rate			
	V_oc[%]	I_sc[%]	P_mpp[%]	FF[%]	V_oc[%]	I_sc[%]	P_mpp[%]	FF[%]
Min	0.02	0.13	4.41	-5.63	0.01	0.02	0.67	-1.28
Max	11.25	22.84	39.08	34.35	3.03	6.76	8.66	6.87
Average	3.19	8.80	13.19	4.58	0.88	2.30	3.55	1.34
Standard deviation	2.24	5.71	6.22	5.44	0.67	1.46	1.74	1.49

Table 2.4: Summary of electrical parameters measurements and degradation rates found in [3].

cell/string or showed signs of PID. Drops on the short circuit current are diverse and seem to be directly related to soiling.

Finally, with respect to the thermal characterization of modules, it was found that, in average they operate 11.67 °C above their respective room temperature, with a maximum of 24.45°C above room temperature. However, average temperatures are strongly influenced by the presence of hotspots. Additionally, due to the lack of a more sophisticated technique to obtain average temperature of the modules, they were calculated by taking the average temperatures of selected square areas fitting as much as possible to the module geometry (that was never perfectly rectangular because of the position of the camera with respect to the module), as shown in Figure 2.15. With tthis method, the extension of each square with respect to the entire module was not weigthed in the average, so a big square of low temperature (say, 10 cells with an average temperature of 38°C) could be averaged with a much smaller square (say, 4 cells with an average temperature of 60°C due to the presence of a hotspot) thus distorting the real average temperature of the module. For this thesis, when necessary, the average temperature of modules was corrected taking the average cell by cell (considering similar areas, again not equal due to the tilt of the image). Regarding to failures found according to known thermal patterns it was found that two modules showed PID pattern, but the vast majority showed a patchwork pattern characteristic of short circuit operating condition (in which all the test were carried out). Regarding to hot cells, several cells were found to operate above 20°C with respect to the average temperature of the modules, but none of the cells was found to operate above 100°C. Although it is undoubtedly detrimental to the overall performance of the modules, it does not represent a major safety issue.

2.5 Methodology

In order to address the objectives of this thesis, as referred in Chapter 1, a methodological strategy is proposed, based on the four stages shown in Figure 2.16. The first stage consists of a theoretical characterization of solar photovoltaic modules, as developed in the present Chapter. To perform the 5-fold analysis proposed in Chapter 1, this characterization involves the understanding of the basic principles that govern solar energy conversion. Furthermore, a basic understanding of the composition of PV module materials, their fundamental properties, and their interaction with the environment is also required. This is essential to identifying the critical aspects that can lead them to fail/degrade in outdoor operation, and how they may affect the electrical parameters of the system. Additionally, a review of the state of

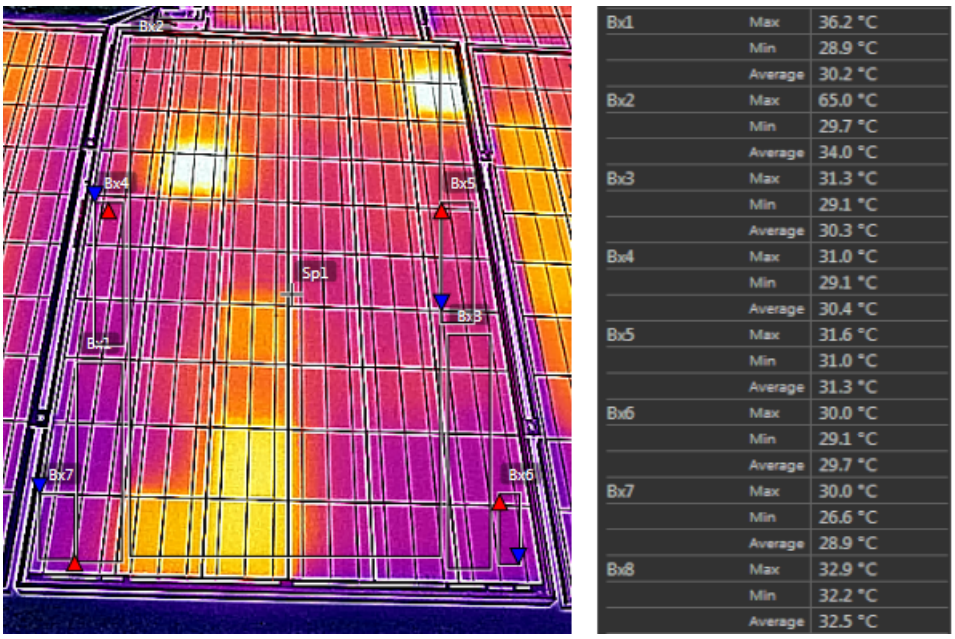

Bx1	Max	36.2 °C
	Min	28.9 °C
	Average	30.2 °C
Bx2	Max	65.0 °C
	Min	29.7 °C
	Average	34.0 °C
Bx3	Max	31.3 °C
	Min	29.1 °C
	Average	30.3 °C
Bx4	Max	31.0 °C
	Min	29.1 °C
	Average	30.4 °C
Bx5	Max	31.6 °C
	Min	31.0 °C
	Average	31.3 °C
Bx6	Max	30.0 °C
	Min	29.1 °C
	Average	29.7 °C
Bx7	Max	30.0 °C
	Min	26.6 °C
	Average	28.9 °C
Bx8	Max	32.9 °C
	Min	32.2 °C
	Average	32.5 °C

Figure 2.15: Determination of average temperature of modules using FlirTools.

the art concerning to the identification and diagnosis of failures based on the application of visual inspections, thermal imaging and electrical measurement procedures.

Background information is completed with a review of the main results obtained from the field test campaign carried out in [3] from where the data used in this thesis was extracted. Nonetheless, considering the number of modules tested (95), it becomes clear that using a statistical approach to analyse the collected data will not offer strong or reliable conclusions regarding the occurrence of failures and/or degradation modes of PV modules in the Atacama Desert. Furthermore, in [3] these three inspection tools (visual, thermal, electrical) were analysed independently. Therefore, a detailed analysis of the information, matching the visual inspection with infrared thermography and the I-V characterization of each module may provide additional information. This detailed analysis represents the core of this thesis, and will be developed on Chapter 3.

As detailed in Chapter 1, with the information obtained from Stage 1, a definition and justification of the objectives, limitations, selection criteria and the scope of the thesis are developed in Stage 2. In stage 3, the identification and analysis of selected failures/degradation modes found in solar photovoltaic modules from the Atacama Desert is conducted, addressed through a five dimensional approach based on the tools available: Statistical information derived from [3], visual inspection, electrical measurements and thermal imaging collected in a previous field test campaign. Finally, a theoretical analysis based on materials science regarding failure/degradation mechanisms identified from the available field testing data was conducted. Note that the analysis of failure/degradation modes is classified by the affected component, and that for each failure/component the available information may vary. For example, as discussed in Section 2.4, only four modules show delamination of the EVA encapsulant, therefore, there is no statistical information regarding this fault. Furthermore, due to its purely theoretical nature, the materials analysis is conducted considering individual components (materials) and their respective interaction with environment rather than

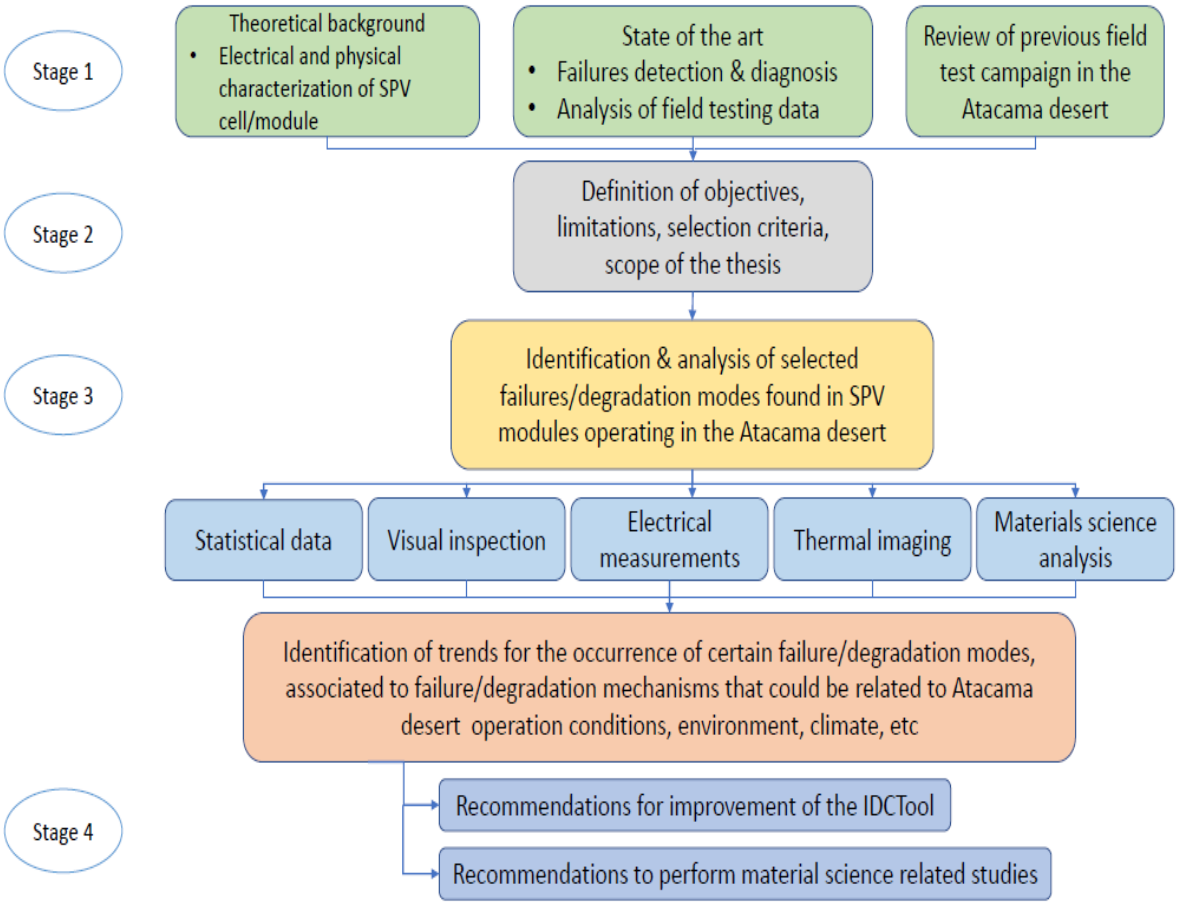

Figure 2.16: Methodological strategy addressed in this thesis.

individual faults. Finally, in Stage 4, recommendations for the improvement of the IDCTool developed in [3] are made, in order to identify the critical aspects to consider when developing future field test campaigns and to maximize the information that can be extracted from the collected data. Additionally, recommendations to conduct material science related studies are proposed in order to establish interdisciplinary bonds that may contribute to a better understanding of the fundamental features of underlying failure/degradation processes detected through in-field measurements.

2.6 Summary

In the present Chapter, all the information needed to fulfill the objectives of this thesis was briefly presented. In Section 2.1 the main features that allow to characterize and measure the performance of solar modules were discussed, from a physical approach. Composition and working principles (if needed) of each component of solar modules were explained, together with the critical aspects which determine the behaviour of PV modules during their lifetime. In Section 2.2, electrical characterization of solar cells and modules was explained. The diode mode, which accurately represents the behaviour of PV devices, together with the I-V characteristics offer a straightforward alternative to identify variations in parameters such as short circuit current, open circuit voltage, series and shunt resistances, and maximum power

point. These parameters are critical to describe analyse the actual state of PV modules, but also can help to track on the primary failure and degradation modes and corresponding mechanisms that affect them.

In Section 2.3 a literature review on failure and degradation modes and mechanisms was performed. The many possible causes for failures and accelerated degradation were discussed: manufacturing issues, improper handling and installation, defective or nonexistent operation and maintenance protocols, among others, can contribute to failure and/or degradation phenomena. Moreover, general guidelines found in literature to properly analyse field testing data are presented.

In Section 2.4 a summary of results from the previous work were briefly commented. Limitations regarding to the methodology applied in [3] were also discussed, setting up the methodology proposed for this thesis in Section 2.5.

Chapter 3

Analysis of failure/degradation modes found in photovoltaic modules operating in the Atacama desert

In this chapter, a detailed analysis of the sample modules is conducted, regarding the information obtained from [3] where a field test campaign was carried out. . The inspection procedure was applied to 95 modules. According to their geographical locations, four zones were delimited, as shown in Figure 3.1: A. coastal zone with two locations (designated by 2,3), B. city zone with 5 locations (4-8), C. inner valley zone with seven locations (9-15) and D. inner coast with one location (1). General information about the inspected modules is shown in Table 3.1. For the analysis, modules are referred as Fi, with $i = 1, .., 95$.

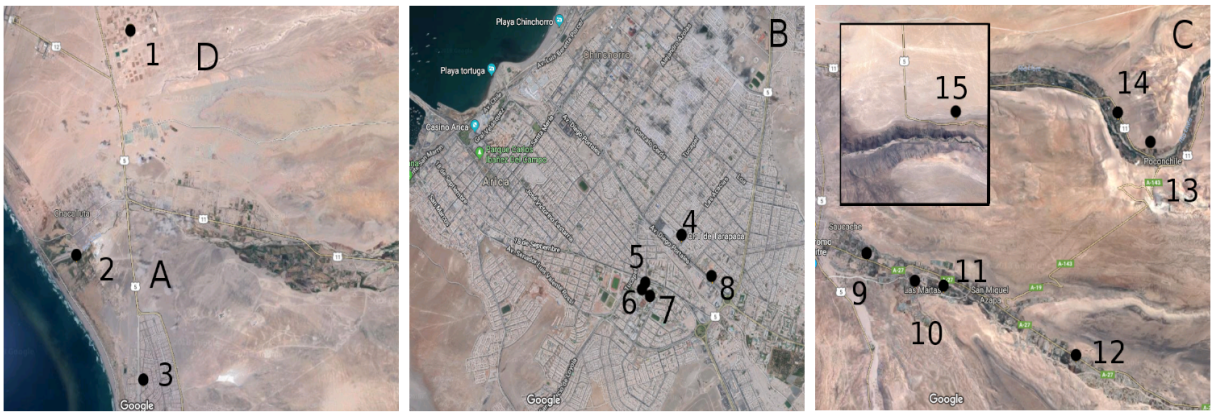

(a) (b) (c)

Figure 3.1: Distribution of inspected modules by zones (a) seashore and inner coast, (b) city and (c) inner valley.

In this Chapter, contents are organized as follows: According to the results obtained from previous work, summarized in Chapter 2, selected failure/degradation modes are analyzed. The three approaches addressed in the IDCTool developed in [3] (visual inspection, infrared thermography and electrical measurements) are used to detect characteristic fault signatures

Manufacturer	Si Technology	Deployment year	Number of modules	Location
BP Solar	multi-Si	–	1	6
Luxor	multi-Si	2011	6	7
SolarWorld	multi-Si	2012,13	30	2, 10-14
Risen Energy	multi-Si	2013,15,16	24	1, 8
ET Towards Excellence	multi-Si	2015	12	3, 4
JA Solar	multi-Si	2015	3	7
SUNEL	multi-Si	2012-16	9	9, 14
Hanwha Solar	multi-Si	2012-15	4	1
Siemens	mono-Si	2005	6	5, 15

Table 3.1: General data of studied modules.

reported in the literature. Additionally, a brief physical analysis is performed for each of the components affected by the failures found. The aim of this is to propose, theoretically, the possible failure/degradation mechanisms involved in each mode. The analysis is based on the information obtained from field test measurements, together with recent research and the structural, electronic and optical properties of materials involved in solar photovoltaic systems exposed to environmental stress. In section 3.1 issues that affect the front cover glass are analyzed: Soiling in different degrees of deposition (section 3.1.1 to 3.1.4) and milky discoloration of the front cover glass (3.1.5). In section 3.2 failures/degradation modes related to the EVA encapsulant are analyzed. In section 3.3, failures related to solar cells and finally in section 3.4, faults that were not detected by simple visual inspection but could be inferred by thermal imaging and/or electrical measurements are mentioned. Thermal images were taken with the Flir One pro IR camera. In order to achieve a better resolution, the images were mapped to density plots using MATLAB. Electrical measurements were obtained with the I-V tracer Seaward PV210.

3.1 Front Cover Glass

3.1.1 Soiling

Rigorously, soiling is not a failure or degradation mode inherent to solar modules. However, it is one of the most common issues that affect them over their entire lifetime, particularly for desert areas. Furthermore, severe and long-term soiling issues may contribute to trigger or enhance the development of failure/degradation. Additionally, as soiling is detected by means of visual inspection, its presence can contribute to cover other visual defects that may help to detect or explain other failure/degradation processes. For this, in this first Section, a complete characterization of soiled modules in each geographical area is conducted, in order to consider (or discard) the presence of soiling layers in further analysis of other failure/degradation modes and mechanisms.

From the universe of 95 modules analyzed, 4 soiling degrees on the front glass are distinguished, according to the intensity of soiling deposition: clean (2 modules), weathered (2 modules), lightly soiled (52 modules) and heavily soiled (39 modules). Although soiling deposition is difficult to quantify, in this study lightly soiled modules are those which present a thin layer of dust particles, pollution particles or drops over the surface. However, the

module is not totally covered, or features like color and metallization components can still be distinguished. On the other hand, heavily soiled modules are highly covered by a thick layer of particles: color and metallization are less, or not distinguishable. For this analysis, only lightly and heavily soiled modules are considered.

A relationship between the drop in the Maximum Power Point (P_{mpp}) and the degree of soiling is shown in Figure 3.2. As shown, 60% of lightly soiled modules (red) show a Maximum Power drop below 10% from their nominal value, and 96.15% of the lightly soiled modules show power drop below 20%. The remaining 3.85% (2 modules) show power drops in the range 21-30% and 61-70%, which can be indicative of additional problems that will be later studied individually. Regarding to heavily soiled modules, 53.85% show power drop between 11-20% while 82.06% present P_{mpp} drop below 30% from the nominal value. As it will be detailed below, those modules with higher power drop belong to a set affected by a particularly thick and uniform layer of dust, which presumably prevents the generation of photo-current in the entire modules surface.

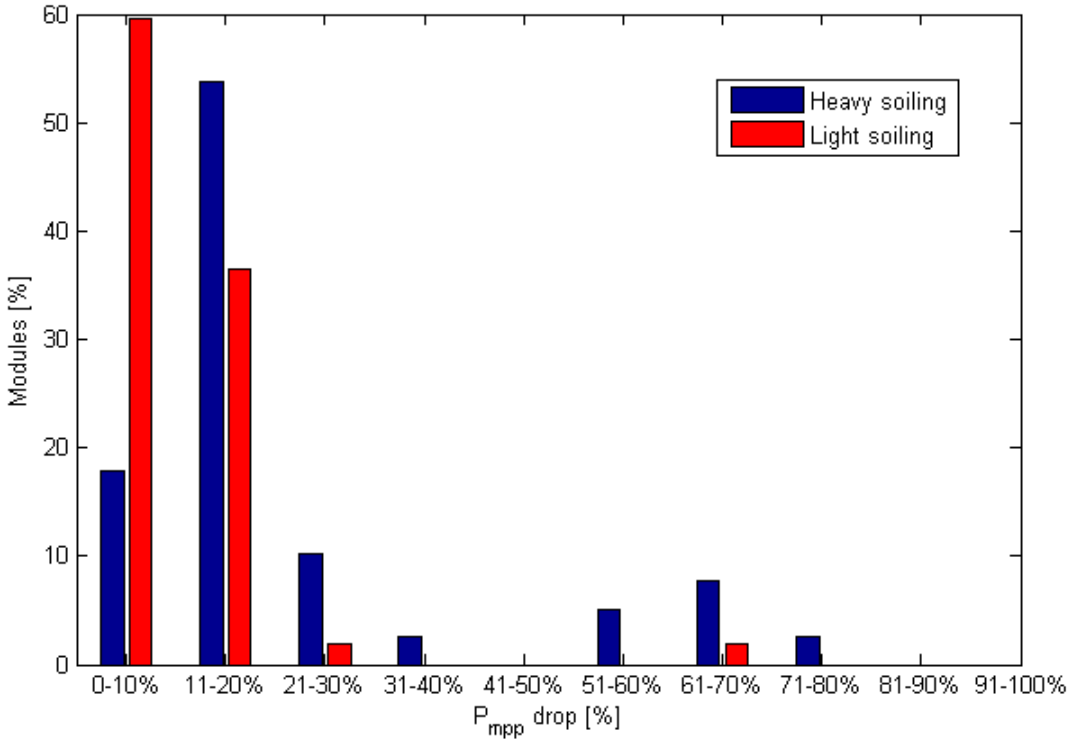

Figure 3.2: Distribution of P_{mpp} drop of heavily (blue) and lightly (red) soiled modules.

Power output of the modules is determined by the Open Circuit Voltage (V_{oc}) and Short Circuit Current (I_{sc}). The parameter that is most related to soiling corresponds to reductions in I_{sc}, given that its effect is equivalent to lower irradiation levels seen by the module (and thus lower generation of charge carriers). As shown in Figure 3.3 (a), the vast majority (84.62%) of lightly soiled modules present a reduction of I_{sc} less than 10% with respect to nominal value, and all of them present less than 20% reduction. For heavily soiled modules, 79.49% of the total sample show less than 20% I_{sc} reduction, but 15% show values higher

than 40%. Regarding to V_{oc}, it is known that changes in irradiance do not affect the open circuit voltage (as temperature does), as it can be seen in Figure 3.3 (b). All heavily soiled modules show V_{oc} reduction less than 10%, while for lightly soiled modules one of them shows a very high drop (64.08%) but this is presumably not related to soiling phenomena.

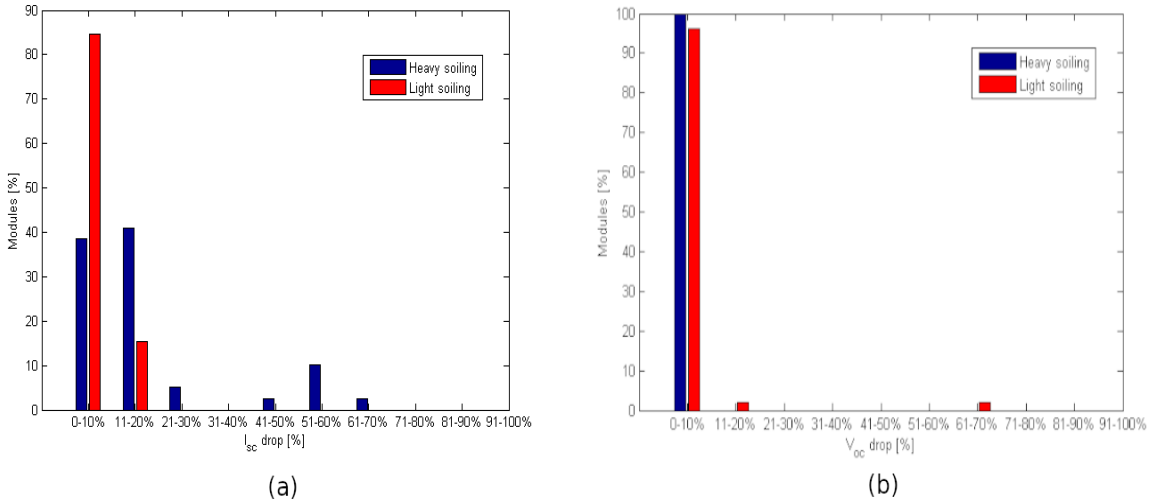

Figure 3.3: Distribution of (a) I_{sc} and (b) V_{oc} drop of heavily (blue) and lightly (red) soiled modules.

Regarding to the operating temperature of the soiled modules, it was found that the average operating temperature on the surface of heavily soiled modules is 40.94°C. For lightly soiled modules this temperature is 46.02°C. Temperatures were calculated from the IRT data, with the same approach shown in Section 2.4, but using a greater amount of squares to fit the desired area.

The distribution of temperatures, divided in four ranges is shown in Figure 3.4. It can be noted that most of the heavily soiled modules remain within the range [38.39,42.69]°C, and three modules operate with an average temperature between 46.99 and 55.59°C. In contrast, most of lightly soiled modules (35) operate below 48.86°C but six modules operate between 55.06 and 67.46°C. This may be because severe and uniform soiling layers, can act as a screen over the surface, preventing the generation of charge carriers and thus, the temperature rising. When a photon of energy larger than the energy *bandgap* of the absorbing material (around 1.1 eV in the cells analyzed in this work) is absorbed, the excess energy is dissipated as thermal energy across the crystal lattice. When the amounts of incident photons is decreased by screening the active surface (in this case with a thick layer of dust), the electron-hole pairs generation rate is also decreased, and consequently the thermal loss. This decreases the total current of the module and consequently the temperature. Additionally, this can also contribute to adjust the short circuit current (I_{sc}) mismatch between the cells on the module, avoiding to force higher currents through defective cells. This is not observed in lightly soiled modules, considering that modules average temperature considers also cells operating at very high temperatures (>70°C) probably due to other (and less evident) reasons, like broken cells, uneven light transmission across encapsulant layers or high shunted cells.

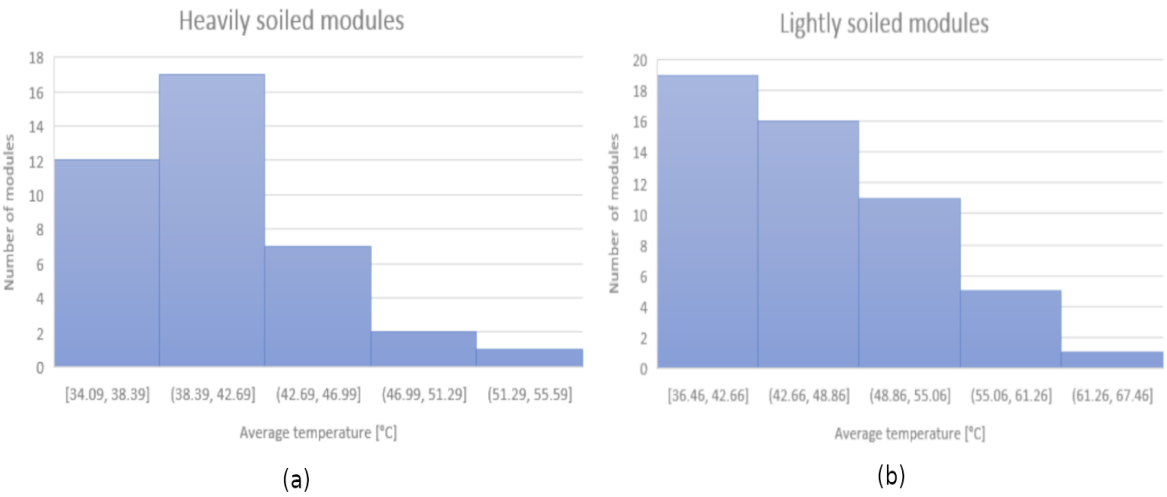

Figure 3.4: Average temperature distribution of (a) heavily and (b) lightly soiled modules.

In the next subsections, soiling over the sample of modules is described and analyzed in detail, in order to detect common features associated to soiling that can be involved in failure/degradation modes of the operating modules in the Atacama Desert. For this, strong and lightly soiled, and weathered modules were classified (when possible, given the unequal number of modules for each case) according to the specific characteristics of soiling deposition, location and operating temperature. Notice that, however, the accumulation of dust on the modules depends highly on the cleaning rates of each individual plant, information that was not available for this research. Moreover, some of the modules were classified as soiled on the survey filled in [3] but were cleaned before taking electrical I-V measurements or thermal images, so these modules were not taken into account to analyze soiling in this work.

3.1.2 Heavily Soiled Modules

Visual Inspection

Heavily soiled modules were found in three different zones: A. Seashore, B. City and C. Inner valley. For these different locations the deposition of soiling shows different signatures over the surface of the modules. As shown in Figure 3.5, modules located in the coastal zone outside the city, 3.5(a), present a groove deposition pattern, possibly related to the higher humidity mixed with wind in this zone (pattern s1). Modules located inside the city, shown in Fig. 3.5(b), present a more circular-like deposition pattern (s2) but with an in-homogeneous distribution over the surface. It can also be noted soiling layers of different composition, probably due to the presence of a greater variety of contaminants in the city than in outside locations. For modules located in the inner valley zones, shown in Fig. 3.5(c) and 3.5(d), soiling show an homogeneous distribution, with circular-like deposition patterns, possibly due to the driest climatic conditions in these zones. Fig 3.5 (d) shows a very thick layer of soiling which barely lets the light penetrate to the module surface. This phenomenon was observed in six modules, which were measured before and after cleaning, in order to evaluate changes in electrical parameters and thermal profiles. Patterns of images (c) and (d) will be assigned as s3 (strong circular-shaped deposition pattern) and s4 (heavy circular-shaped

deposition pattern), but keeping in mind that the main difference between them seems to be just the severity of soiling deposition. The difference between s3 and s4 is that s4 pattern completely covers the module surface.

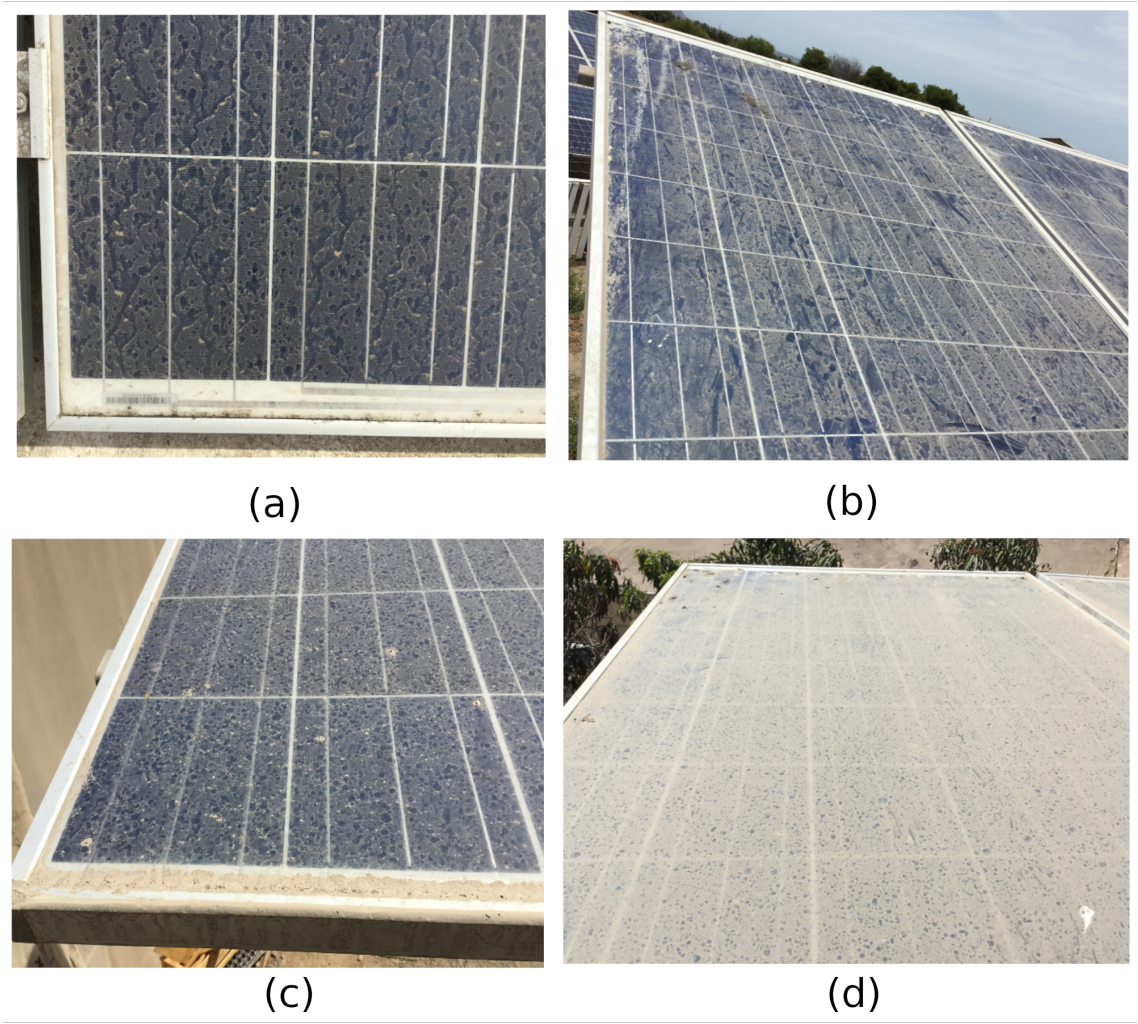

Figure 3.5: Heavily soiled modules in (a) coastal zone, (b) coastal zone inside city, (c) and (d) inner valley.

Infrared Thermography

Regarding to the thermal signatures of heavily soiled modules, the common feature found in all modules was an approximately even temperature profile over the surface (temperature variations no higher than 3°C between cells within a module). Despite individual thermal patterns of hot cells that were more probable to be associated to other failures (like shading by drops or objects, micro-cracks or shunts). Temperature variations < 10°C of cells within modules correspond to patchwork thermal patterns (random distribution of cells with different temperatures, but no differences higher than 10°C between each other) that can be associated to electrical current mismatch.

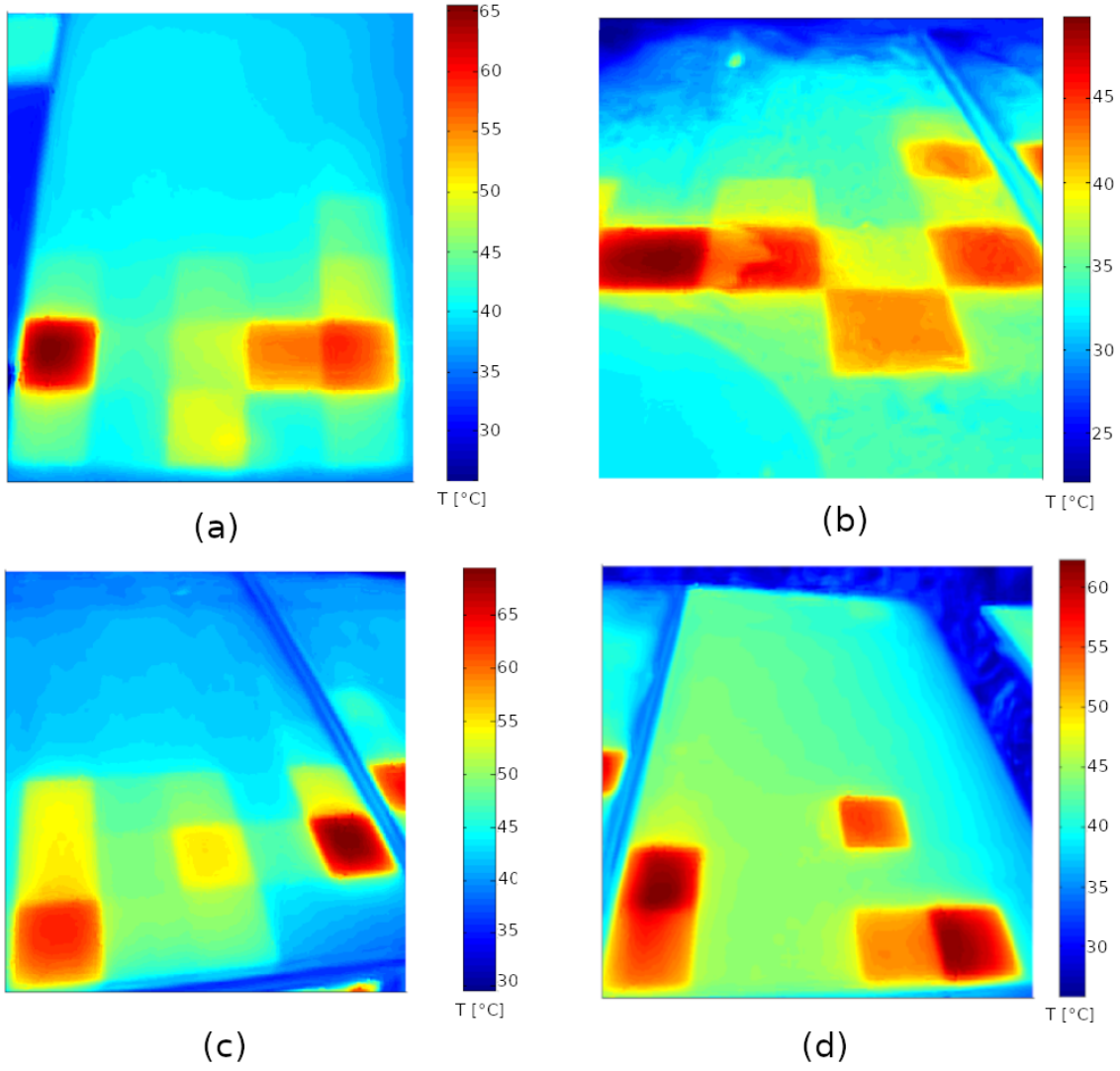

Figure 3.6: Thermal images of heavily soiled modules operating in (a) coastal zone, (b) city, (c) and (d) inner valley

Characteristic thermal images of modules located in the geographical zones described above are shown in Figure 3.6. Similar thermal patterns were found in modules corresponding to each area. Coastal-based modules, shown in Fig. 3.6(a) were all found to have hot cells in the bottom part of the module, while in the upper part an even temperature was measured with an average of 38.7°C, without any particular heat pattern on the cells. For coastal-based modules inside the city, shown in Fig. 3.6(b), it can be seen that on the top of the modules, soiling shades the surface, thus producing a temperature difference between shaded and non-shaded areas of the modules. In the upper part of the module, an average temperature of 28°C was measured while in the central and lower zones the temperature raises up to 36°C (not considering the very hot cells at the center). The clean area on the left corner shows a temperature drop to around 32°C. For modules located in the inner valley, shown in Fig. 3.6(c) and 3.6(d), the average temperature of the modules (not considering hard hotspots) was 41.5°C and 41.9°C respectively, and also all hot cells were located in the lower part of

the modules. In Table 3.2 the temperature ranges found in modules of each zone, specified by region of the module are shown.

		Temperature [°C]		
Zone	Soiling pattern	Upper	Central	Lower
Coast (A)	s1	36.2 - 39.6	36.7 - 40.8	35.6 - 65.3
Coastal city (B)	s2	22.1 - 36.8	32.7 - 49.8	32.0 - 36-0
Inner valley (C)	s3	38.5 - 42.0	41.3 - 43.3	39.8 - 69.4
	s4	35.9 - 40.8	34.0 - 53.1	34.7 - 60.0

Table 3.2: Variation of temperature of heavily soiled modules according to module regions (upper, central lower) and zone (coast, coastal city, inner valley).

Figure 3.7 shows the visual images of the modules of Figure 3.6, where it can be seen that soiling layers distribute homogeneously over the modules surface, except for the city-coastal modules (b). These modules show higher temperature variations (around 5°C) between upper and lower regions, probably due to the higher soiling deposition in the lower part, and the more diffuse distribution of soiling in the upper part. Regarding to hot cells and hotspots, it cannot be seen a direct relationship between hotter cells in the modules and the distribution of soiling over the surface. However, in the partially clean module of Figures 3.7 and 3.6 (b) the partially clean hot cell at the center of the module shows a temperature reduction from 45°C (dirty zone) to 42°C (clean zone), variation that can be also appreciable in the cell immediately below (35.2 to 32.7 °C from dirty to clean zones).

While it is not possible to determine why these modules show a similar temperature distribution, and hot cells distribution by geographical location, attention on transport, handling and installation processes must be paid as a first approach. As for each location, packed modules arrive together, stacked in a pile where they may be subjected to mechanical stress in determined areas (the same areas for the entire pile). Moreover, mishandling and/or negligent installation are commonly related to micro-fractures, which can further enhance thermal stress and the appearance of hotpots.

Electrical Measurements

The effect of heavy soiling on the electrical parameters of the affected modules can be associated to a reduction in I_{sc}. This is because of the screening effect of soiling layers over the surface of the module, which prevents the arrival of photons on the active surface. As shown in Figure 3.8, modules of the three zones (coast, coastal city, and inner valley) are affected by a severe reduction of I_{sc} and a less significant reduction of V_{oc}. Since $P_{mpp} = I_{mpp}V_{mpp}$, a reduction in maximum power point is significant due to the high reduction in the Short Circuit Current. Average values of reduction on the electrical parameters are shown in Table 3.3. It can be seen that, as expected, the largest reduction of I_{sc} and thus P_{mpp} was found in the most heavily soiled modules (pattern s4) located in the inner valley. The second highest drop was found on the other set of modules of the inner valley (pattern s3) followed by the coastal-based modules (s1) and the less affected modules were those located in coastal city (s2). This effect can be due to the homogeneous distribution of soiling of patterns s1, s3 and

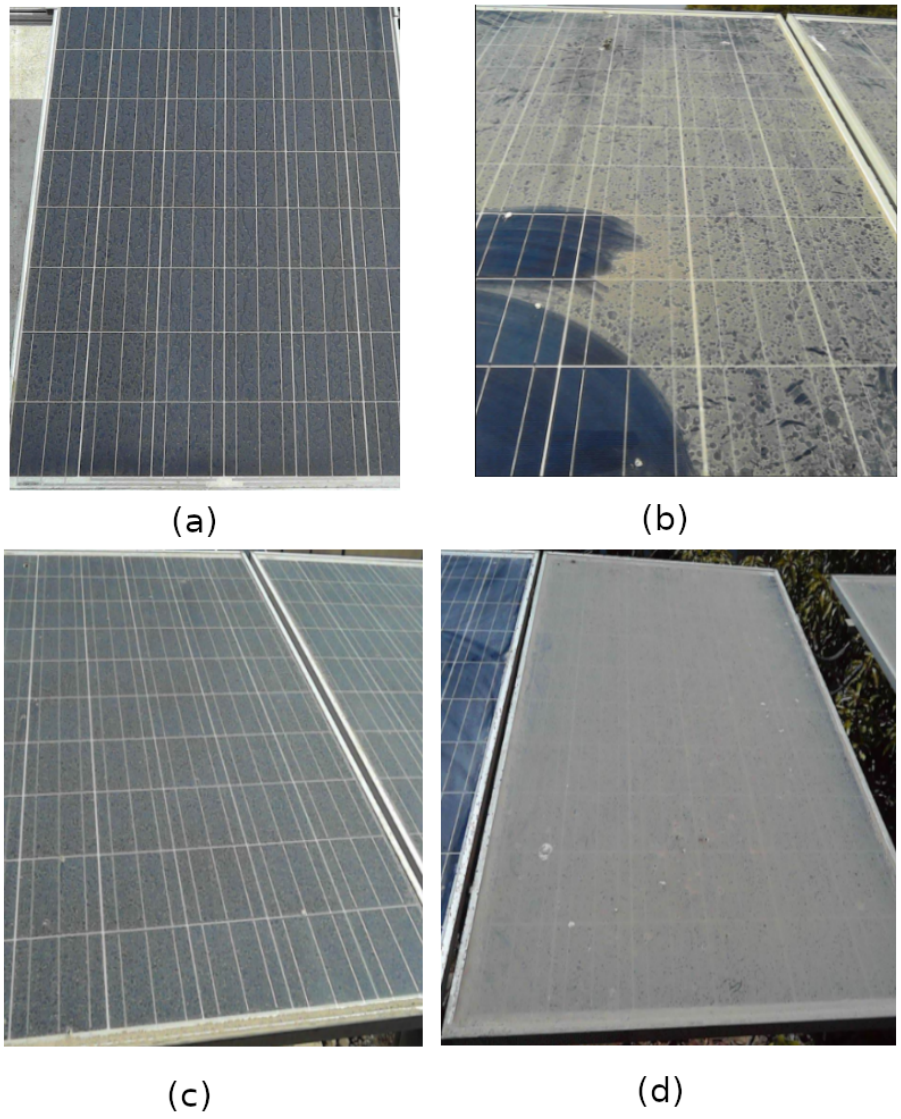

Figure 3.7: Visual images of heavily soiled modules operating in (a) coastal zone, (b) city, (c) and (d) inner valley

s4, which prevents part of the incoming light to reach the semiconductor to generate charge carriers over the entire surface of the module. However, the maximum power point P_{mpp} also depends on V_{oc}, whose reduction is not negligible and in this case happens to be the greatest for s4 modules, followed by s2, s3 and s1.

Regarding to voltage, the relationship between the temperature of modules and the V_{oc} drop is known, and can be related to hard shading issues. However, in this case a correlation between the soiling patterns, temperature and V_{oc} is not clear. What it visible, is that the s3 modules (inner valley, not severely soiled) show the highest temperature, probably due to the higher average room temperature of this zone (31.8°C) with respect to coastal zones. In contrast, s4 modules (inner valley, extremely soiled) show a lower average room temperature (27.79°C), and also lower module average temperature probably due to the less generation of current due to the thick uniform layer of soiling on the surface. Coastal-based modules show

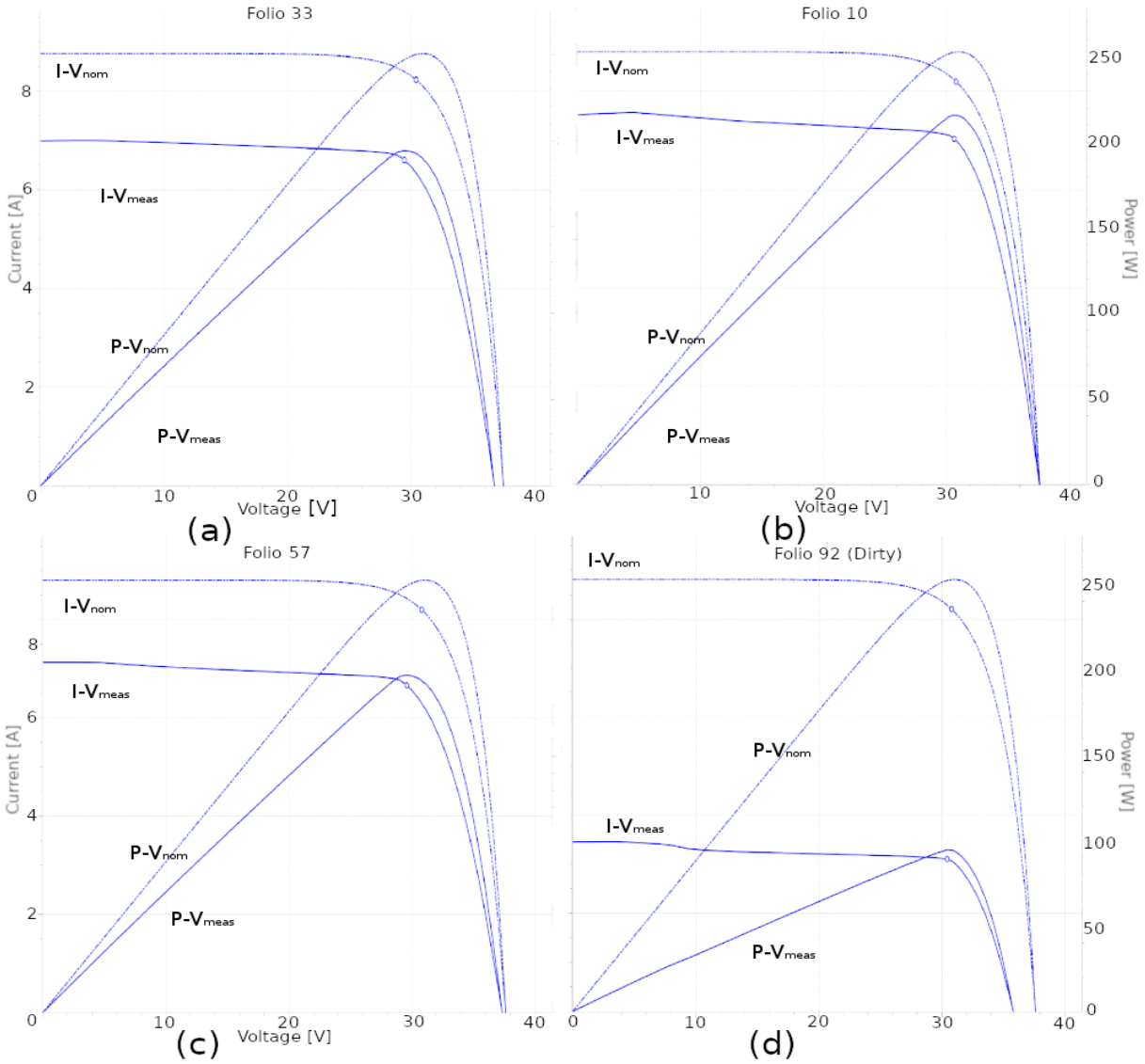

Figure 3.8: I-V characteristics of heavily soiled modules (I-V$_{meas}$, P-V$_{meas}$) operating in: (a) coastal zone, (b) city, (c) and (d) inner valley (solid line) compared with nominal values at STC (I-V$_{nom}$, P-V$_{nom}$).

lower average temperatures probably due to the lower average room temperature (25.62°C for s1 and 29.9°C for s2 modules) .

Zone	Soiling pattern	Average temperature [°C]	Voc	Isc	Pmpp
Coast (A)	s1	37.94	-3.71%	-15.08%	-18.45%
Coastal city (B)	s2	38.36	-4.69%	-10.06%	-14.22%
Inner valley (C)	s3	47.93	-3.47%	-36.53%	-19.08%
	s4	42.49	-4.73%	-55.31%	-63.16%

Table 3.3: Average variation of electrical parameters of heavily soiled modules.

3.1.3 Heavily Soiled Modules Before and After Cleaning

A set of six modules located within the inner valley zone (Zone C, location 11 in Figure 3.1) were found to be operating under severely soiled conditions, covered by homogeneous-thick layers of dust. For these modules, two measurements were performed in order to quantify the relationship between the electrical parameter variations, and thermal profiles with the presence of heavy soiling deposition. The first measurement was performed keeping modules as they were found (soiled), and a second measurement was performed once the modules were cleaned. The complete inspection by visual inspection, thermal imaging and I-V/P-V characterization is shown in Figures 3.9 and 3.10. The modules of this set are labeled as F90 to F95. A quick inspection of the visual and thermal images shows that most of the hot cells in the modules are not the same (in location and/or temperature) before and after cleaning. Also, the six modules show two different I-V trends on their signatures: Module F90 is shown in Figure 3.11, and modules F91-95 are shown in Figure3.12.

Visual Inspection and Infrared Thermography

For module F90, Figure 3.9(a) shows that apart from the soiling layer, there was a plant partially shading the left bottom corner of the module. In the thermal image shown in Fig. 3.9(b) this appears as a colder area (around 30°C), but the non-shaded areas within the shaded region do not show notably higher temperatures than the rest of the module. This is due to the very low current the module is generating, due to the heavy soiling layer that covers the entire surface, so mismatches on the current delivered by differents strings are almost unexistent.

After cleaning and removal of the plant shadow at the corner, Figure 3.9(c), shows that after most soiling was removed, the thermal pattern of the module Fig. 3.9(d) changes substantially. The hot cell previously detected at the second string in Fig. 3.9(b), which had a maximum temperature of 66.7°C in the soiled module decreases to 47°C after cleaning. The hot cell of the third string increases its temperature to 70°C and the cell immediately below increases from 45.5 to 70.9°C. Additionally, the top left corner cell also rises its temperature from 45.4 to 98.5°C. Apparently, the bypass diode was acting when the module was shaded (and soiled), because of the presence of the plant, preventing the corresponding sub-string from excessive heating. Additionally, the temperature distribution across the cell on the right is not uniform, as shown in Fig. 3.9(b). The left half of the cell is hotter than the right half by an average of 5.8°C, because of an additional layer of dust deposited around the edges of the module, which contributes to cool down the cell partially. This uneven temperature distribution disappears after cleaning.

Modules F91-F95 also present a varying thermal pattern, as shown in Figure 3.10. As the I-V signature is similar for all modules, measurements corresponding to F91 are shown. In Figure 3.9(b) the heavily soiled module of (a) shows a thermal pattern with three hot cells at 52.9, 60.7, 69.9 and 72.9 °C. The rest of the module shows a relatively homogeneous temperature over the surface of around 44°C.

After cleaning, the thermal pattern of Figure 3.10(d) shows that the hot cell of the top left corner detected in the soiled module disappears, showing a temperature of 43.7°C on the clean module, just like the cell of the second string. The bottom right corner cell remains hot

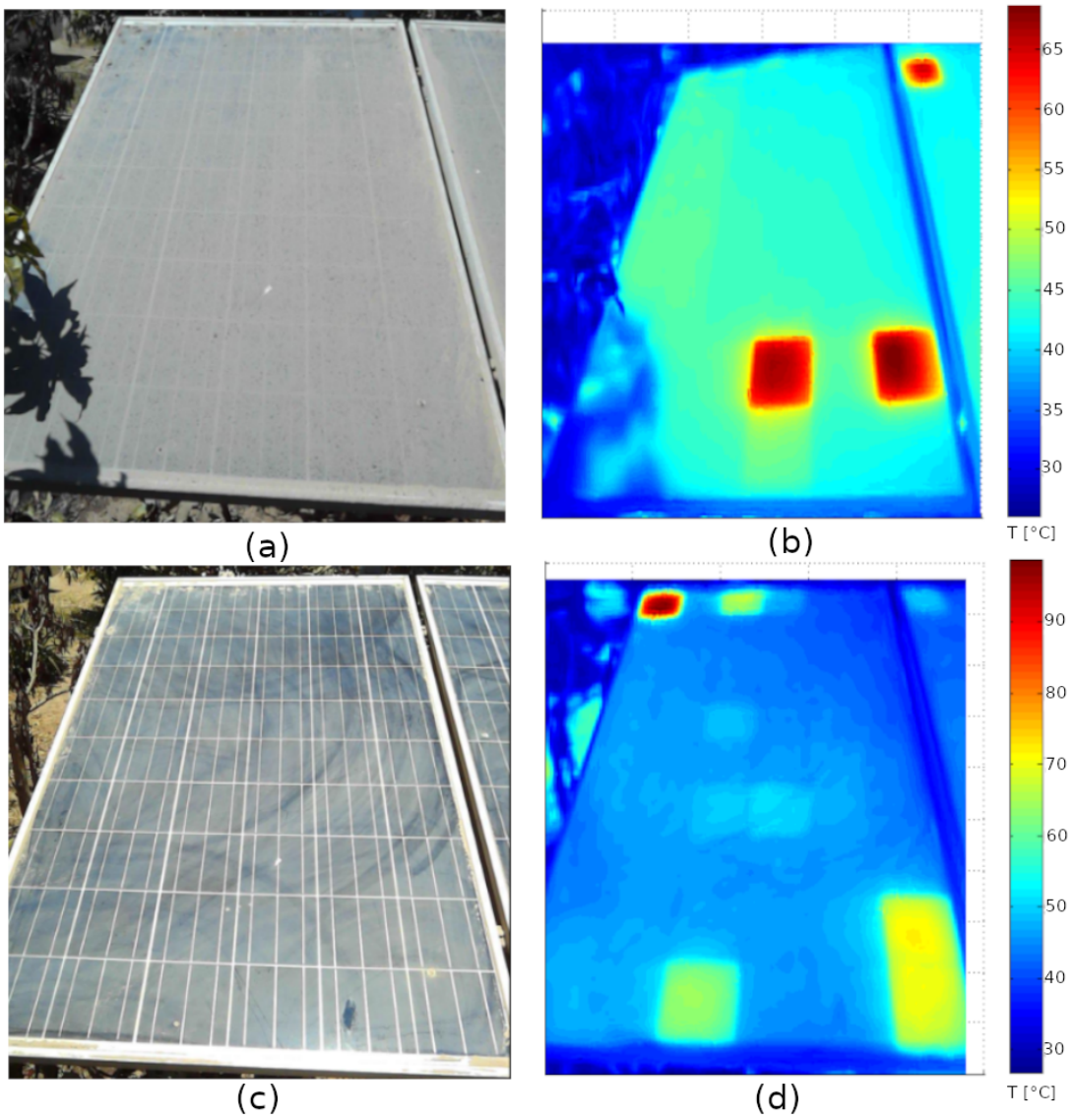

Figure 3.9: Visual and thermal images of a heavily soiled module (F90) from zone C (a), (b) before and (c), (d) after cleaning.

at 74.9°C, 14 degrees hotter than before. At bottom of the module, two other cells appear hot in the clean module at 86.7 and 99.4 °C. However, unlike the F90 module, which shows an important current mismatch, F91 shows an I-V characteristics with a smooth current but a slightly increased shunt resistance, indicative of a possible leakage current across one or more cells.

Electrical Measurements

The I-V/P-V characteristics of modules are shown in Figures 3.11 and 3.12. Dirty and clean modules are shown on the left and right graphs respectively. The electrical signatures shown by modules F91 to F95 were similar in shape, so for clarity only is shown the curve corresponding to F91 in Fig. 3.12. The detailed variations in parameters for all curves will be shown further.

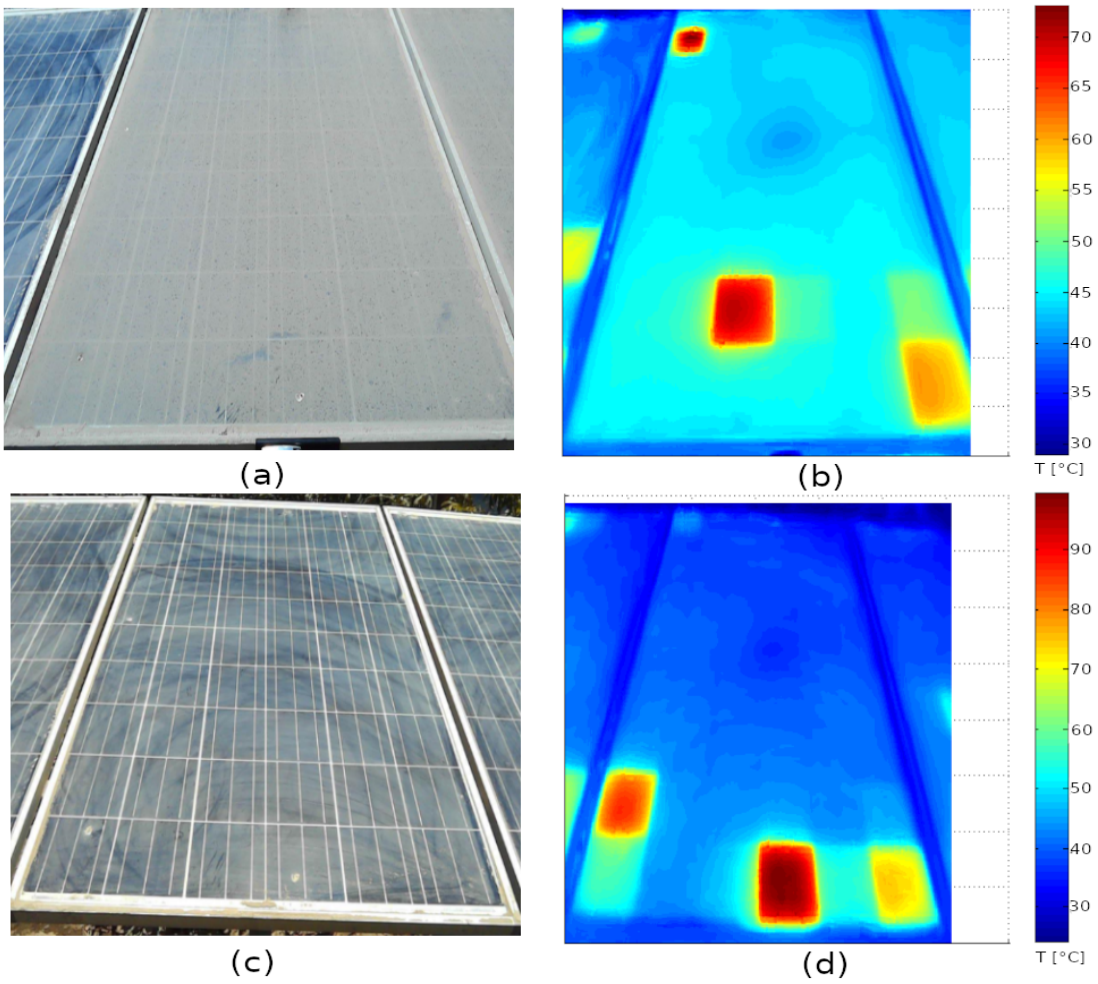

Figure 3.10: Visual and thermal images of a heavily soiled module (F91) from zone C (a), (b) before and (c), (d) after cleaning.

As shown in Figure 3.11(a) the Maximum Power Point (I_{mpp},V_{mpp}) is located at the second step of the solid line curve (measured values) and corresponds to 2.818$[A]$ - 20.892$[V]$. In contrast, the maximum power point of the nominal curve is located at 8.81$[A]$ and 37.6$[V]$. The steps shown in the curve are an indicative of severe current mismatch between the strings, with the consequent operation of the bypass diode. At P_{mpp}, set in the second step of the I-V curve, some cells are forced to operate above their I_{sc}, so hotspots can be generated under these operating conditions.

An extremely hot cell acts as a power dissipation point but, as it can be seen in solid line of Figure 3.11(b) there is activation of the bypass diode (the P_{mpp} remains at the first knee of the curve), and the maximum is set at 7.36$[A]$ - 20.86$[V]$. However, in the bypassed string there is still an important power dissipation through the hot cell.

The I-V characteristics of the soiled module, shown in Figure 3.12(a,) shows a severe decrease of I_{sc} and the P_{mpp} is located 3.07$[A]$ - 31.08$[V]$. It can be seen that this point is with the cells of minimum I_{sc}. However this does not prevent the heating of some cells to very high temperatures.

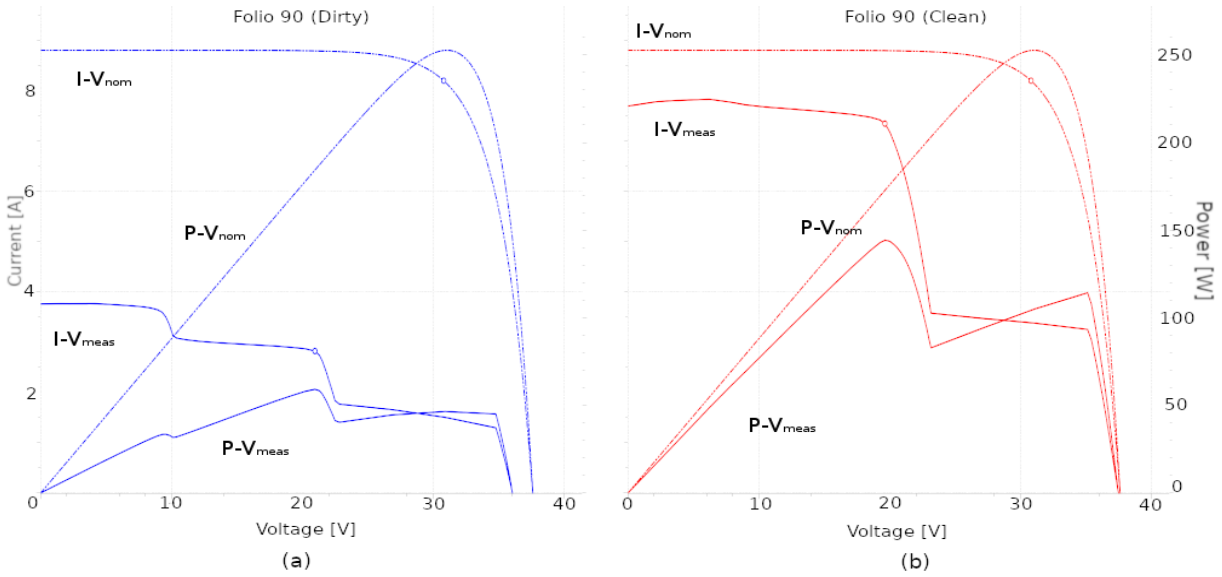

Figure 3.11: I-V and P-V characteristics of heavily soiled module (a) before and (b) after cleaning (F90).

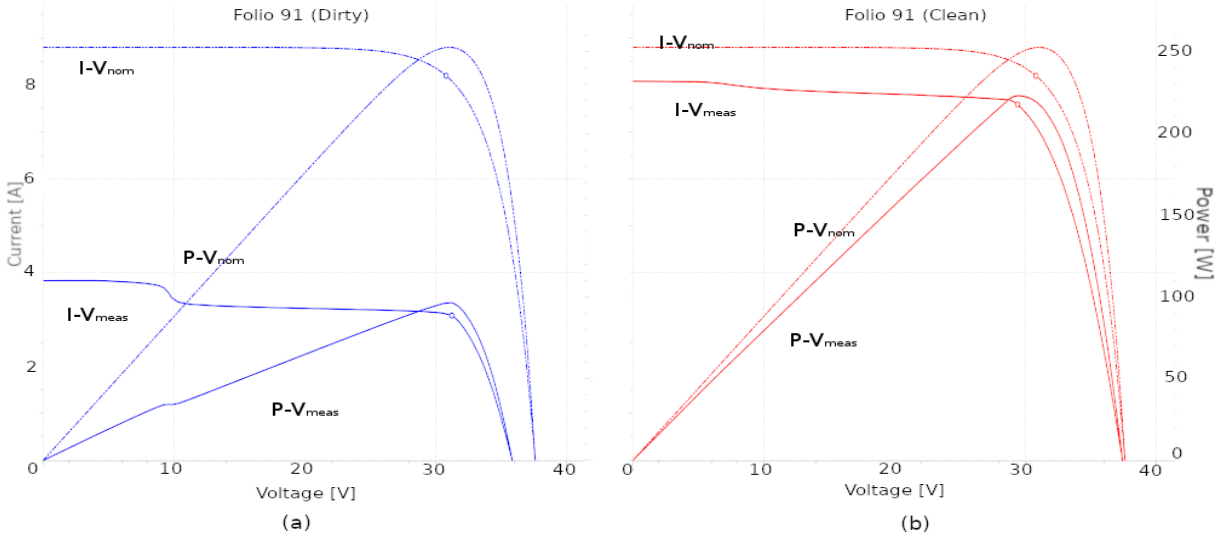

Figure 3.12: I-V and P-V characteristics of heavily soiled module (a) before and (b) after cleaning (F91).

Although there is no intuitive explanation for the sudden changes of temperature of some extremely hot cells when going from soiled to clean module, it is possible that those cells that appeared hot only in the clean modules were delivering less current than their maximum, even if this was low by other undetermined failures. The low irradiance seen by the module because of the thick layer of soiling, can be evidenced comparing the two I-V curves of Figure 3.11. The I_{mpp} of the soiled module, around $2.8[A]$ in Fig. 3.11(a), which is obviously less than that of the minimum current of the clean module Fig. 3.11(b), of $7.8[A]$. In the case of module F91 (Fig. 3.11) the bypass diode did not activate, thus forcing the damaged cells to operate with a current higher than its I_{sc}.

In Table 3.4 the electrical parameters variations and average temperature of all modules from this set are presented. For all modules, the temperature variation between the dirty/-clean module is between 1.85 and 4.6 °C respectively, with an average variation of 2.87°C. In average, the modules rise their temperatures after cleaned. The reason for this can be that, when the module is partially clean, as shown in Figure 3.6(b) from Section 3.1.2, the effect is similar to that of partial shading, thus the clean part of the cell forces the partially shaded part to produce a current higher than it is able to deliver. In this case, the module is completely covered by the soiling layer, then after cleaning it starts delivering a higher current, and thus rising its temperature. Regarding to the electrical parameters deviation, results are not very disperse in the case of V_{oc} drop (between 0.18-1.74% in clean modules and 3.83-5.43% in dirty modules). Therefore, there is a minor contribution of heavy soiling layers on the open circuit voltage drop. As discussed before, the I_{sc} drops on dirty modules can be mainly attributed to soiling, being the values very similar (between 53.18-61.6%). For clean modules, the I_{sc} varies in a more wide range due to other reasons, possibly related to the very hot cells that remain after cleaning. However, under very low irradiation conditions, drops in V_{oc} are unavoidable.

	Temperature °C			Voc		Isc		Pmpp		FF	
Module	Clean	Dirty	ΔT	Clean	Dirty	Clean	Dirty	Clean	Dirty	Clean	Dirty
90	45.44	42.44	3	1.74%	5.46%	12.82%	58.12%	39.08%	75.31%	34.45%	42.69%
91	44.25	41.68	2.57	1.32%	5.33%	8.35%	57.27%	9.80%	61.76%	3.12%	7.75%
92	43.82	41.97	1.85	1.29%	4.91%	8.54%	61.60%	10.81%	62.80%	3.80%	-0.32%
93	47	42.4	4.6	0.84%	4.81%	2.91%	53.18%	6.17%	61.10%	5.64%	14.16%
94	47.34	44.96	2.38	0.18%	3.83%	4.22%	55.17%	5.34%	60.76%	4.16%	10.03%
95	44.34	41.5	2.84	0.82%	4.05%	2.79%	56.00%	5.69%	57.23%	4.88%	17.57%

Table 3.4: Comparison of temperature and electrical parameters of heavily soiled modules before and after cleaning.

3.1.4 Lightly Soiled Modules

Visual Inspection

Lightly soiled modules were found in zones D (inner coast, 12 modules), B (city, 17 modules) and C (inner valley, 23 modules). Light soiling vary from fine layers of dust over the surfaces (detectable by a close inspection), to thicker layers deposited (both uniformly or non-uniformly) over the surface of the modules. In Figure 3.13 different soiled modules are shown according the classification by geographical zone: Fig. 3.13(a) corresponds to city modules, Fig. 3.13(b),(c) and (d) correspond to inner valley modules and (e) to inner coast modules. Lightly soiled modules located in the city show a very thin layer of dust. This can also be observed in inner coast modules. Inner valley modules show thicker layers of dust on their surfaces, similar to heavily soiled modules. However, metallization components and cell color are not totally blocked. In particular, in Fig. 3.13(b) it is shown a module from a set of 6 modules with a combination of light soiling and milky discoloration on the lower cells, which will be further analyzed.

Even though it is not possible to distinguish soiling deposition pattern for lightly soiled modules by simple visual inspection, as it was done for heavily soiled modules, for the analysis

they will be still classified by locations (B and D for city and inner coast modules). In the case of inner valley-based modules, they will be separated in C1 (lightly soiled modules combined with milky discoloration), C2 (lightly soiled modules with a thin layer of dust) and C3 (lightly soiled modules with a thicker layer of dust).

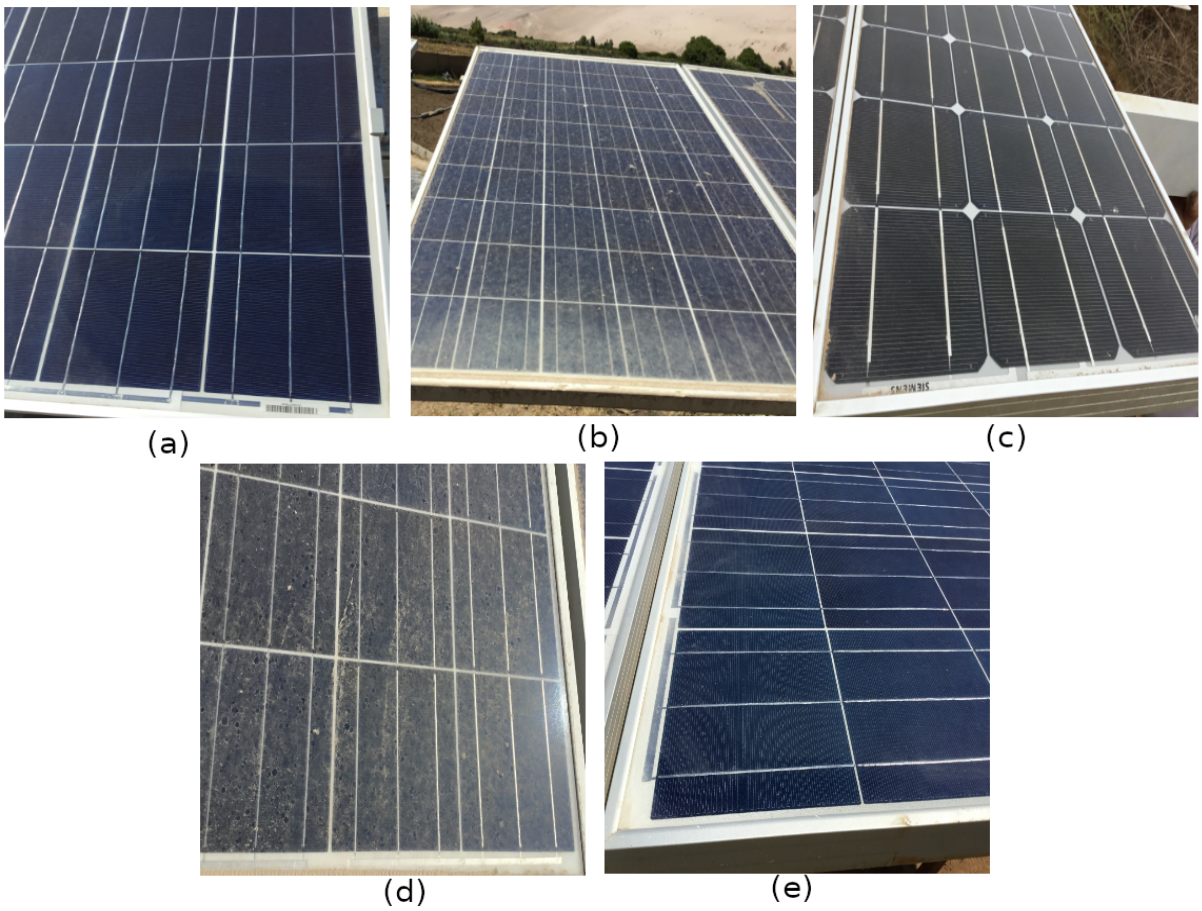

Figure 3.13: Close visual inspection of lightly soiled modules operating in (a) city zone, (b), (c), (d) inner valley, and (e) inner coast.

Infrared Thermography

The thermal patterns of modules shown in Figure 3.13, are shown in Figures 3.14 and 3.16. In the city, 16 modules of Risen and 1 from BP Solar manufacturers were measured. However, a clear correlation between light soiling layers deposited on the surfaces and thermal patterns of the modules was not found. The module shown in Figure 3.16 (a) show several hot cells distributed at the central area of the module with temperatures ranging 38-49°C. A colder zone at the bottom of the module ranging 34-36°C is shown, but as the soiling layer is very thin, it is more probable that the observed patchwork pattern is due to the short circuit conditions in which the measurements were taken. Form the total amount of modules in zone B, 1 module, in Fig. 3.15(a) show a uniform temperature distribution, and 13 modules show patterns with hotter cells distributed randomly across the module (Fig. 3.14a). Only one (1) module shows a uniform temperature profile in most part of its surface, but with few and localized strongly heated cells, as shown in Figure 3.15(b). This pattern can be most associated to localized and severe failures, as shunts. One module, shown in Fig. 3.15(c)

show a pattern with hotter cells in its bottom area, which can be associated with Potential Induced Degradation (PID).

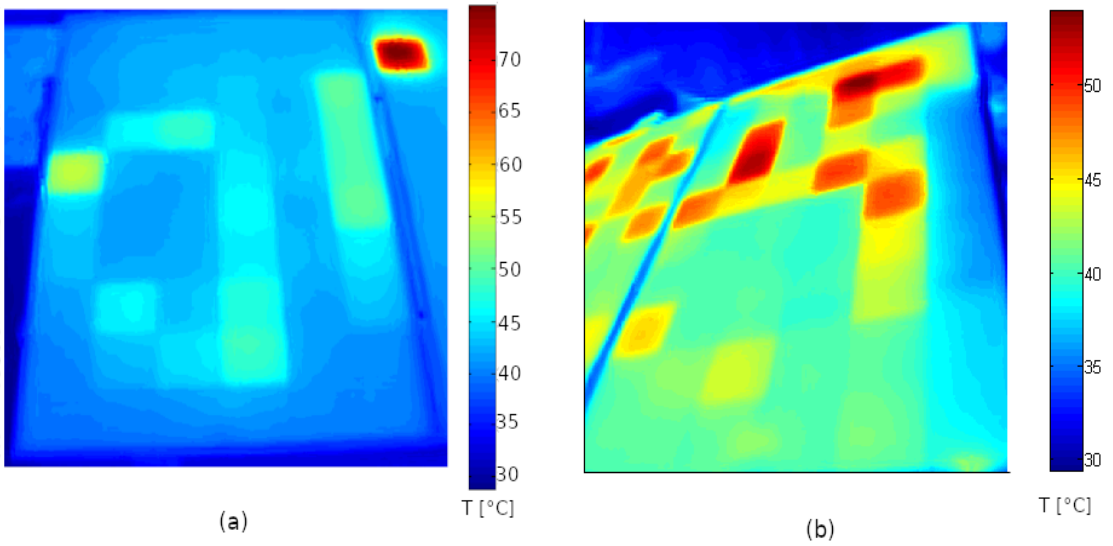

Figure 3.14: Thermal profiles of lightly soiled modules located in (a) city and (b) inner coast zones.

Regarding to the inner coast-based modules, there were also found different thermal patterns, as shown in Figure 3.14 (b). From the set of 12 modules located in D, 3 of them show hotter cells at their top area, 6 show single/few localized hot cells mainly at the bottom of the modules and 3 show hot cells distributed randomly across the module surface, similar to patterns shown in Figure 3.15.

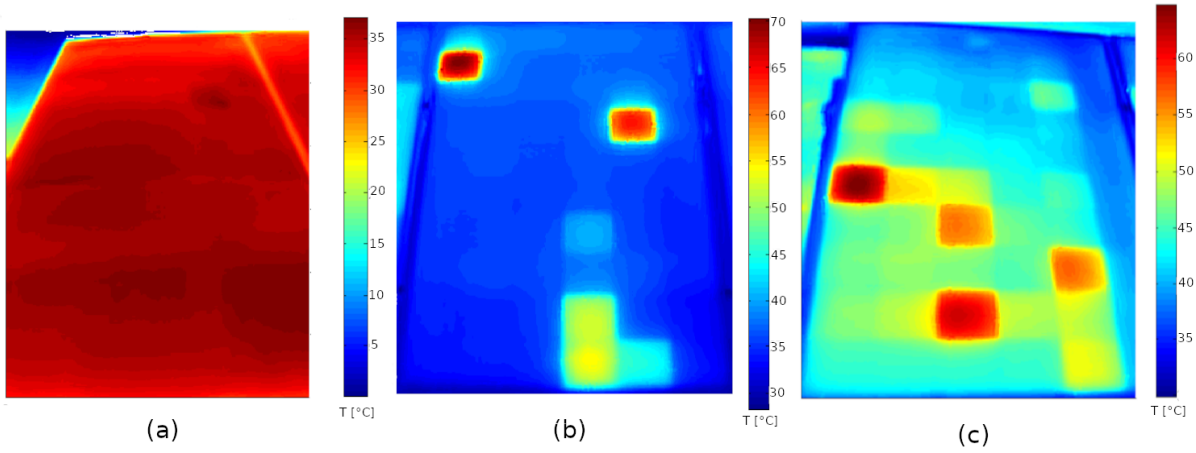

Figure 3.15: Thermal profiles of lightly soiled modules of zone B (a) uniform temperature distribution, (b) uniform temperature distribution with single/few hot cells and (c) modules with hotter cells at the bottom.

For the modules located in the inner valley zone (C), there can be found three different thermal distributions: Modules with uniform temperature distribution and few localized hot

cells at the bottom, modules with few hot cells distributed randomly across the surface, and modules with a random patchwork pattern, as shown in Figure 3.16.

Lightly soiled modules located in the city (note the difference between modules located in the coastal areas of the city, which were analyzed as strongly soiled) are located in School and University roofs. This location, on one hand, may help to keep them apart from some degree of street-level pollutants. On the other hand, it is more probable that in these buildings there exists a more sophisticated cleaning protocol than in other zones. However, in the other geographical areas where lightly soiled modules were found, varied thermal signatures can also be distinguished. Therefore, in general terms for this sample, as the light soiling layers do not cause a significant disturbance on thermal profiles, it is more likely to observe different thermal pattern associated to other failure/degradation processes.

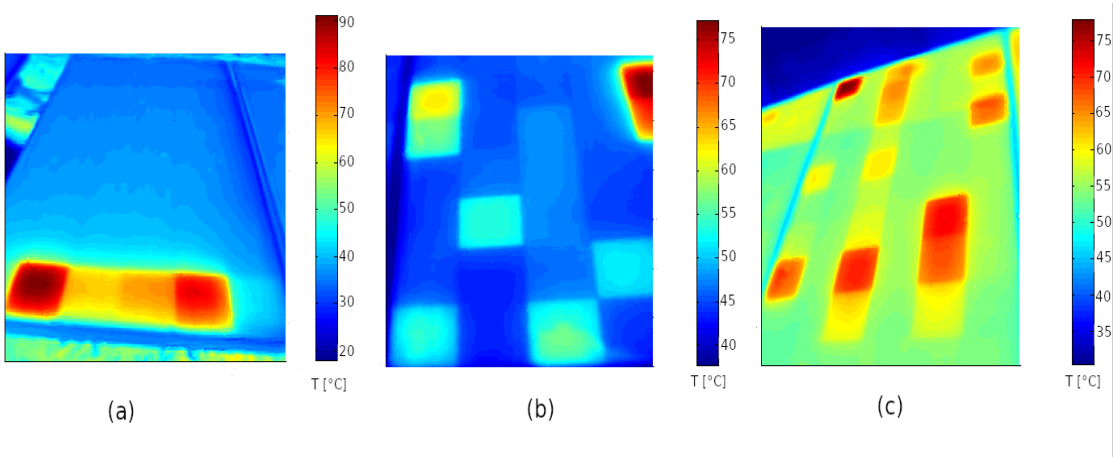

Figure 3.16: Characteristic thermal profiles found in lightly soiled modules located in inner valley zone.

Electrical Measurements

Severely heated cells and short circuit patterns cannot be associated to light soiling (since there is not a visible shading effect). Therefore, the net effect of soiling on the I - V curve is mainly a reduction of the short circuit current. In most cases, the variations on the curve are a uniform drop of current with respect to the nominal values; in some cases with a slight increase of the slope, indicative of a reduction of the shunt resistance, which can be due to the presence of hot cells. I-V and P-V characteristics measured for lightly soiled modules of zones B and D are shown in Figure 3.17. Modules located in zone C are shown in Figure 3.18. City and inner coast-based modules show a drop of I_{sc} around 5.09% and 6.52% respectively, and a V_{oc} drop of 1.76% and 3.21% respectively.

The I-V and P-V characteristics of modules located at the valley zone (C) are shown in Figure 3.18. The average variation of electrical parameters with respect to nominal values is shown in Table 3.5. It can be seen in Figure 3.18(a) that those modules affected by light soiling and milky discoloration at the bottom areas (labeled as C1 in Table 3.5) show the highest I_{sc} drop (11.99%) but a positive average variation of V_{oc}. This last feature may indicate the presence of severely reverse biased cells due to high I_{sc} mismatch inside the modules. As light soiling does not induce a significant screening effect over the surfaces,

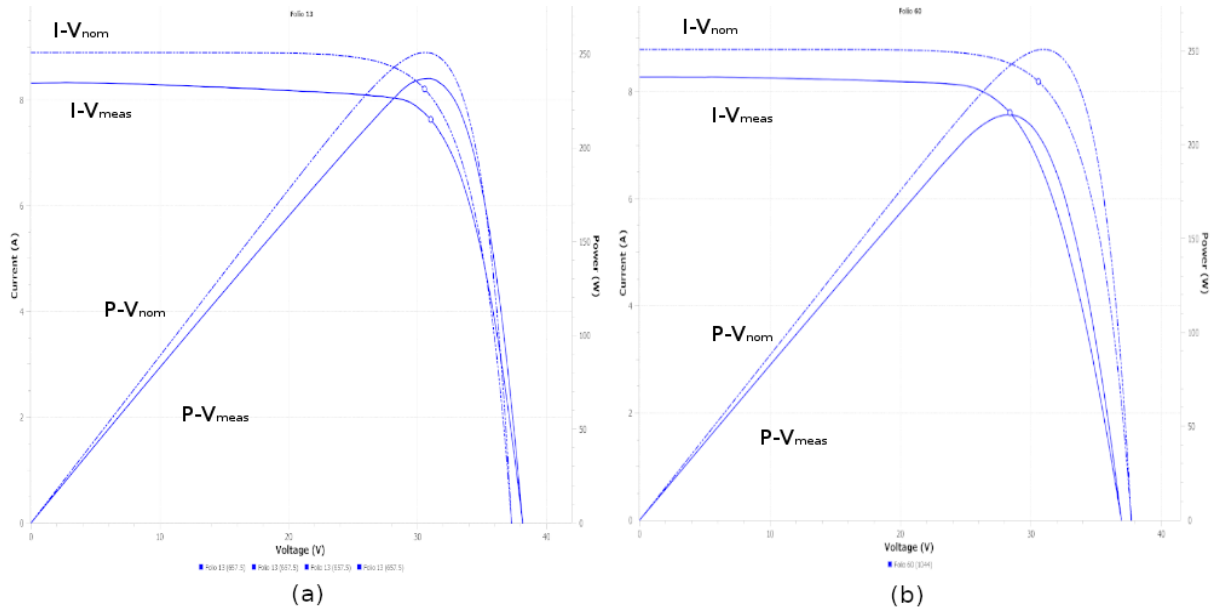

Figure 3.17: I-V and P-V characteristics of lightly soiled modules located in (a) city and (b) inner coast zones (solid line) compared with nominal values at STC (dotted line).

and localized dust concentrations or drops are not observed, this cannot be considered as a consequence of soiling. On the other hand, as shown in Figure 3.18(c) modules with thin layers of soiling in zone C show I_{sc} drops similar to those found in zones B and D (6.09%) but also the highest V_{oc} drop of all modules (20.59%). This causes in the highest P_{mpp} drop of the entire sample. Finally, modules with the thickest layer of soiling (C3 in Table 3.5) show I_{sc} drops slightly smaller than C1 modules (9.26%) but higher average V_{oc} drop, as shown in Table 3.5.

For lightly soiled modules of all geographical areas, it has been found that small amounts of soiling does not represent a major stress factor, and despite of a thin layer of contaminants, other failure/degradation modes can be independently detected and analyzed. For heavily soiled modules, thicker soiling layers, which however still allow to distinguish features as the color or metallization components, as shown in Section 3.1.2, exert a non-negligible screening effect on the surfaces. Certain temperature variations across the surface of modules are found in those affected by in-homogeneous soiling layers, are clearly attributable to soiling, as shown in Figure 3.6. However, other abnormalities, like hotspots, can still be detected and not attributable to soiling. In contrast, for those modules shown in Section 3.1.3, severe soiling layers may contribute to cover some failure/degradation processes, like hotspots, shunted cells, or delamination, visible defects, etc.

3.1.5 Milky Discoloration

Visual Inspection and IR Thermography

From the 95 modules inspected, two modules were found to have extensive milky discoloration, as shown in Figure 3.19 and 6 modules show localized milky discoloration on their bottom cells, as shown in Figure 3.20, all of them manufactured by SolarWorld and deployed

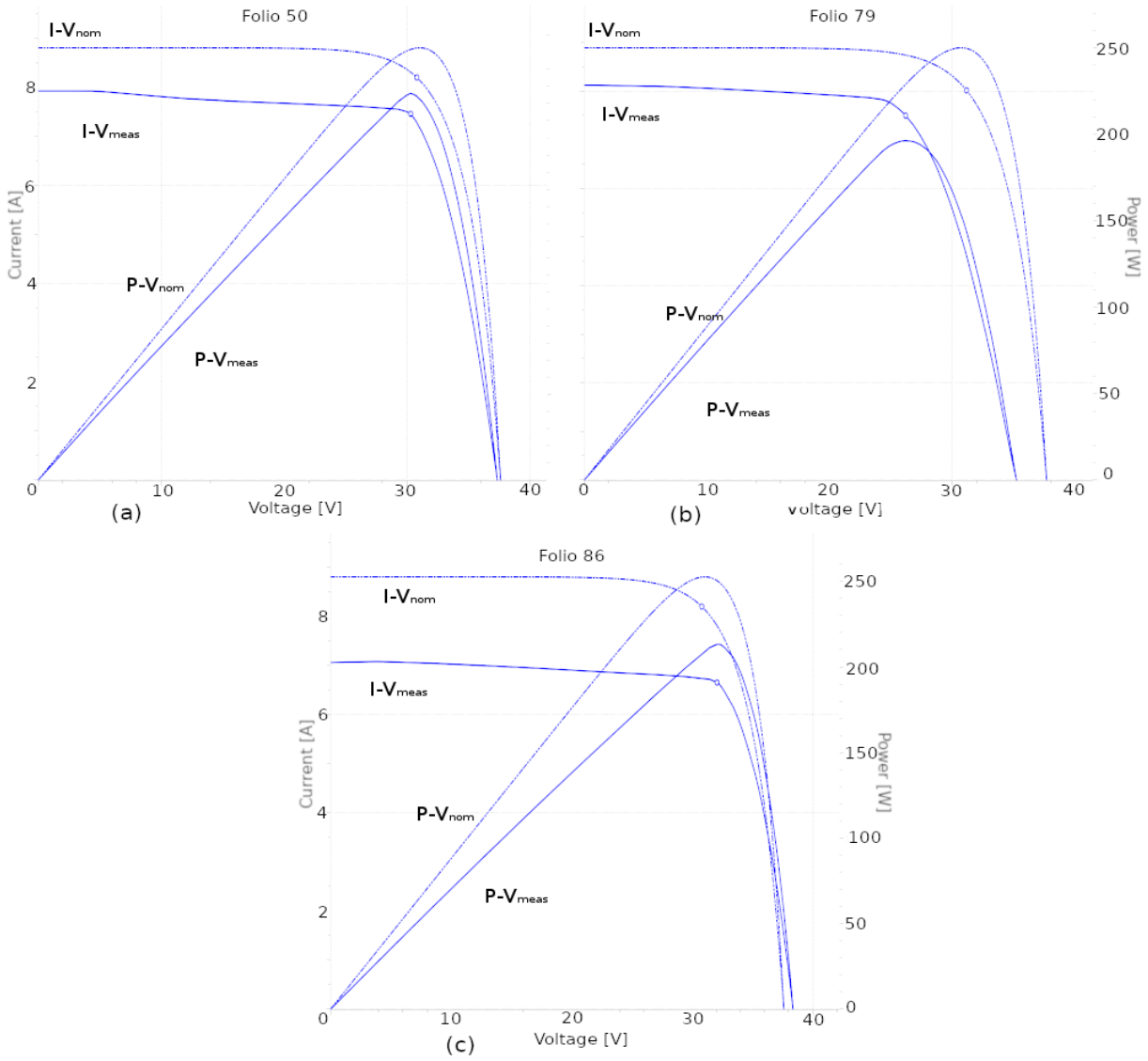

Figure 3.18: I-V characteristics of lightly soiled modules located in inner valley zone (solid line) compared with nominal values at STC (dotted line).

in years 2013 and 2012 respectively. All these modules are located in zone C (inner valley).

Figure 3.19 shows that the two modules with extensive milky discoloration also present a light soiling layer on the surface concentrated in their top area, which difficult the detection of discoloration, added to a weathered glass surface appearance. Discoloration appears as whitish areas, which are not removed by the cleaning of the surface, mostly distinguishable at the bottom of the modules. In the case of module F8, shown in Figure 3.19 (a) and (b), the temperature of cells ranges from 31.7 to 38.9 °C, with the hottest areas on the bottom of the module. However, the module also show hot zones at the top cells, due to the presence of in-homogeneous dust layers that shade the cells in this area. For the module F9, shown in Figure 3.19 (c) and (d), a similar temperature distribution is found but somewhat higher than that of module F8, ranging from 36.3 to 50.3 °C, however, only one cell reaches the highest temperature. All the other cells show temperatures below 46°C. The temperature

Zone	Soiling type	Average temperature [°C]	Voc	Isc	Pmpp
City (B)	B	41.83	-3.21%	-6.52%	-9.82%
Inner coast (D)	D	49.15	-1.76%	-5.09% -	9.71%
Inner valley (C)	C1	46.80	0.20%	-11.99%	-9.42%
	C2	42.11	-20.59%	-6.09%	-25.34%
	C3	50.17	-4.68%	-9.26%	-14.26%

Table 3.5: Average temperature and percentage variation of electrical parameters of heavily soiled modules.

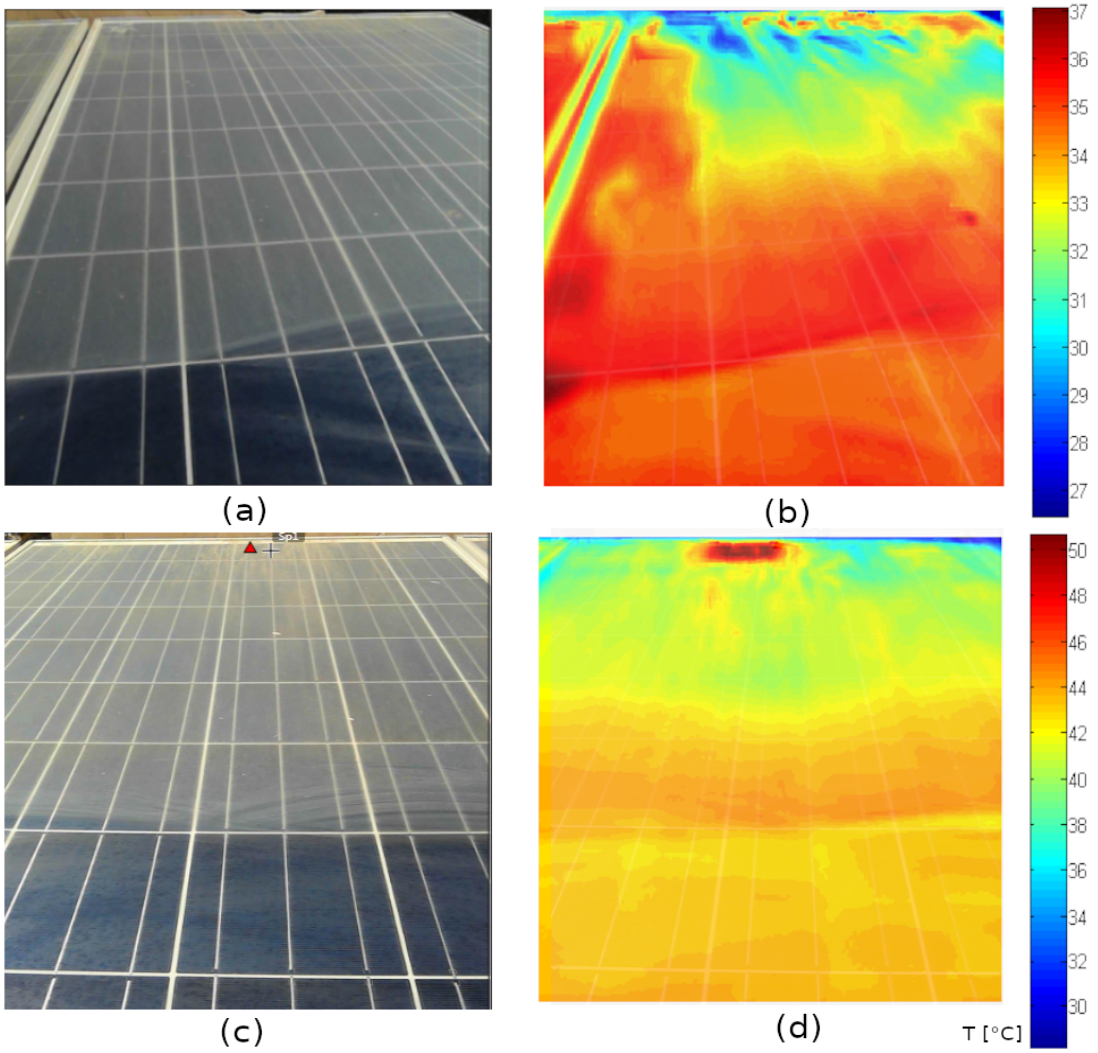

Figure 3.19: (a) (c) Visual inspection and (b) (d) thermal images of extensive milky discoloration found in two modules.

distribution appears to be in-homogeneous, however, it can be seen that the hottest cell is notably more soiled than the rest of the module. Therefore, its temperature is probably related to the shading effect of dust. Comparing the bottom cells shown in the IR images of Figure 3.19, it can be seen that slight temperature variations agree with the visual detection of milky discoloration. However, these variations are no greater than 2°C.

Regarding to modules with small (referred to the extension of affected areas of the module) and localized milky discoloration, they all present this abnormality on cells located at the lowest row of the module, and a similar thermal signature, as shown in Figure 3.20. The average temperature of these modules ranges from 38.77 to 43.35°C, with cell temperatures ranging from 30-36.9°C to 80.9-93.8 °C. Visual inspection in Figure 3.20(a) reveals that light soiling concurs with milky discoloration on the bottom cells which could slightly enhance the temperature rising. In this case, the tilt of modules can also play a role on the distribution of soiling, and the discolored areas. Milky discolored zones lead to loss of transmittance and thus a higher current mismatch affects these cells. It it also noticeable from Figure 3.20(b) that the rest of the module shows an approximately even temperature profile around 39°C, apart from a drop that shades cells partially on the top of the module, causing a rise in temperature to a maximum of 44°C.

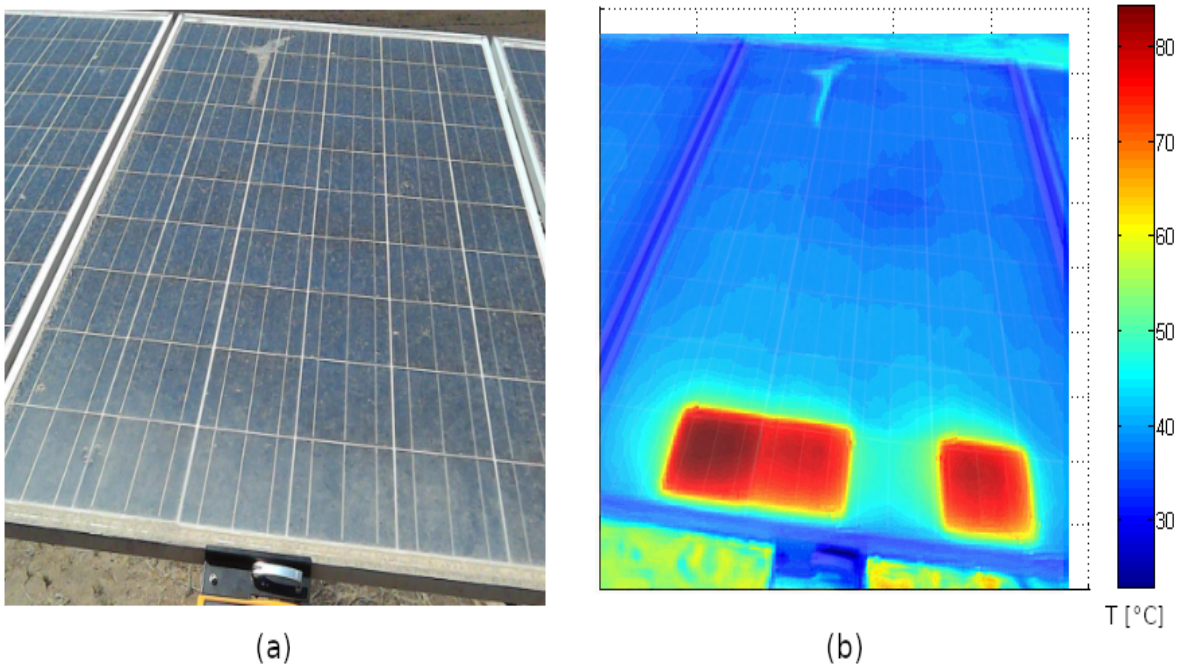

Figure 3.20: (a) Visual inspection and (b) thermal image of a module with milky discoloration localized in the bottom cells, combined with light homogeneous soiling.

Comparing the visual inspection and thermal image shown in Figure 3.20 (a) and (b) respectively, it can be seen that discolored areas can influence excessive temperature rising: the hottest cells show temperature differences over 40°C with respect to the rest of the module. Moreover, the screening effect on these areas, caused by the discoloration may help to trigger further defects as massive shunts and reverse biasing. Although temperature rising up to 100°C is not considered hazardous to the cell or the EVA encapsulant, operation of cells under these abnormal conditions may accelerate degradation and shorten the lifetime of modules.

Electrical Measurements

The I-V/P-V characteristics of extensively and localized milky discolored modules are shown in Figure 3.21(a) and (b) respectively. It can be seen in Fig. 3.21(a) that module F9 shows

steps on its I-V curve. However, the current mismatch is not enough to cause activation of the bypass diode, and also this does not affect the P-V curve, for which P_{max} is still reduced by the operation point on the I-V curve but multiple peaks of P_{max} are not detected, as it would be for hardly shaded modules. Considering the information given by the I - V curve with visual and thermal images in Figure 3.19, upper areas of the modules are significantly colder: under 30°C in Fig. 3.19(b) and 36°C in Fig. 3.19(d). This could indicate that certain regions of the module are not generating, or generating considerably less current than they should.

For localized discolored modules, labeled as F48-53, steps in the I-V curve are not observed. However a decreased shunt resistance can be detected, as shown in Figure 3.21(b). Moreover, for both modules it is observed an increase of V_{oc} above the nominal value.

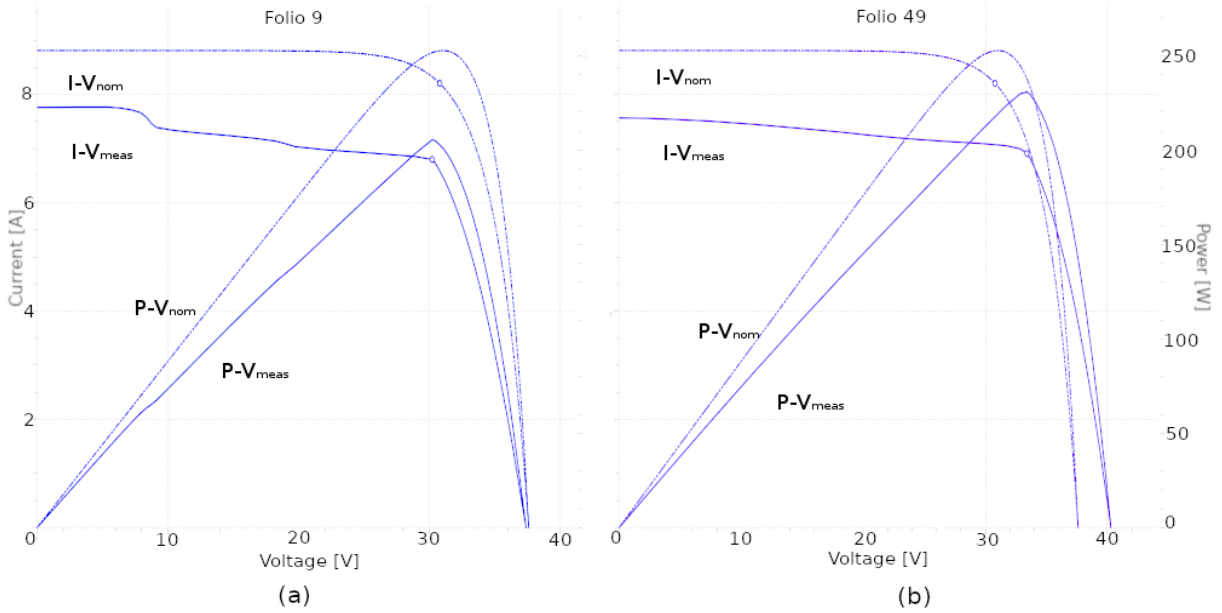

Figure 3.21: I-V/P-V characteristics of modules with milky discoloration (a) extensive, (b) localized in bottom cells.

Data related to milky discolored modules is shown in Table 3.6. The electrical parameters measurement of the six affected modules reveals that the short circuit current drop is between 7.87 and 16.15%. Considering that all of these modules also have a light soiling layer on the surface, the I_{sc} drop of both localized and extensive milky discolored modules are the highest of all lightly soiled modules (compare Tables 3.5 and 3.6). Thus, it is feasible that this particular defect plays a role on the degradation of short circuit current, possibly by the loss of light transmittance. The open circuit voltage drop is between 0.42 and 2.50%, but two modules show a positive variation of V_{oc}. This may indicate the presence reverse biased cells, also evidenced by the extremely high operating temperatures shown by the bottom cells of modules F48-53. This can be caused by severe shunts due the circulation of reverse currents across the affected cells. It must be noted that those modules, which show the hottest cells (F50, F52 and F53) are not the ones that show the highest drops in I_{sc}, V_{oc}; but the modules with highest drop of I_{sc} are the ones with positive V_{oc} variation. Regarding to operating temperature of the modules, although the extremely high temperature of the hottest cells of this set of modules, the rest of the modules remain at an approximately homogeneous

temperature, so average temperature of the modules is not necessarily the highest.

General Data			Electrical parameters deviation [%]				Temperature	
Milky Discoloration	Module	Year	V_{oc}	I_{sc}	P_{mpp}	FF	Average T[°C]	Cells temp. range [°C]
Extensive	8	2013	-2.50%	-10.56%	-14.72%	- 5.40%	31.60	31.7-38.9
	9	2013	-0.42%	-12.22%	-15.91%	-7.01%	41.70	36.3-50.3
Small/localized	48	2012	1.95%	-16.65%	-10.51%	2.42%	38.77	31.7-84.4
	49	2012	5.36%	-14.51%	-6.96%	-0.53%	39.77	34-84.1
	50	2012	-1.58%	-10.17%	-9.07%	-0.35%	43.35	32-92
	51	2012	-1.83%	-12.07%	-11.01%	-0.83%	41.68	30-80.9
	52	2012	-1.15%	-10.67%	-9.44%	-0.31%	42.44	32-93.6
	53	2012	-1.53%	-7.87%	-9.54%	-2.58%	42.87	36.9-93.8

Table 3.6: Average variation of electrical parameters and temperature data of milky discolored modules.

3.1.6 Materials Analysis of Failures Related to Front Cover Glass

As shown in previous sections, the main impact of soiling on solar modules, in all ranges of severity and deposition patterns, is related to a reduction of the short circuit current. It is highly probable that these reductions are due to the blocking role of the dust particles over the glass surface, which can prevent the incoming sunlight to pass through the glass layer to reach the semiconductor. Although, according to the results found in [3], soiling layers were not very easy to remove, and in some cases it was strongly attached to the surface. This can indicate that deposition (and permanence) of the particles on the glass is not only mediated by gravity, but suggest the existence of chemical or physical adsorption processes over the surface, which could permanently alter the electronic or optical properties of glass. Moreover, weathered modules were found in a location belonging to the valley zone (C), which evidences the interaction (mediated by water deposition in this case) between environmental particles and the glass surface.

Apart from information recorded by visual inspection about the deposition of soiling on modules, to perform material analysis further information is required, in order to understand the behaviour of the material (glass in this case) and interactions with the environment. For example, the composition of dust particles involved in this process. However, in [101] it was determined that for modules operating in different locations of the Atacama Desert, the particles size deposition tend to present in general diameters smaller than 63 μm with spherical geometry. The elementary composition of particles is most frequently O (44%), Si (28%) and to a lesser extent Na, Mg, Al (5-10%) and Fe, S, Cl, K, Ca (<5%). Particularly in Arica, the mineral compounds found in the modules are mainly Quartz (SiO_2), Anorthite ($AaAlSi_3O_8$), Cristobalite (SiO_2), Halite (NaCl), Muskovite ($KAl_2(AlSi_3O_{10}(OH)_2)$) and Orthoclase ($KAlSi_3O_8$). Performing a quick inspection of these minerals, the electronic band-structures of (crystalline) quartz compounds are well known, showing energy gaps of about 5-6 eV [111] [112], while for sodium chloride it has been calculated as 8.4 eV [113]. The energy gap of Muskovite has been estimated around 5 eV [114]. Since all the compounds found present wide energy gaps, so in a very rough manner it is not direct to infer that these minerals could be interfering with the light absorption, but further analysis is recommended to investigate the nature of the interactions. However, this can vary in the case of considering interactions between the isolated compounds and the surface of modules, for which specific

determinations of features associated to these interactions are recommended.

The electronic and optical properties of amorphous silicon dioxide are well known for decades [115], and the wide transmittance spectrum of glasses makes them suitable to perform protective purposes on solar modules. Electronic band-structure of glass shows energy *band gaps* of about 10 eV, which ensures that incident photons with energies in the range of the optical spectrum do not interact with it. However, if deposited soiling particles interact with the glass surface, they could induce additional intermediate electronic states in the energy gap of glass, particularly in the range of silicon (around 1 eV). This may induce absorption of useful energy on the glass surface, preventing these photons to reach the semiconductor surface further than just blocking the incoming light. Moreover, understanding of the bond properties (bond strength, arrangement of atoms) linked to adsorption of molecules or compounds over the glass surface could help to improve cleaning methods by development of more efficient techniques or additional coatings that could prevent a strong deposition of impurities.

Since weathered modules were found in one location (zone C), some environmental compounds could be reacting with the glass cover surface in the presence of water. Glass absorption spectrum (which vary slightly from one type of glass to another) shows absorption in the UV range [116] and transmittance up to 90% of light in the visible range. Research on the response of soda lime glass under damp heat tests show that transmission in the UV range increases, letting a more fraction of radiation pass through which could damage the subsequent layers under long term exposure [51]. Additionally, in [51] it was found that network modifiers of soda lime glass (Na, Ca, K) participate on aging processes under damp heat and enhance corrosion [51].

Finally, concerning to the milky discoloration of the glass surface found in 8 modules there has not been found specific information in the literature about this issue, so very few can be said due to the lack of concrete information. However, it results evident by simple visual inspection that milky discoloration interferes with the solar light transmission across the glass, which is enhanced by the fact that most of the cells covered by the discolored areas show very high temperatures, and also some of the I-V curves show signatures characteristic of reverse biased cells. This could be due to a combination of poor transmittance of light of the glass and poor shunt resistance in the affected cells, because not all of these cells were found to be extremely hot (as it would be expected if the heating phenomenon was attributed only to the loss of transmittance). In this line, to validate or reject the hypothesis raised above, it would be necessary to perform additional tests.

3.2 EVA Encapsulant

3.2.1 Delamination

Visual Inspection

Delamination of EVA was found in 4 modules, three of them manufactured by JA Solar labeled as F35, F36 and F37,deployed in 2015 and located in zone B (location 7), and one by Siemens (F83) deployed in 2005, located in zone C (location 15). The electrical

parameters of JA Solar modules were taken under bad irradiance conditions (G<600) so they will not be analyzed due to the lack of reliability of collected data. For module F83, the I-V characteristics shows the activation of two bypass diodes (one third of the total open circuit voltage is measured) so this measurement was not useful to investigate delamination.

For modules of zone B, extensive delamination was found by visual inspection, affecting wide areas of the modules. Module F35, as shown in Figure 3.22 shows delamination mainly across the cells between two busbars, Fig. 3.22(a), and localized around the busbars, Fig. 3.22(b).

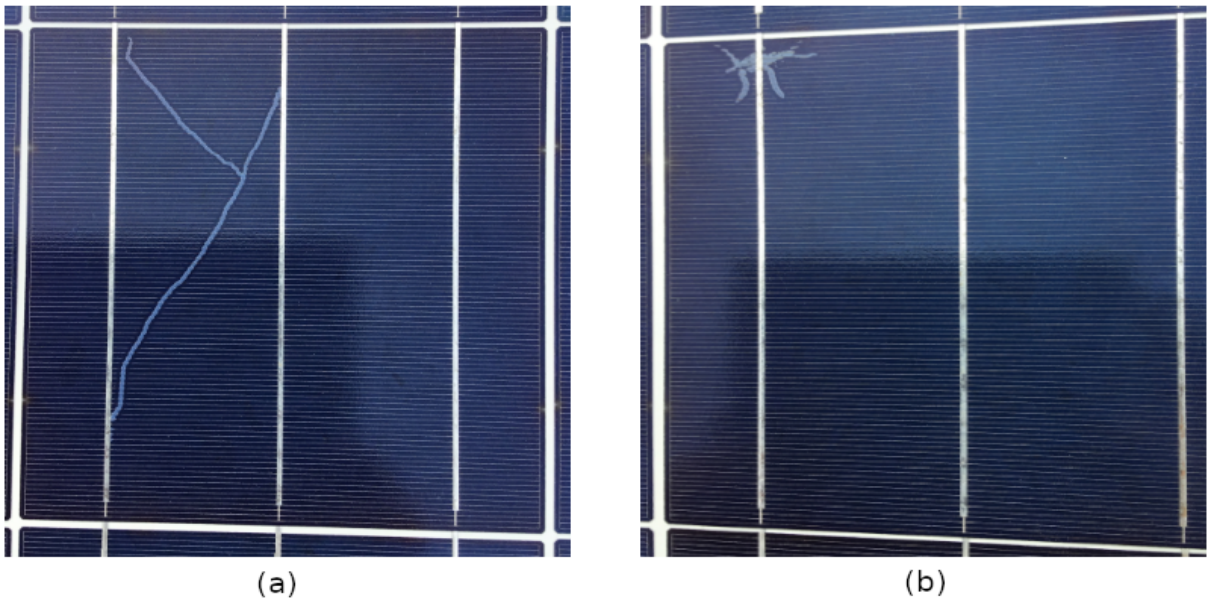

Figure 3.22: Visual inspection of module F35 showing localized delamination (a) over cells and gridlines and (b) around busbar.

Module F37, as shown in Figure 3.23 shows extensive delamination both across the surface of the cells or localized besides the busbars, but much more severe than modules F35.

Modules F36 and F83 are shown in Figure 3.24. F36, the remaining module of the set located in zone B shows small and localized delamination areas in the gridlines and besides a busbar only in three cells, being the one shown in Figure 3.24(a) the most delaminated of the entire module. For the Siemens module F83, visual inspection shows delamination localized besides busbars but extended for most of the cells of the module. F83 belongs to a set of 4 modules of the southern geographical location (15) of zone C, as shown in Figure 3.1, but none of the other modules from this set show this type of failure.

It must be noted that the three JA Solar modules with delamination were detected after just three years of outdoor operation. It has been reported that this failure normally appears later during solar modules lifetime [102]. In the Siemens module, shown in Figure 3.24, the very small and localized delaminated areas are found after 13 years of operation. Since delaminated modules represent just 4% of the total sample, very few conclusions can be reached with available information. However, it is recommended for further field campaigns to pay special attention on manufacturer and deployment date of modules. Geographical

Figure 3.23: Visual inspection of a module with extensive delamination (a) over cells and (b) around busbars.

location of the modules may also be relevant because delamination can be related to humidity and the presence of pollutants. Therefore, in modules located inside the city more factors influencing delamination can be found than those outside the city.

Infrared Thermography

Thermal images of delaminated modules are shown in Figure 3.25. Comparison between delaminated cells detected by visual inspection and thermal images do not show a relationship between observations and thermal signatures. In fact, hotter cells do not necessarily correspond to delaminated cells, or delamination paths. For module F35 (a) it is observed a thermal pattern of several hot cells distributed across the entire module, with temperatures ranging 30-36°C. Module F36 shows two hot cells in the bottom of the module up to 45 °C, another cell near 40 °C and a cell in the upper part of the module around 38°C. The rest of the module shows an even temperature profile around 31°C. Module F37 shows hot cells at the bottom and top of the module ranging from 35 to 37.8°C, and F83 shows a hot cell up to 47°C in the bottom part of the module. Moreover, as found in visual inspection, thermography does not reveal any pattern common to all delaminated cells, so temperature variations due to delamination were not detected in this campaign. This can be due to early-stage delamination, or a negligible effect in transmittance caused by the observed delamination.

Figure 3.24: Visual inspection of delaminated cells of two modules around gridlines (a) and busbars (b).

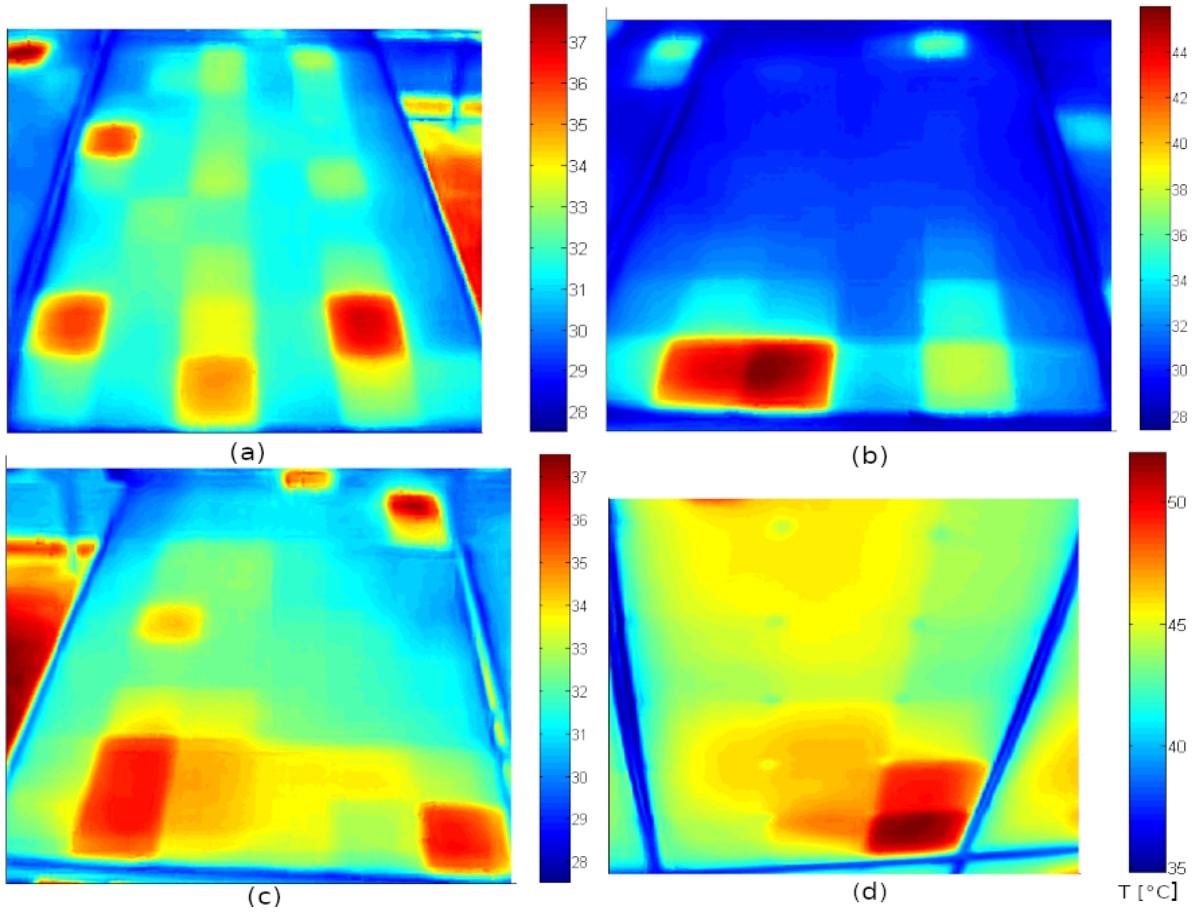

Figure 3.25: Thermal images of delaminated modules.

3.2.2 Materials Analysis of Failures Related to EVA Encapsulant

Delamination of EVA encapsulant can be caused both by environmental triggers (prolonged exposure to UV radiation at high temperatures or humidity) or defective manufacturing processes (such as poor adhesive bonds in the stack during lamination) [52]. Chemically, delamination can be induced by interaction between UV radiation and the polymer, which can cause scission reactions in the chain and thus a loss of mechanical properties. EVA is the most often used encapsulant in solar cells because it is practically inexpensive, but it still lacks of ideal mechanical and thermal properties [59], apart from the well known production of acetic acid under exposure to UV radiation and/or moisture [117].

The additive that promotes adhesion between EVA and glass/backsheet (normally silanes) which enhances the formation of Si - O bonds between the interfaces have been found to be susceptible to moisture ingress. This promotes bond decomposition and a reduction of the physical adsorption forces across the interface, processes that are accelerated by high temperatures. Additionally, due to the high diffusivity of EVA, it is difficult to prevent moisture ingress, with the subsequent possibility of condensation and corrosion, during the 20-30 years of modules lifetime [118].

Regarding to modules inspected in Arica, from the four modules affected by delamination, three of them belong to the same manufacturer (JA Solar) and the deployment data indicate that these modules are operating since 2015 (approximately three years when the campaign was performed in January 2018), and one of the modules manufactured by Siemens was deployed in 2005. JA Solar modules seem to be affected with a much more extensive delamination that Siemens module, which in turn happened to be the only one delaminated from its set, considering manufacturer and location. For this reasons, it is possible that extensive delamination is related to defective manufacturing issues than environment itself. However, extensive delaminated modules were found in zone B, which is near the coast. Therefore, humidity (although low due to the desert environment) could be enhancing the loss of adhesion.

3.3 Solar Cells

3.3.1 Partial Shading

In rural/residential solar photovoltaic power plants, it is very common to find objects that project shadows on the modules surface. Due to the multiple use of the land there can be found buildings, trees, water pumps or power lines nearby the PV facilities. Partial shading of one or more cells in a module, or one or more modules of a series array can be detrimental to the final power output of the PV plant and cause the risk of excessive heating of the affected components, which may lead to safety issues. From the analyzed sample of 95 modules there were found 2 modules partially shaded by trees or plants, 5 modules with cells shaded by thick bird drops/mud that caused non-negligible temperature differences and 2 modules with partially shaded cells due to localized dust deposition. Examples of these shading types are shown in Figures 3.26 and 3.29.

Visual Inspection

Localized dust deposition was observed in modules belonging to zone B. Note that, although measurements were performed to modules which show cells partially covered with dust, this is not necessarily a consequence of dust deposition itself, but it also seems to be related to non-uniform cleaning of the modules. Anyway, the in-homogeneous distribution of soiling over the surface of cells shows disturbances in their thermal profiles. Bird drops and mud drops (1 case each) were found in zones A and B (coast/city), but not within the inner zones, probably due to the major presence of birds and moisture on the coast and city zones. Extended shading caused by objects, in this case trees, was found in zone C, in two modules, as shown in Figures 3.9(a) and 3.29(a). This is because, in the city the modules are located at roofs, and the absence of very high buildings in Arica prevents the projection of shadows over the modules. Meanwhile, in the inner zones the modules are normally located at the ground level. In this places, the terrain is normally shared with facilities for agriculture, crops and tree plantations. Also, in one module located in zone C was found a shadow projected by an overhead power line, but an appreciable change in temperature on the surface of the affected module was not observed. This is possibly because of the presence of a heavy soiling layer, which, as discussed before, contributes to lower the overall current delivered by the modules, so it was not considered for analysis.

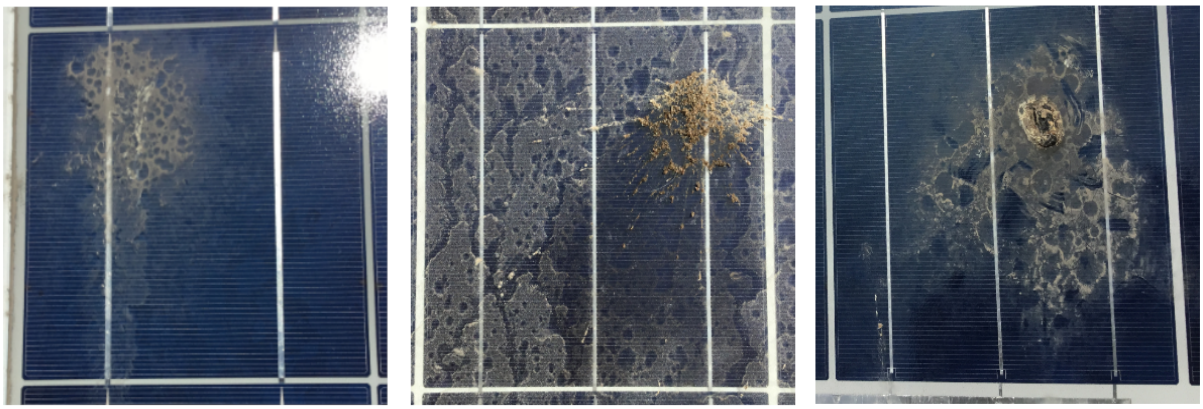

Figure 3.26: Visual inspection of cells with (a) localized dust deposition, (b) mud drop and (c) bird drop.

Infrared Thermography

Thermal profiles of cells affected by localized dust deposition and drops are shown in Figure 3.27, which correspond to: (a) module F5 located in zone B7, (b) module F30 located in A3 and (c) module F39 located in A2. Module F5 shows two cells partially covered by dust, but the thermal profile of cell shown in Figure 3.26 was not coincident with this failure but more with a shunt, due to the pronounced temperature difference with respect to the rest of the module ($\Delta T = 40.6$°C). Also, the location of the hottest point inside the cell, which is inconsistent with the drop. For the other cell, which thermal profile is shown in Figure 3.27(a) the temperature distribution partially coincides with the drop, in the upper central part of the cell with $\Delta T = 26.8$ °C, but the hottest region of the cell, localized in the left corner is more attributable to an edge shunt, also with a very high $\Delta T = 30.7$°C with respect

to the rest of the module. Thermal profile of the dropped cell of module F30, shown in Fig3.27(b) shows a hot zone in the upper right corner of the cell, which coincides with the mud drop shown in Fig3.26(b) with a temperature difference of 6.7 °C with respect to the rest of the module and 3.3 °C with respect to the average temperature of the affected cell. The drop found in module F39, in Figure 3.27(c) shows a temperature difference of 6.8 °C with respect to the rest of the module and 4.9 °C to the average temperature of the cell. In this module and the entire set of modules located in A2 (the nearest zone to the seashore) were found several drops combined with dust deposition (as shown in Fig3.29) and all of these showed temperature differences nor greater than 7 °C with respect to their average operating temperatures.

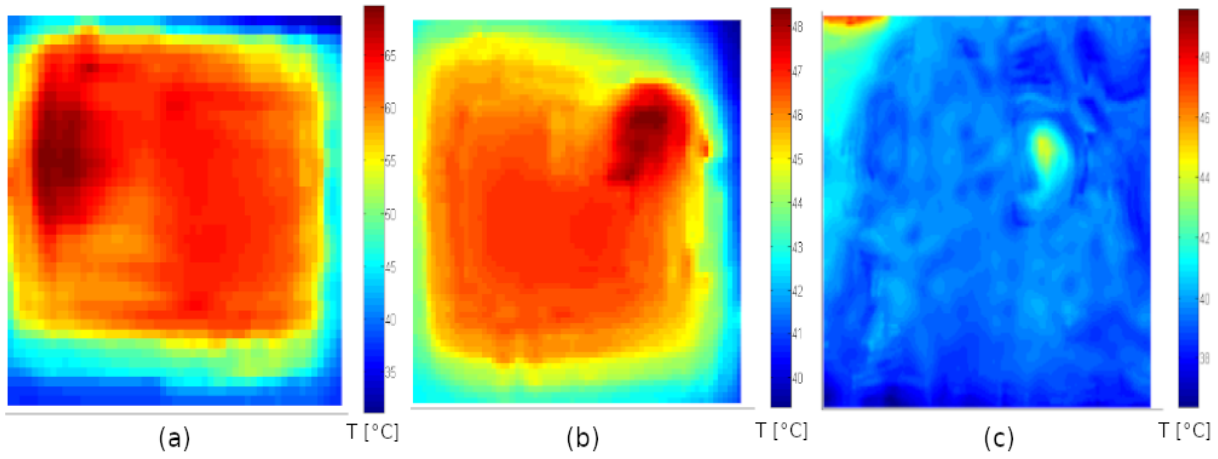

Figure 3.27: Close up of thermal images of cells with (a) localized dust deposition, (b) mud drop and (c) bird drop.

The thermal profile of a module affected by thick bird drops in several cells are shown in Figure 3.28. It can be seen that the drops (localized in the top cells) do not cause extreme temperature differences. The thermal pattern of the hot cell observed in this module does not match with the drop distribution, as the cell surrounding colder region with temperatures around 48 °C does (it is slightly hotter than non-dropped regions). Therefore, in this case the severely hot regions in the cell are more attributable to a shunt, as evidenced also by the I-V/P-V characteristics in 3.28(b) with an increased shunt resistance.

Regarding to modules with extended shading caused by trees, as shown in Figure 3.29(a), which correspond to module F72 located in zone C9, several cells were affected. This reduces severely the power output, and, as discussed in section 3.1.3 it can cause the activation of bypass diode to avoid excessive heating of cells.

In the case of module F72 a light layer of soiling is observed, which, as discussed in section 3.1.4 can cause a homogeneous drop in I_{sc} depending on the severity of soiling deposition. The thermal profile of Figure 3.30(a) shows an important temperature difference in shaded cells, ranging from 35°C to 52 °C because the complete current is forced in the unshaded zones of the affected cells causing heating. This effect is similar to that found in fractured cells with electrically isolated regions (that do not contribute to generation). This can be checked by looking at the I-V/P-V characteristics (b) which shows steps that evidence the I_{sc} mismatch because of the shadow.

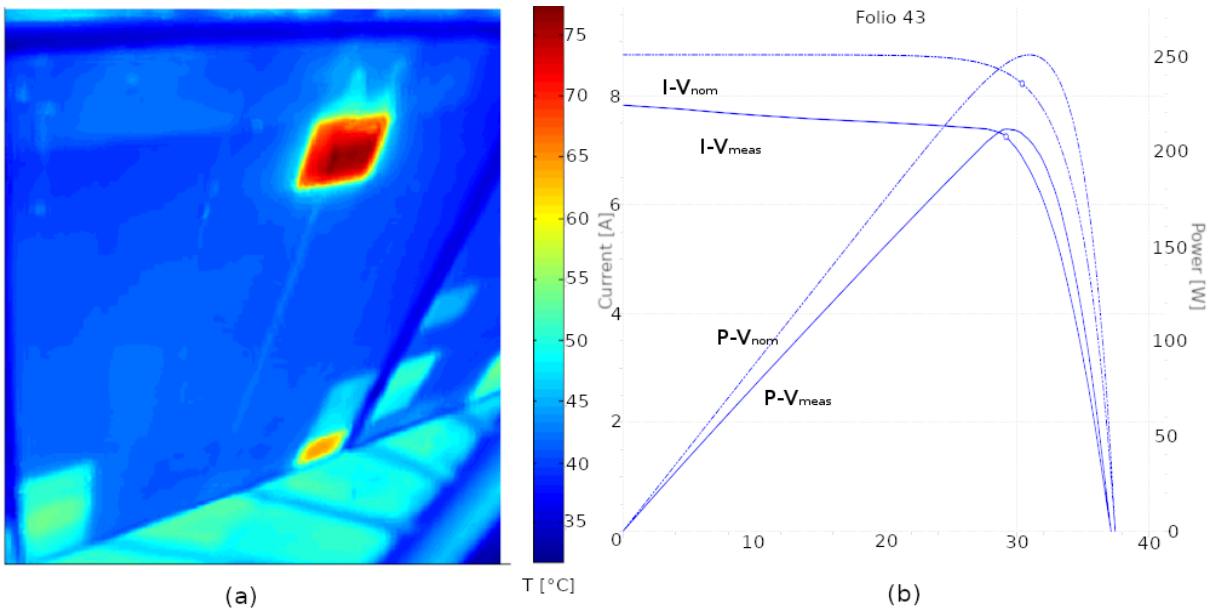

Figure 3.28: (a) Thermal image and (b) I-V/P-V characteristics of a module with partial shading caused by a thick bird drop.

Figure 3.29: Visual inspection of modules with partial shading caused by (a) a plant and (b) a thick bird drop combined with dust deposition.

A summary of temperature variations for the inspected modules affected by partial shading is shown in Table 3.7. They are classified by the root cause of partial shading (dust, drop, object), and the zone where they operate. Only for ordering purposes, the affected module tag (Fi) is also included. Additionally, the location of the drop within the module is given, because, as it can be seen for modules affected by drops the rise in temperature for shaded

busbars is slightly less than that of semiconductor shaded areas, but considering also the presence of other failures. For example, modules F5 and 43, for which extreme temperature rising dominates the thermal profiles of affected cells, causing temperature differences over 30 °C. For modules shaded by trees the temperature differences in affected cells with respect to the module average temperature (dT_{mod}) is varied, because the average temperature of the rest of the module is normally higher than that of shaded cells.

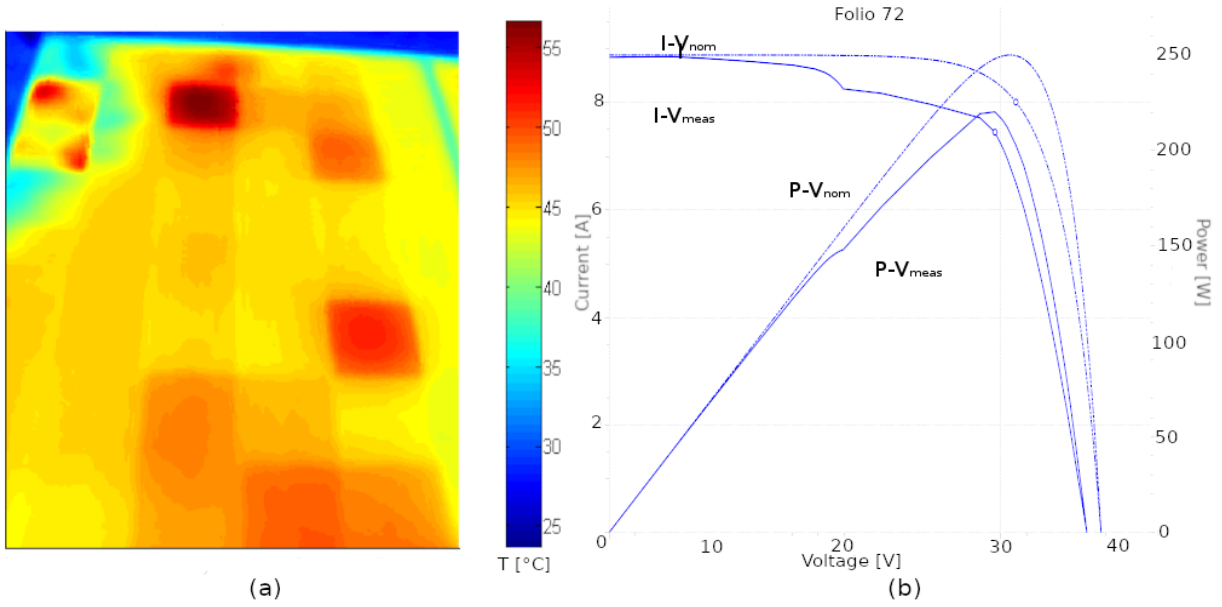

Figure 3.30: (a) Thermal image and (b) I-V/P-V characteristics of partially shaded module by a tree.

Electrical Measurements

The variation of electrical parameters with respect to nominal values and degradation rates are shown in Table 3.8. As it can be seen, the decrease in V_{oc} for all modules is no higher than 7.55%. In the case of I_{sc}, it is varied because of the strong dependence of this parameter on the amount of soiling. Again, it is evidenced that for modules lightly soiled (F5 and F72) the drop of Short Circuit Current is much smaller than for heavily soiled modules (all the rest of partially shaded modules). Additionally, for module F90, which was also affected by a thick heavy soiling layer this reduction is very large (58.12%). Considering that, in average the reduction of I_{sc} of the set of heavily soiled modules F90-95 (see Section 3.1.3) was calculated around 56%, and no other modules of this set showed partial shading, the contribution of shading to I_{sc} reduction in % should not be very large. Although, this is not possible to calculate this exactly with the available data. A simple way to investigate the effect of the tree and soiling separately in I_{sc} could be to perform the measurement in three stages: with the module, 1. partially shaded and heavily soiled, 2. by removing the tree but not the soiling layer and 3. after cleaning the module. This could also give an idea of the behaviour of all other parameters in a simple way, and it can be extended to the remaining types of shading (dust, drops).

In summary, it can be concluded from this section that localized drops deposited in individual cells act as a small blocking object, which difficult the generation of charge carriers in

Partial Shading	Module	Zone	Location	Type	dT_{mod}(°C)	dT_{cell} (°C)
Dust	F5	B7	Busbar	Dust	46.6	17.6
			Semiconductor	Dust	30.7	13.7
Drop	F30	A3	Busbar	Mud	6.7	3.3
	F39	A2	Semiconductor	Bird	6.8	4.9
	F40	A2	Busbar	Bird	6.2	4.2
	F41	B4	Semiconductor	Bird	10.9	4.1
	F43	B4	Semiconductor	Bird	40	14.3
	F42-44-45-46	B4	-	Bird	<3	<3
Object	F72	C9 (Multiple cells affected)	-	Tree	-15.3	5.8
			-		0.1	8.6
			-		-4.2	6.9
			-		-10.3	4.6
			-		-9.2	1.2
			-	Tree	-7.2	5.2
			-		-8.8	2.7
	F90 (Dirty)	C11 (Multiple cells affected)	-	Tree	1.2	6.1
			-		-2.1	2.4
			-		-3.1	2.8
			-	Tree	1.9	3.9
			-		0.3	4

Table 3.7: Temperature variations of partially shaded cells with respect to average module operating temperature and average cell temperature.

		Deviation				Degradation			
Type of shading	Module	Voc	Isc	Pmpp	FF	Voc	Isc	Pmpp	FF
Dust	F5	3.47%	0.78%	5.98%	3.90%	0.50%	0.11%	0.85%	0.56%
Drop	F30	4.38%	17.85%	20.75%	1.74%	1.46%	5.95%	6.92%	0.58%
	F39	2.53%	22.84%	20.88%	-3.46%	0.51%	4.57%	4.18%	0.69%
	F40	3.18%	16.37%	19.03%	2.17%	0.64%	3.27%	3.81%	0.72%
	F41	2.48%	9.01%	13.91%	4.94%	0.83%	3.00%	4.64%	1.65%
	F42	4.26%	9.87%	14.41%	3.60%	1.42%	3.29%	4.80%	1.20%
	F43	2.70%	10.66%	14.31%	4.58%	0.90%	3.55%	4.77%	1.53%
	F44	4.36%	10.70%	15.39%	3.64%	1.45%	3.57%	5.13%	1.21%
	F45	6.76%	9.83%	11.12%	-3.84%	2.25%	3.28%	3.71%	1.28%
	F46	7.55%	10.29%	16.16%	6.11%	2.52%	3.43%	5.39%	1.02%
Tree	72	4.16%	0.49%	9.49%	8.81%	2.08%	0.24%	4.74%	4.41%
	90	5.46%	58.12%	75.31%	42.69%	1.09%	11.62%	15.06%	8.54%

Table 3.8: Variation of electrical parameters for three different types of shading detected.

the affected cells. However, the net contribution to the I_{sc} decrease cannot be quantified with the available data, because there exists a major contribution from soiling. Also, localized drops contribute to heat the shaded areas but the temperature difference between blocked regions and the average temperature of the entire cells is no larger than 7°C. With respect to tree shading, it can be seen that the effect of shadow is inverse (temperature decreases in the shaded areas with respect to non-shaded areas of the cell). Therefore, it can be inferred that there is no generation of charge carriers and the total current is being forced to the

non-shaded areas, thus heating them above the modules average temperature.

3.3.2 Hotspots

In this section, given the large amount of modules with hot cells in different temperature ranges, and because much of them have been already commented in previous sections, the analysis will be performed following the approach given in [3], based more on statistical criteria than in individual analysis of hot cells/modules.

According to the information reported by [3], from the 90 modules inspected (5 were taken out of the analysis because of bad measurement conditions), 68 modules (75%) showed hot cells with temperatures in the range between 10 - 20 °C (H1) above the average temperature of the module, while 50 modules (55.5%) showed hot cells with temperature differences higher than 20°C (H2) above the modules average temperature. Except by zone A, for which all modules showed hot cells of type H1, the presence of cells H1 in modules of the remaining zones ranged from 66 to 83%. The presence of hot cells H2 in modules of zones B and D was around 40% and 67% for modules in zones A and C. When sorting by manufacturer, the most affected modules by both H1 and H2 hot cells happened to be SolarWorld (higher than 75%) followed by Risen, Sunel and ET ([78-83]% of modules affected by cells H1), and the less affected modules were Luxor (50% for H1 and H2), Siemens (33%) and Hangwha (25% for H1 and H2). For hot cells H2, Risen shows notably less affected modules (33%) while Sunel and ET show 55% each. No modules from Siemens show strong hotspots. Finally, when sorting by operating time it was found that modules most affected by H1 cells have been operative by 5, 3 and 2 years (86, 85 and 75%) followed by 6, 7 and 13 years of exposure (62, 50 and 25%). For cells of type H2 the decreasing order is 6 (92%), 5 (79%), 2 (50%), 3 (38%), 7 (50%) and 13 (0%) years of exposure.

From the information above, the first we can note is that in all zones more than 50% of the total amount of modules operate with type H1 hot cells, and two zones have more than 50% of modules with cells H2. However, in zone A and C also are installed the modules with hotter cells sorted by manufacturer (SolarWorld, ET), and in zone C there is a large number of SolarWorld modules (24) and Sunel, which also show high amount of cells H1 and H2.

For further analysis, in this work the same sample was divided in more limited intervals. While under thermal stress, the affected components (semiconductor, encapsulant, front glass) normally support temperatures over 100°C before being damaged, the nature and severity of heating can give clues about the failure modes and mechanisms involved in it. However, something to remind is that, for in field measurements in most cases the primary phenomenon that thermal cameras measure is the glass cover infrared radiation (which is indeed determined by the cell thermal behaviour) but as the heat spreads over the glass surface good spatial resolution of local heat sources in images is difficult [119]. Although, as it has been exposed in previous sections, for failures that cause current mismatch like partial shading the temperature rising is not so extreme (below 10°C) and temperature variations across the cell are detectable by simple inspection, as shown in Figure 3.30. But for failures that cause severe temperature rising (for example reverse biased cells) it is difficult to detect the hottest point, which is presumably the source of the heat dissipation. Moreover, for the case of reverse biased cells, heat dissipation is determined both by the reverse voltage

magnitude and the shunt resistance of the cell. Therefore, a cell which is reverse biased by, for example -10 [V] but has a high shunt resistance will dissipate less heat than other cell reverse biased by 5 [V] but with a much lower R_{sh}. This information (both reverse voltage and shunt resistance) is not possible to be inferred with the available information.

The amount of modules affected by hot cells and the amount of hot cells on the intervals I_1 = [10-20)°C, I_2 = (20-30]°C, I_3 = (30-40]°C, I_4 = (40-50]°C and I_5 = > 50°C is shown in Figures 3.31-3.33 (a). The bars indicate the % of modules which show hot cells with respect to the total amount of modules considered for each criteria (zone, manufacturer, time). Above each bar it can be seen the number of affected modules. As it can be seen, when sorting by geographical operating zone, the hottest cells (I_5) are found only in zone C, and cells belonging to the range inmediately below (I_4) are found in the inner zones (valley and inner coast) rather than coastal zones (A, B).

Regarding to hot cells themselves, graphical information is shown in Figures 3.31 to 3.33 (b), and is based on the temperature deviation of cells with respect to the average temperature of the respective modules. By sorting the information in terms of operating zone, it can be seen in Figure 3.31 (b) that the trend is similar to that of modules, but here the amount of hot cells in the range I_1 is the highest for zone C, while modules from zone C were the less affected by hot cells in this range, shown in Figure 3.31 (a). Hence, in this zone a small amount of modules concentrate a big amount of hot cells. The same can be observed in zone B, which shows the second highest amount of affected cells but also the second smaller amount of modules affected, and the inverse occurs with modules from zones A and D, where it can be seen that the hot cells found within range I_1 (30 and 28 respectively) are distributed in (almost) all the modules of the zone sample (12 for each zone).

Sorting the information by manufacturer, the results show that modules from SolarWorld are the only ones with cells in the range I_5 (17% of the total amount of SolarWorld modules). In the next range, there can be found, apart from SolarWorld, modules from Hangwha (25%) and Luxor (17%). However, given that these samples were only 4 and 6 modules for each manufacturer respectively, these results lack of statistical validation. Moreover, both Hanwgwha and Luxor show only one and two cells in the range I_4 respectively, and in the case of Luxor (module F5, described in section 3.3.1) the thermal profile of the cells is more likely to be related (very roughly speaking) to severe defects such as shunt paths across the cells. Slightly hot cells (I_1) were shown by all manufacturers, but this seems to be more related to the processes of cell sorting (when modules are manufactured) for which each manufacturer apply their own selection criteria, and normally power mismatches between cells of the same module less than ±5% are not considered as harmful [79].

Regarding to hot cells, it can be seen in Figure 3.32 (b) that SolarWorld concentrates the larger amount of hot cells in all ranges, followed by Risen and ET, which show hot cells up to range I_3. Here, comparing with Figure 3.32 (a) it can be seen that in the case of lower temperature differences (ranges I_1 and I_2) the total amount of hot cells is distributed by more than 50% of modules (except for Siemens) and, except for Luxor, more than 70% of the total amount of modules of each manufacturer. In the case of higher temperature ranges, as commented before, certain isolated modules (1 in the case of Luxor and Hangwha) show one or two hot cells. In the case of SolarWorld, as stated before, is the only one that present

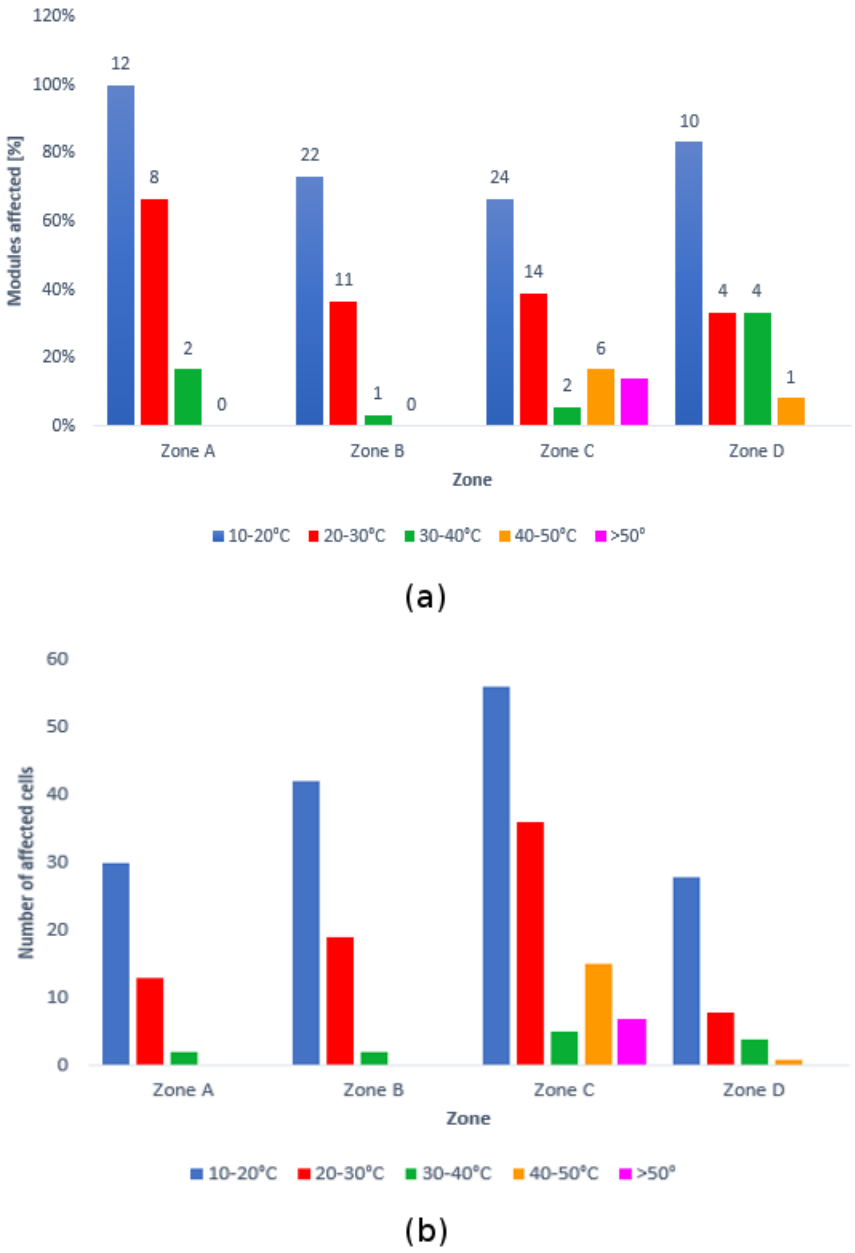

Figure 3.31: Distribution of modules with hot cells, sorted by operating zone.

cells with temperature differences higher than 50°C than modules average temperature.

Sorting by time of exposure, as shown in Figure 3.33, it can be seen that modules of range I_5 belong to two separate sets, deployed in 2012 (6 years) and 2013 (5 years) respetively. As discussed in previous paragraphs, these modules belong to only one manufacturer (SolarWorld) and are located exclusively in zone C. Regarding to the remaining temperature intervals, the trend associated to manufacturer is still evident (for I_4 only Luxor, SolarWorld and Hangwha, deployed in 2011, 2012-2013 and 2015 are found), and the only modules that did not show temperatures higher than range I_1 belong to Siemens (2005).

For cells, when sorting by time of exposure, it can be seen in Figure 3.33(b) that hot cells

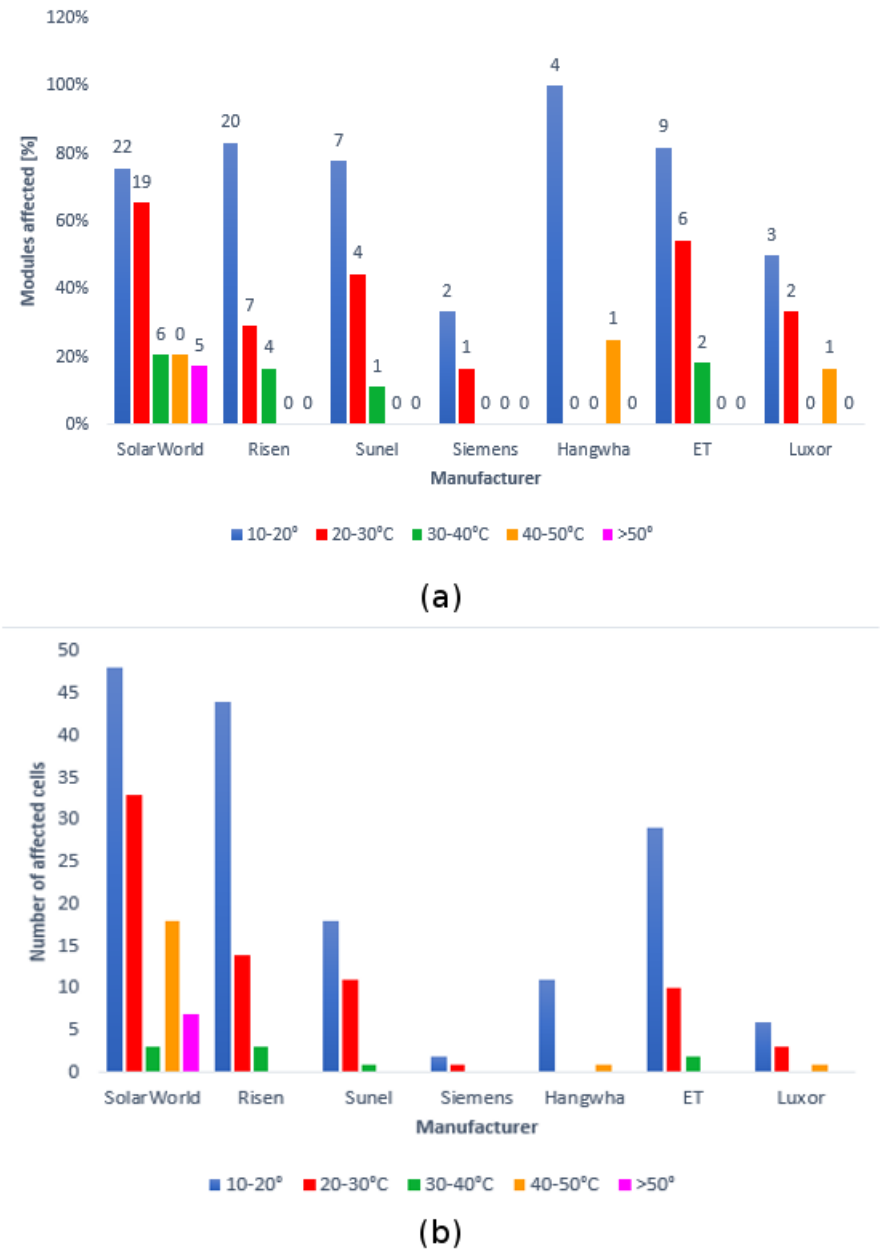

Figure 3.32: Distribution of modules with hot cells, sorted by manufacturer.

belonging to range I_1 are by far more numerous (82 hot cells in total) for those modules deployed in 2015, distributed in the 85% of modules deployed that year, comparing with Figure 3.33 (a). For modules deployed in 2013 (5 years) 86% of them show hot cells (12 modules), and they concentrate 28 hot cells. In the second range I_2 the largest amount of hot cells is again found for 3 years old modules (21 cells in 12 modules), while for higher temperature cells the amount of affected cells decreases for all intervals (less than 10).

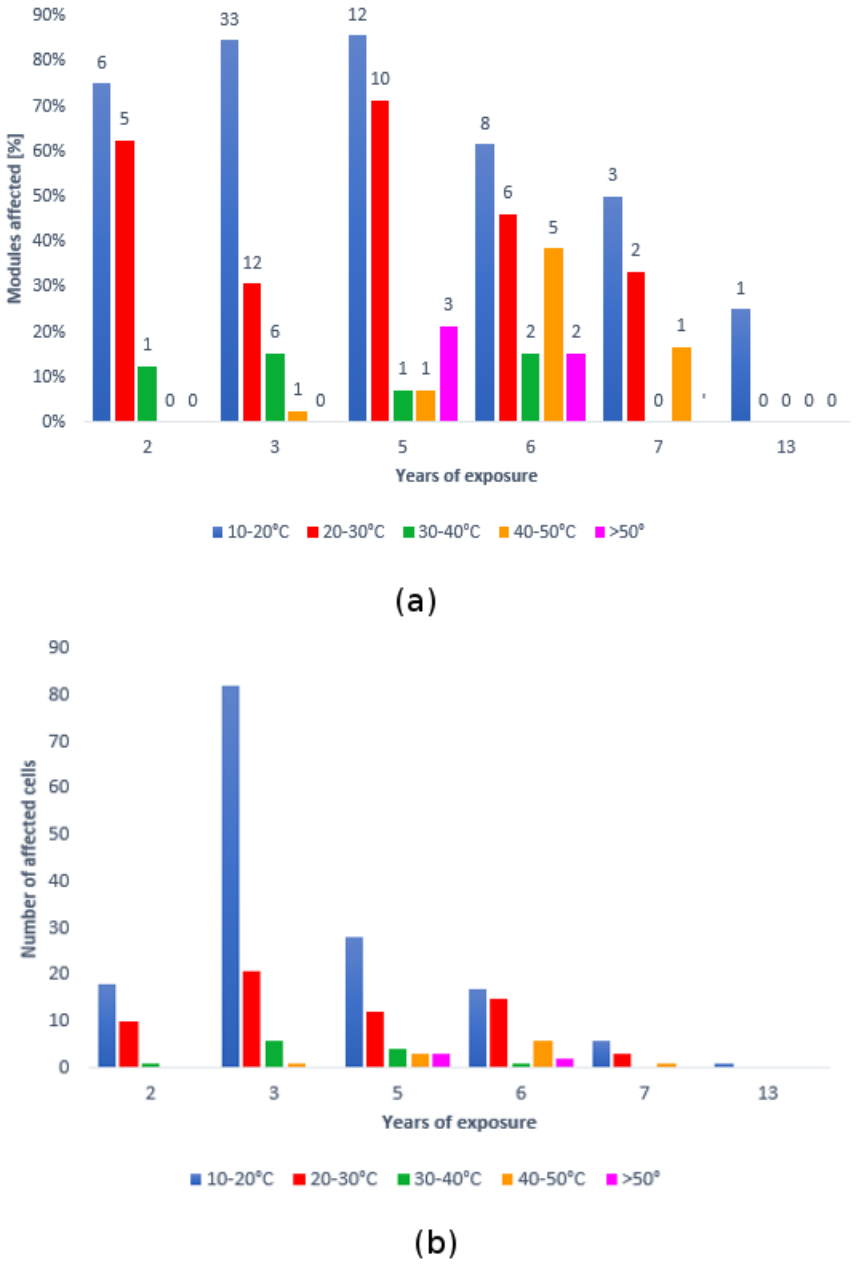

Figure 3.33: Distribution of modules with hot cells, sorted by years of exposure.

3.3.3 Materials Analysis of Failures Related to Solar Cells

The abnormalities related to solar cells (as a component of the module) analyzed in this work correspond to phenomena triggered by thermal stress originated by different causes (partial shading, loss of transmittance, among others). The semiconductors response is closely linked to its specific composition (presence and amount of impurities or doping levels), which determines the behaviour of the cells against thermal stress, derived from current mismatch between cells within a module. As discussed in previous sections, the main sources of current mismatch (and subsequently non-uniform temperature distribution within cells or between cells in a module) are partial shading, the presence of in-homogeneous layers of soiling and the localized deposition of drops (bird drops, mud, dust). From thermal measurements, it

can be noted that these sources of light interference in general do not cause important current mismatch and thus either cause large increase in temperature.

The measurements performed to most of severely hot cells do not show visible blockages to the incident light neither visible cracks or fractures, with exception of the six modules described in Section 3.1.5. However, it is possible the presence of micro-cracks that are not detectable by simple visual inspection. This suggests that in some cases disproportionate temperature rising of cells can be related to internal causes, such as cell quality and shunt resistance, which depends on the semiconductor characteristics of each cell. This can be related to the marked trend of the analyzed modules to show similar thermal behaviour according to their manufacturer. Therefore, for example, we found the case of modules from SolarWorld, deployed in 2012-2013 which show the highest cell temperatures (above 50°than modules average temperature). Moreover, five of these modules correspond to the set analyzed in section 3.1.5 which show milky discoloration of the glass, particularly located at the bottom region of the module. The remaining modules belong to the set analyzed in section 3.1.3 with modules severely soiled.

In the case of milky discolored modules, intense heating seems to be related to a severe current mismatch caused by a reduction of the transmittance, due to the fault added to a layer of soiling also present in these modules. For the set of heavily soiled modules (section 3.1.3) the relationship between the rising in temperature and the fault that causes it can be not so direct, because the distribution of hot cells changes notably (both in the location and magnitude of the temperature rising) from dirty to clean module. However it seems to be related with the current demanded.

The rest of the modules with hot cells show the same trends by manufacturer. However, strong conclusions cannot be stated, because some samples were very small (< 10 modules) and also these were located together in the same zones. For example, ET only has modules in the coast (A, B), and Sunel only in zone C. Nevertheless, in the case of modules from Siemens (6 modules), which were found in 2 zones (B and C) they are also the oldest (11 years of exposure). For this set, there were not found excessively hot cells, but for more precise conclusions it is recommended to expand the sample by performing additional measurements. Balancing the amount of data regarding time of exposure, manufacturer and operating zone is highly required.

From a purely materials perspective, the effect of thermal stress on solar cells can lead to detrimental effects by several causes: first, as the Si substrate is interconnected with metallization components, and due to the expansion behaviour of solar cells under temperature rising, the difference in coefficients of thermal expansion between the semiconductor, glass frit and metallic components will lead to mechanical stress that can cause cracks, power dissipation and even complete fault of the cell [46]. On the other side, the behaviour of the cell under reverse bias conditions determines the temperature rising for determined reverse voltage. For cells with low shunt resistance, temperatures above 100°C can be achieved at very low reverse voltages [106]. In the case of modules of Arica, the hottest cell was operating at a temperature near 100°C, and such temperatures are usually associated with severe cell fractures [68], or severe power dissipation across the affected cell.

3.4 Other Failures

3.4.1 Faulty Soldering

In this section, failures for which identification not enough information was available, or the quality of this information was not completely reliable to perform a concrete diagnosis are described.

In figure 3.34 it is shown a module with several hot cells in its bottom half, but it can be observed that one is half-heated, with a temperature difference of 4°C between the hotter and the colder halves. This can be indicative of a faulty soldering on the cell [68]. In this particular case, visual inspection did not give further information about the failure, because the module was affected by a heavy layer of soiling. Moreover, the I-V curve is dominated by the reduction in the I_{sc}, characteristics of this last phenomenon. However, it was possible to discard the cell fracture as a possible failure due to the shape of the curve, which does not show steps (characteristics of isolated fractured sections of the cell). However, it can be noticed a change in slope near V_{oc}, which can be related to increased series resistance, ussually associated to a faulty soldering (since the series resistance is directly related to metallic components).

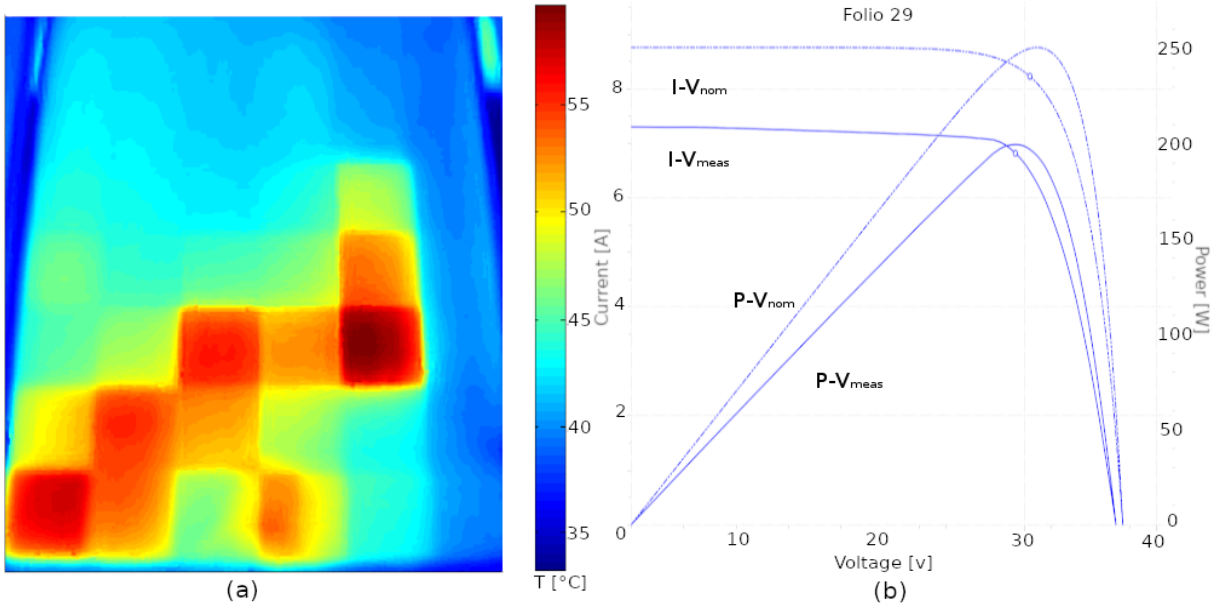

Figure 3.34: (a) Thermal image and (b) I-V/P-V characteristics of a module with one bottom cell half heated.

3.4.2 Cell Fracture

A thermal pattern coincident with cell fracture was found in a module operating in zone C, which was also affected by a light soiling layer and localized bird drops, as shown in Figure 3.35. The pressumed fractured cell (R1C3) shows a non-uniform temperature distribution and a well defined temperature difference across a straight line in the right edge of about three °C, which may indicate the presence of electrically isolated regions caused by a fracture.

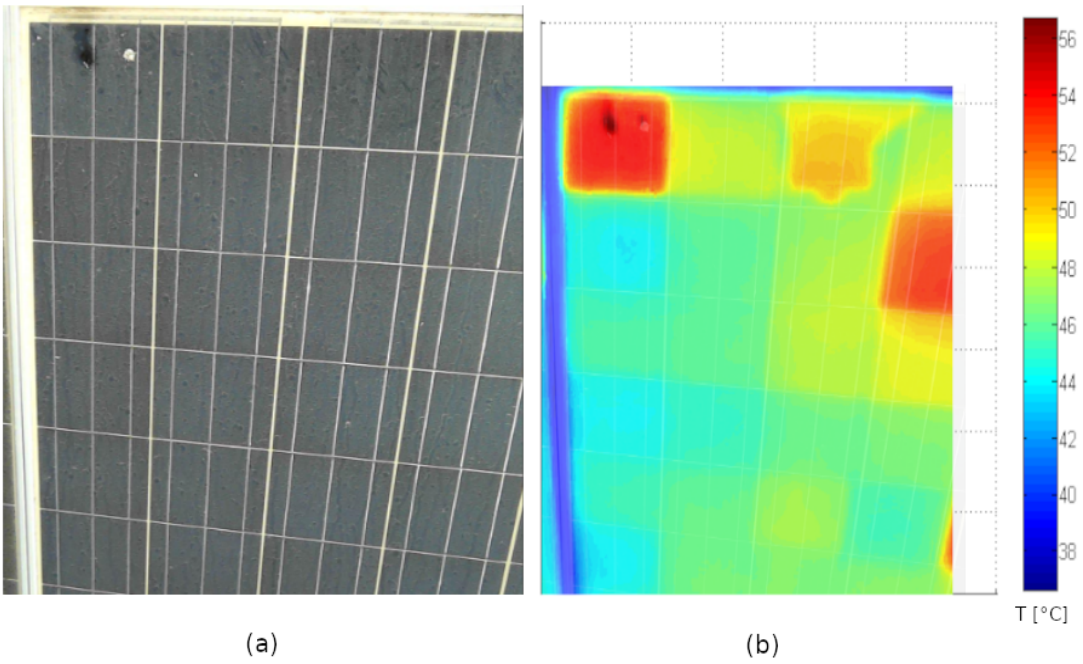

Figure 3.35: (a) visual inspection and (b) thermal image of module with a drop in cell R1C1 and a presumed fracture in cell R1C3.

A close up of the defective cells of the studied module is shown in Figure 3.36. For the presumably fractured cell (c), it is not possible to detect the failure by visual inspection because of a soiling layer covering the modules surface. Additionally, these type of failures is not always detectable by bare eye. Additional tools like electroluminiscence (for fielded modules) or microscopy (for laboratory samples) are needed. Moreover, the I-V/P-V characteristics, as shown in Figure 3.37 does not evidence a characteristic plateau [68] caused by the reduction of current delivered by the defective cell, but this also depends on the severity of the fracture and the fraction of isolated cell. However, it can be seen both a reduction in the shunt resistance and increase in series resistance. Nevertheless, for the characterization of this failure mode an additional inspection and additional tools are needed.

3.5 Discussion and Recommendations for Future Work

As a result of the detailed analysis performed in the present Chapter, it has been found that the vast majority of modules shows multiple failure/degradation modes at the same time. This makes their analysis a manifold task, and the correct interpretation of the information for failures diagnosis is an even more difficult challenge.

Considering the three approaches that the IDCTool contemplates (visual inspection, thermal imaging and electrical measurements), an integrated analysis of each of the failure/degradation modes found has been done. In principle, trends for their occurrence in field have been discussed. However, the main limitation for this analysis was, precisely, that it was not possible to isolate each fault for a separated analysis, therefor well delimited conclusions about each fault cannot be done. Despite this, certain phenomena exhibited by the Atacama desert

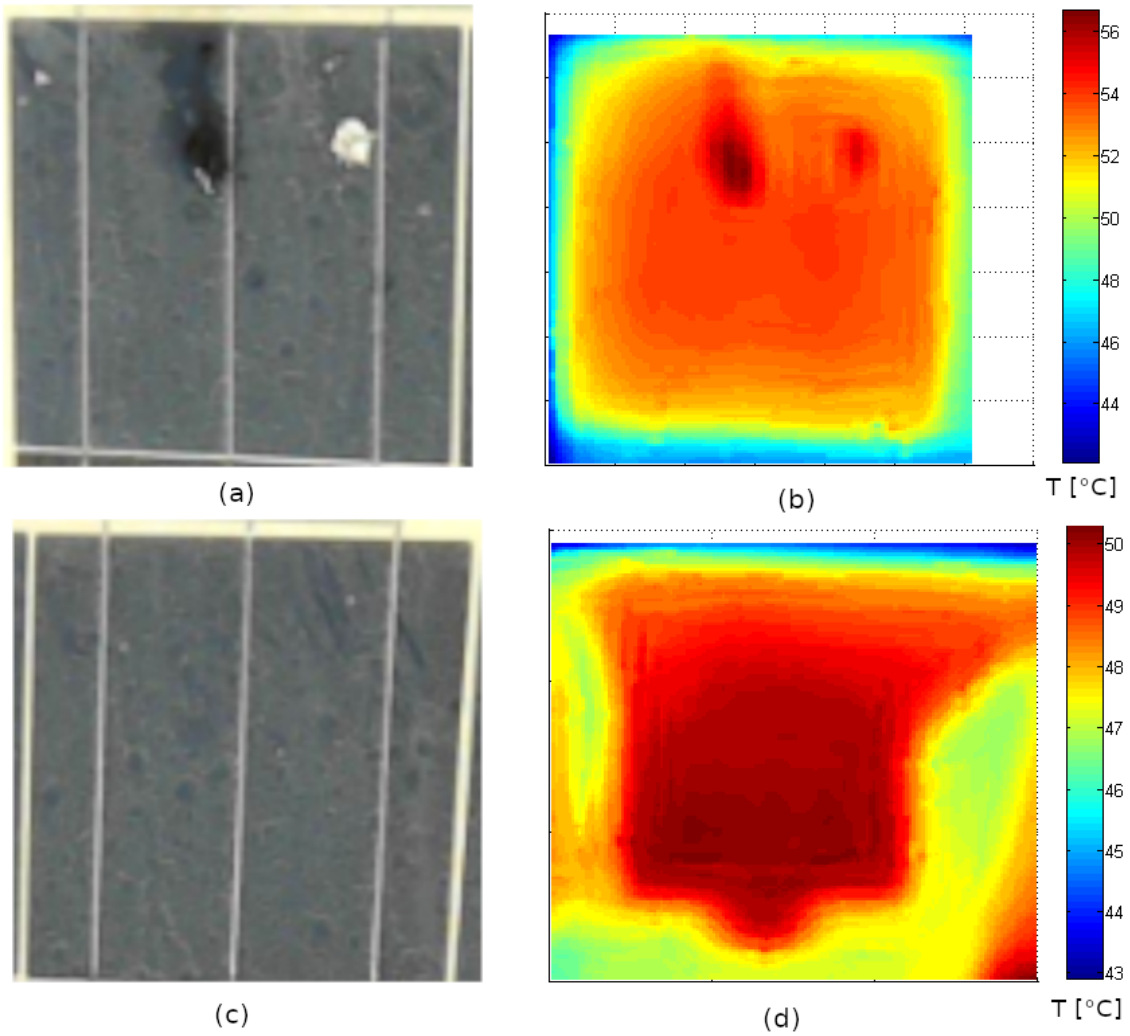

Figure 3.36: (a), (c) visual inspection and (b), (d) thermal image of a dropped and a presumably fractured cell.

modules could be enlightened. First of all, derived from visual inspection it can be noted that the P_{mpp} reduction for both heavily and lightly soiled modules is not larger than 20% from the nominal value, and, as expected, heavily soiled modules show higher drops in power than lightly soiled modules, which indicates that severity of soiling deposition affects directly the power output. Moreover, the drop in power seems to be more related to the reduction in short circuit current than that of voltage, because soiling screens the incident light that reaches the cells. For voltage, the relationship was not so direct. Regarding to temperature, in general, it was found that heavily soiled modules operate with lower temperatures than lightly soiled modules, because of the screening effect of soiling layers that prevent heating caused by thermalization losses.

For heavily soiled modules, there were identified four different patterns of soiling deposition, and related to the location of modules and the specific environmental features of each zone. As for most modules the distribution of soiling layers over the surface was approximately homogeneous, noticeable temperature changes because of this were not detected.

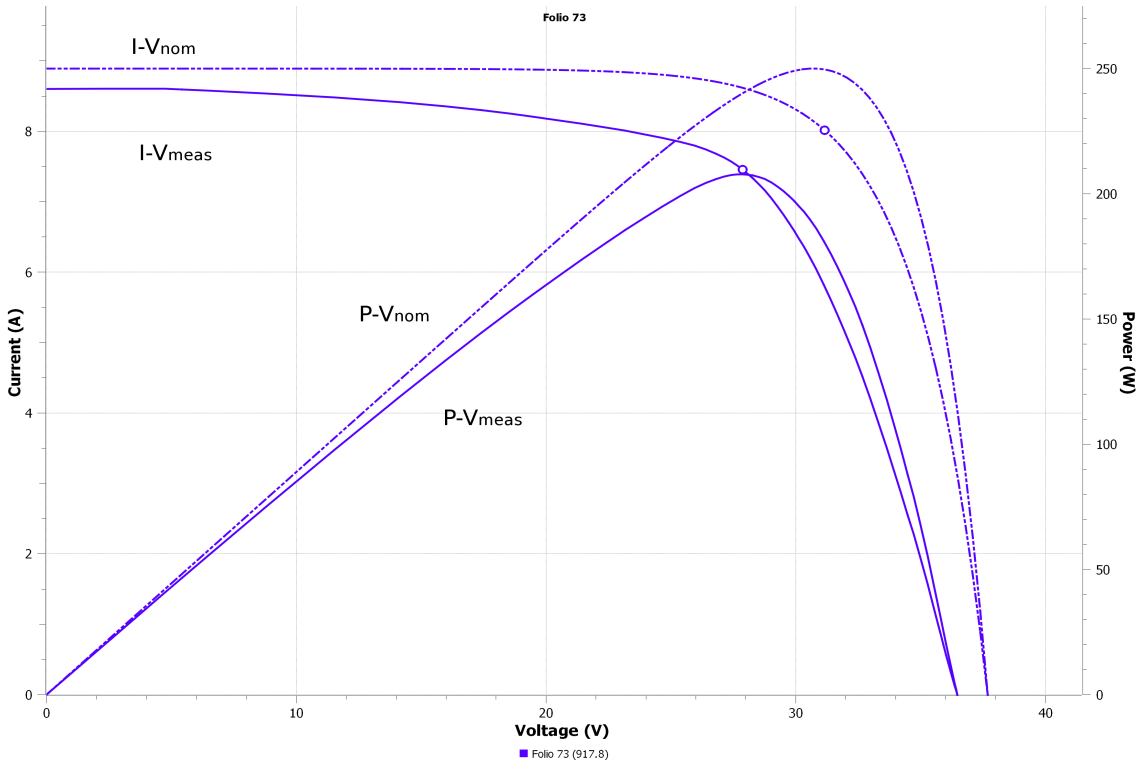

Figure 3.37: I-V/P-V characteristics of a module with a thick drop on one cell (R1C1) and a presumably fractured cell (R1C3).

However, the drop in electrical parameters shows that modules affected by the thickest layers of soiling also show the highest reductions in I_{sc}. Moreover, in general, modules from inner zones show higher decreases in I_{sc} than coastal-based samples. The set of heavily soiled modules which were measured before and after cleaning indicate that the lack of cleaning protocols in a desert location can lead to severe output reduction, but at the same time, soiling layers contribute to attenuate the overheating of current-dissipating cells. This can be positive in the sense that the materials get less stressed but at the same time, the underlying problems can be underestimated. For lightly soiled modules, given that the effect of soiling layers is not highly pronounced, thermal patterns cannot be directly related to this phenomenon in particularly severely heated cells, and in most cases the only attributable effect was a slight reduction in I_{sc}. The only set of modules which show significant Short Circuit Current drop was also observed to have localized milky discoloration of the glass surface in the bottom cells, which is because of the local loss of transmittance in the discolored area and thus severe heating by current mismatch.

Regarding to delamination of the EVA encapsulant, this was found in four modules from the entire sample, three of them were the only modules manufactured by JA Solar and deployed just three years before the inspection, in a location inside the city near the coast. In a very rough manner this particular failure seems to be more attributable to manufacturer issues, but, for concrete conclusions more information is required, as well as a bigger sample. In thermal images, none of the delaminated modules showed thermal patterns attributable to delamination, but this can be either due to the fact that measurements were not taken under ideal irradiation conditions (in the case of JA Solar modules which were the most

extensively delaminated), the extension of delaminated areas was very small and localized as in the case of the Siemens module, or the existence of cells severely hotter in the modules opaqued the thermal abnormalities derived particularly from delamination. In this case, for further field inspections could be useful to take better resolution images or (due to the lack of a more sophisticated method like real time monitoring), perform the inspection twice: one for identifying the thermal abnormalities in a general way and the second time to focus, as possible on isolated issues.

For issues that affected primarily isolated solar cells or groups of cells, which were partial shading and hotspots, it was found that, none of the objects or localized drops that partially shaded a cell or module produced severe heating in the affected regions (always less than 10°C). Moreover, the vast majority of abnormally heated cells did not show issues detectable by visual inspection, for which (in the case of severely heated cells) processes related to the internal functioning of the cell (like shunts or micro-cracks) were more probable to be related to thermal patterns (excluding the set of milky discolored Solarworld modules, for which thermal patterns are more attributtable to loss of transmittance of the glass cover). Additionally, two thermal profiles were identified with a possible cell fracture and a faulty soldering, phenomena that should be checked in future research, complemented with additional measurements.

About the performance of the IDCTool developed by [3], there is not very much to improve from a technical point of view, given that it is solidly based in international standards and norms. The survey and methods of inspection are not very different from international inspection procedures, which, for the scope of an IDCTool (to collect information) meets the expectations. However, improvements or modifications can be proposed, considering the future research needs. In one hand, if the main objective is oriented to simply gathering information about the general state of modules operating in the Atacama Desert considering issues related to the environment (soiling, presence of surrounding buildings, humidity, temperature) the main efforts should be focused on the automatization of the inspection procedure in order to optimize the inspection procedure. For this aim, mobile application development could be useful (for the fillable form) together with the use of a tripod or mobile platform to improve the quality of thermal images, which also affects the final results. Other possible application of these tools could be the real time detection/diagnosis of failures, for which the use of UAV devices to perform the visual and infrared inspection with real time image processing to detect abnormal patterns that would require individual, additional evaluation. On the other hand, if research requirements concern with the detailed analysis of failures to find further relationships with specific features of the Atacama Desert, in order to make contributions in a scientific fashion, it is recommended to consider the use of additional tools. For example, electroluminiscence allows to detect structural defects in solar cells/modules in a qualitative way, which are not detectable by visual inspection like cracks or micro-cracks. Thermal/electrical signatures of these two issues were found in this sample, but with the available information it is impossible to conclude the presence of these failures in the inspected modules. Another useful technique could be the lock-in thermography, which allows to characterize more complex thermal phenomena like hotspots derived from shunts.

Finally, some recommendations to perform further investigation in materials science field can be roughly done. From the detailed characterization and analysis of failures, performed

in [3] and the present thesis work, it can be inferred that, local environmental conditions of the Atacama desert seem to be affecting modules components. In particular, the front cover glass (which is the most exposed component) but also with the underlying components. The physicochemical interactions that mediate these processes are well documented, but relevant information could be extracted by studying the specific effects of the local environment dust particles and contaminants over the surfaces, which could be altering the properties and degradation of glass, further than just deposited and blocking the incident light.

Chapter 4

Conclusions

In this thesis work, a detailed analysis of the occurrence of failure/degradation modes found of solar PV modules operating in the Atacama Desert has been conducted. Based on the data collected in a previous field test campaign, the analysis considered information from visual inspections, IR thermography, I-V curve characterization and statistical trends. Additionally, a general supplement from a physical perspective was added to the analysis, considering well-known features of materials, together with recent literature research. This allowed to relate the information collected by each tool (visual, electrical, thermal) separately, to infer or detect the presence of certain failure/degradation modes. The physical analysis allowed to propose certain mechanisms that may be involved in these failure/degradation modes. However, this last approach is very rough and all assumptions need to be confirmed through formal research, which is highly encouraged in this work. The abnormalities detected and analysed were: soiling, milky discoloration of the front glass, weathering, delamination of EVA encapsulant, partial shading, and hotspots. Additionally, certain thermal patterns were found to show uneven temperature distributions that may correspond to defective soldering and cell fracture, but these were only described as possible faults and hence proposed for further studies.

Based on the results, the most common issue found in inspected modules is soiling, which is something expected for a desert region. Following the approach used in a previous work [3], soiling was classified in two intensities: light soiling and heavy soiling. For further analysis, as for the heavy soiling classification, a set of modules affected by a particularly severe soiling layer was studied separatedly. In heavily soiled modules, different deposition patterns were found, attributable to individual features of respective locations. For coastal-based modules, soiling deposition seems to be influenced by humidity and wind, while city-based modules show uneven soiling patterns (both in composition and distribution) attributable to the presence of varied pollutants. In inland locations, the absence of water allows for an even deposition that prevents sharp temperature variations in modules, but this zones, in contrast, show the highest covering levels, thus producing the highest power drops. In contrast, lightly soiled modules show less pronounced patterns, but again, modules located in inland areas show thicker soiling layers than other locations. The parameter most affected by soiling is short circuit current, as soiling layers act as a screen that uniformly prevents photocurrent generation. This has a direct influence the P_{mpp} drop, and, as expected, lightly

soiled modules show better performance than heavily soiled modules. The strong influence of soiling in I_{sc}, P_{mpp} can be evidenced by the immediate improvement on the electrical performance of modules after cleaning. Additionally, voltage is also affected at very low irradiance levels, received by the cells due to thick soiling layers. Temperature variances were measured at different soiling degrees, as well as strong temperature variations between dirty and clean modules. However, the presence of hotspots cannot be directly related to soiling.

In addition to its effect on I_{sc}, the presence of soiling layers (other than severe soiling) does not considerably affect the detection of other abnormalities. Nonetheless, in order to enhance the degree of success and accuracy for detecting other failure/degradation modes, proper module cleaning is recommended for further inspection procedures.

Aside from purely gravitational deposition, dust particles seem to interact with the front cover glass. Weathered modules and milky discoloration of the glass were found in inland areas. Weathering may suggest that, despite the arid environment, small amounts of water/moisture seem to be enough to produce chemical reactions on glass surfaces. Two of the weathered modules also show extensive milky discoloration on their covers, hence chemical reactions may be altering the optical properties of the glass, therefore severely affecting its transmittance. Other modules showed localized milky discoloration at the bottom, where also strong hotspots ($\Delta T > 50$°C with respect to the average temperature) were localized. The latter may be due to severe current mismatches caused by loss of the transmittance capacity of the front cover glass, while the remainder areas of the modules showed even temperature profiles.

Hotspots represented extended issue in operating modules. 75 percent of the total sample showed cells with temperatures $\Delta T > 10$ °C hotter than the average temperature of modules, which may be attributed to small defects or slight current mismatches between cells. On the other hand, more than half of the modules of the total sample (55 percent) showed cells with temperatures $\Delta T > 20$ °C hotter than the average temperature of modules. Broad temperature range differences are less probable to be caused by current mismatches, owever other failures may be involved, such as shunts, reverse bias operation, cracks or low shunt resistance. Nonetheless, cell temperatures above 100°C were not found. Therefore, although thess temperatures still carries safety concerns, these does not represent a catastrophic hazard (EVA melting is around 150°C). Temperature variations due to other failures suchas delamination, partial shading, cell fracture and defective soldering could not be determined.

As for the primary objective of this thesis, it has been possible to describe and analyse failure/degradation modes found in PV modules operating in the Atacama Desert, by using the information recorded in previous works. As overview and, in order to generate discussion about the failures found and their possible causes, the information available enabled the obtaining of satisfactory results. It was possible to identify (at least qualitatively) seven (7) different abnormalities. Upon the analysis, based on the theoretical and experimental results found in literature, it is expected this lays the groundwork for future developments in detecting and diagnosing failures/degradation modes of solar modules. The performance of the IDCTool developed in a previous work shows satisfactory results from a technical point of view, since it is based in well tested standards and regulations. However, researches and

developments based on local standards may contribute to improve future results [120].

As for the specific conditions of the Atacama Desert, mainly the aridity and high UV radiation , these does not show to be excessively harmful (given the current state of modules) for the studied sample. According to literature, the most detrimental climate for solar modules is the hot and humid climate. The aridity of Atacama Desert, and its moderate room temperatures seem to placate the negative effects that can derive from rough environmental operating conditions. Although there is no statistical evidence, inspected modules did not show degradation/failures with more frequency/potency associated to UV radiation (and, in general to any environmental factor). This could be an indicative that UV by itself does not play a major role as a degradation trigger, but otherwise as a catalyst in presence of other agents. Nevertheless, all the modules inspected are fielded near the coast (the farthest inner-based modules are located 25 km away from the seashore) and at the sea level. These locations are characterized by more presence of clouds and lower UV radiation levels than those of more elevated terrain such as the Andean plateau [92]. Therefore, a complete characterization of the influence of the Atacama Desert climatic conditions on the occurrence of failure/degradation modes in solar photovoltaic modules should also involve the application of field inspection campaigns in power plants with different geographical altitude.

Bibliography

[1] Marc Köntges, Sarah Kurtz, Corinne Packard, Ulrike Jahn, Karl Berger, Kazuhilo Kato, Thomas Friesen, Haitao Liu, Mike Van Iseghem, john Wohlgemuth, David Miller, Michael Kempe, Pete Hacke, Florian Reil, Nicolas Bogdanski, W Herrmann, C Buerhop, Guillaume Razongles, and Gabi Friesen. Review of failures of photovoltaic modules. 01 2014.

[2] (Mani) GovindaSamy TamizhMani and Joseph Kuitche. Accelerated Lifetime Testing of Photovoltaic Modules. Technical report, University of Arizona, 07 2013.

[3] María Ignacia Devoto. Solar module characterization via visual inspection in the field, i-v curve and thermal-image analysis. Master's thesis, Universidad de Chile, Santiago, Chile, 2018.

[4] How to inspect visually a solar pv panel? `https://www.renewablesinafrica.com/how-to-inspect-visually-a-solar/`. Accessed: 2018-20-07.

[5] Solar panel construction. `https://www.cleanenergyreviews.info/blog/solar-panel-components-construction`.

[6] S.M. Karazi, I.U. Ahad, and K.Y. Benyounis. Laser micromachining for transparent materials. In *Reference Module in Materials Science and Materials Engineering*. Elsevier, 2017.

[7] W.D. Callister. *Materials Science And Engineering: An Introduction*. John Wiley & Sons, 2007.

[8] Single Diode Equivalent Circuit Models. `https://pvpmc.sandia.gov/modeling-steps/2-dc-module-iv/diode-equivalent-circuit-models/`.

[9] Mohammad Reza Maghami, Hashim Hizam, Chandima Gomes, Mohd Amran Radzi, Mohammad Ismael Rezadad, and Shahrooz Hajighorbani. Power loss due to soiling on solar panel: A review. *Renewable and Sustainable Energy Reviews*, 59:1307 – 1316, 2016.

[10] K. A. Kim and P. T. Krein. Photovoltaic hot spot analysis for cells with various reverse-bias characteristics through electrical and thermal simulation. In *2013 IEEE 14th Workshop on Control and Modeling for Power Electronics (COMPEL)*, pages 1–8,

06 2013.

[11] Michael Simon and Edson L. Meyer. Detection and analysis of hot-spot formation in solar cells. *Solar Energy Materials and Solar Cells*, 94(2):106 – 113, 2010.

[12] Huang Jian-Bin, Wang Shao-Wu, Luo Yong, Zhao Zong-Ci, and Wen Xin-Yu. Debates on the causes of global warming. *Advances in Climate Change Research*, 3(1):38 – 44, 2012.

[13] Ipcc fifth assessment report, 2014. `http://www.ipcc.ch/pdf/assessment-report/ar5/syr/AR5_SYR_FINAL_SPM.pdf`. Accessed: 2018-20-07.

[14] Michael Stephenson. Chapter 3 - artificial global warming: The 'fossil economy'. In Michael Stephenson, editor, *Energy and Climate Change*, pages 47 – 69. Elsevier, 2018.

[15] E.A. Feilat, S. Azzam, and A. Al-Salaymeh. Impact of large pv and wind power plants on voltage and frequency stability of jordan's national grid. *Sustainable Cities and Society*, 36:257 – 271, 2018.

[16] Energía 2050, política energética de chile. `http://www.minenergia.cl/archivos_bajar/LIBRO-ENERGIA-2050-WEB.pdf`.

[17] Stephen J. Fonash. Chapter one - introduction. In Stephen J. Fonash, editor, *Solar Cell Device Physics (Second Edition)*, pages 1 – 8. Academic Press, Boston, second edition edition, 2010.

[18] Nrel solar cell best efficiencies chart. `https://www.nrel.gov/pv/assets/images/efficiency-chart-20180716.jpg`. Accessed: 2018-20-07.

[19] Nilofar Asim, Kamaruzzaman Sopian, Shideh Ahmadi, Kasra Saeedfar, Mohammad Alghoul, Omid Saadatian, and Saleem H. Zaidi. Review on the role of materials science in solar cells. *Renewable and Sustainable Energy Reviews*, 16:5834–5847, 10 2012.

[20] Utpal Gangopadhyay, Sukhendu Jana, and Sayan Das. State of art of solar photovoltaic technology. *Journal of Energy*, 764132, 04 2013.

[21] Photovoltaics report. `https://www.ise.fraunhofer.de/content/dam/ise/de/documents/publications/studies/Photovoltaics-Report.pdf`.

[22] Samy Almosni, Amaury Delamarre, Zacharie Jehl, Daniel Suchet, Ludmila Cojocaru, Maxime Giteau, Benoit Behaghel, Anatole Julian, Camille Ibrahim, Léa Tatry, Haibin Wang, Takaya Kubo, Satoshi Uchida, Hiroshi Segawa, Naoya Miyashita, Ryo Tamaki, Yasushi Shoji, Katsuhisa Yoshida, Nazmul Ahsan, Kentaro Watanabe, Tomoyuki Inoue, Masakazu Sugiyama, Yoshiaki Nakano, Tomofumi Hamamura, Thierry Toupance, Céline Olivier, Sylvain Chambon, Laurence Vignau, Camille Geffroy, Eric Cloutet, Georges Hadziioannou, Nicolas Cavassilas, Pierre Rale, Andrea Cattoni, Stéphane Collin, François Gibelli, Myriam Paire, Laurent Lombez, Damien Aureau, Muriel Bouttemy, Arnaud Etcheberry, Yoshitaka Okada, and Jean-François Guillemoles. Material challenges for solar cells in the twenty-first century: directions in emerging technologies.

Science and Technology of Advanced Materials, 19(1):336–369, 2018. PMID: 29707072.

[23] What happens when low quality, unproven materials are used in solar panels? `http://www.saurenergy.com/solar-energy-articles/what-happens-when-low-quality-unproven-materials-are-used-in-solar-panels`.

[24] Tetsuo Soga. Preface. In Tetsuo Soga, editor, *Nanostructured Materials for Solar Energy Conversion*, pages v – vi. Elsevier, Amsterdam, 2006.

[25] Nian Chen, Keith Tate, and Abasifreke Ebong. Generalized analysis of the impact of emitter sheet resistance on silicon solar cell performance. *Japanese Journal of Applied Physics*, 54(8S1):08KD20, 2015.

[26] Martin Heinrich, Achim Kraft, Martin Lieder, Bram Hoex, Armin G. Aberle, and Markus Glatthaar. Quantification of front side metallization area on silicon wafer solar cells for background plating detection. *Energy Procedia*, 77:717 – 724, 2015. 5th International Conference on Silicon Photovoltaics, SiliconPV 2015.

[27] A. Ebong and N. Chen. Metallization of crystalline silicon solar cells: A review. In *High Capacity Optical Networks and Emerging/Enabling Technologies*, pages 102–109, 12 2012.

[28] William Shockley and Hans J. Queisser. Detailed balance limit of efficiency of p-n junction solar cells. *Journal of Applied Physics*, 32(3):510–519, 1961.

[29] Loic Tous. *Nickel/Copper Plated Contacts as an Alternative to Silver Screen Printing for the Front Side Metallization of Industrial High Efficiency Silicon Solar Cells*. PhD thesis, 01 2014.

[30] Alexis Vossier. Effect of non-ideal losses on the optimal bandgap arrangement of multijunction solar cells comprising up to 5 subcells. volume 1679, 04 2015.

[31] Florian Schindler, Bernhard Michl, Jonas Schön, Wolfram Kwapil, Wilhelm Warta, and Martin Schubert. Solar cell efficiency losses due to impurities from the crucible in multicrystalline silicon. *Photovoltaics, IEEE Journal of*, 4:122–129, 01 2014.

[32] N.G. Sakiotis. Role of impurities in silicon solar cell performance. *Solar Cells*, 7(1):87 – 96, 1982.

[33] B. Sopori. Impurities and defects in photovoltaic si devices: A review. 11 1999.

[34] O. Breitenstein, J. Bauer, and J. P. Rakotoniaina. Material-induced shunts in multicrystalline silicon solar cells. *Semiconductors*, 41(4):440–443, 04 2007.

[35] Pannientakandi Somasundaran and Rajesh Gupta. Evaluation of shunt losses in industrial silicon solar cells. *International Journal of Photoenergy*, 2016:1–9, 06 2016.

[36] O. Breitenstein, J. P. Rakotoniaina, M. H. Al Rifai, and M. Werner. Shunt types in crystalline silicon solar cells. *Progress in Photovoltaics: Research and Applications*,

12(7):529–538.

[37] S A. Correia, Jan Lossen, and Mario Bähr. Eliminating shunts from industrial silicon solar cells by spatially resolved analysis. 01 2006.

[38] Dieter Schroder and Daniel Meier. Solar cell contact resistance—a review. *Electron Devices, IEEE Transactions on*, 31:637 – 647, 06 1984.

[39] Metal-semiconductor junctions. `https://nptel.ac.in/courses/113106062/Lec9.pdf`.

[40] SLAC National Accelerator Laboratory, United States. Department of Energy. Office of Science, United States. Department of Energy. Office of Scientific, and Technical Information. *The Formation Mechanism for Printed Silver-contacts for Silicon Solar Cells*. United States. Department of Energy. Office of Science, 2016.

[41] M.K. Mat Desa, S. Sapeai, A.W. Azhari, K. Sopian, M.Y. Sulaiman, N. Amin, and S.H. Zaidi. Silicon back contact solar cell configuration: A pathway towards higher efficiency. *Renewable and Sustainable Energy Reviews*, 60:1516 – 1532, 2016.

[42] P N Vinod, B C Chakravarty, Mohan Lal, Ravi Kumar, and S N Singh. A novel method for the determination of the front contact resistance in large area screen printed silicon solar cells. *Semiconductor Science and Technology*, 15(3):286, 2000.

[43] Yuping Tai, Guojun Zheng, Hanying Wang, Hui Wang, and Jintao Bai. Effect of glass frit in ag paste on the electrical properties of front-side ag contacts for crystalline-silicon solar cells. *RSC Adv.*, 5:92515–92521, 2015.

[44] Juehui Zhou, Nuoxin Xu, Hui Yang, and Qilong Zhang. Effect of ag powder and glass frit in ag paste on front contract of silicon solar cells. *Procedia Engineering*, 94:1 – 5, 2014. International Conference on Materials for Advanced Technologies (ICMAT2013), Symposium E - Solid-state devices for light emission and detection.

[45] T. Aoyama, M. Aoki, I. Sumita, Y. Yoshino, and A. Ogura. Characterization of glass frit in conductive paste for n-type crystalline silicon solar cells. *IEEE Journal of Photovoltaics*, 7(5):1313–1318, 09 2017.

[46] He Wang, Ao Wang, Hong Yang, and Jingsheng Huang. Study on the thermal stress distribution of crystalline silicon solar cells in bipv. *Energy Procedia*, 88:429 – 435, 2016. CUE 2015 - Applied Energy Symposium and Summit 2015: Low carbon cities and urban energy systems.

[47] Shan Jiang, Kemin Wang, Hongwen Zhang, Yonghong Ding, and Qiang Yu. Encapsulation of pv modules using ethylene vinyl acetate copolymer as the encapsulant. *Macromolecular Reaction Engineering*, 9(5):522–529, 2015.

[48] M. Hasanuzzaman, A. Rafferty, M. Sajjia, and A.-G. Olabi. Properties of glass materials. In *Reference Module in Materials Science and Materials Engineering*. Elsevier, 2016.

[49] Sebastian Pingel, O Frank, M Winkler, S Daryan, Torsten Geipel, H Hoehne, and Juliane Berghold. Potential induced degradation of solar cells and panels. pages 002817 – 002822, 07 2010.

[50] Michael F. Ashby. Chapter 15 - material profiles. In Michael F. Ashby, editor, *Materials and the Environment (Second Edition)*, pages 459 – 595. Butterworth-Heinemann, Boston, second edition edition, 2013.

[51] Vincent Guiheneuf, Fabien Delaleux, Olivier Riou, Pierre-Olivier Logerais, and Jean-Félix Durastanti. Investigation of damp heat effects on glass properties for photovoltaic applications. *Corrosion Engineering, Science and Technology*, 52(3):170–177, 2017.

[52] Michele Candida Carvalho de Oliveira, Antônia Sonia Alves Diniz Cardoso, Marcelo Machado Viana, and Vanessa de Freitas Cunha Lins. The causes and effects of degradation of encapsulant ethylene vinyl acetate copolymer (eva) in crystalline silicon photovoltaic modules: A review. *Renewable and Sustainable Energy Reviews*, 81:2299 – 2317, 2018.

[53] Muhammad Tayyib, Jan Ove Odden, and Tor Oskar Saetre. Uv-induced degradation study of multicrystalline silicon solar cells made from different silicon materials. *Energy Procedia*, 38:626 – 635, 2013. Proceedings of the 3rd International Conference on Crystalline Silicon Photovoltaics (SiliconPV 2013).

[54] M. R. Vogt, H. Hahn, H. Holst, M. Winter, C. Schinke, M. Köntges, R. Brendel, and P. P. Altermatt. Measurement of the optical constants of soda-lime glasses in dependence of iron content and modeling of iron-related power losses in crystalline si solar cell modules. *IEEE Journal of Photovoltaics*, 6(1):111–118, 01 2016.

[55] Papadopoulos and Christina-Amalia Drosou. Influence of weather conditions on glass properties. *Journal of the University of Chemical Technology and Metallurgy*, 47:429 – 438, 01 2012.

[56] Giovanni Palleschi, Marzia Caproni, D Falcos, A Giacomelli, P Fabbri, A.W. Czanderna, and F.J. Pern. Encapsulation of pv modules using ethylene vinyl acetate copolymer as a pottant: A critical review. *Solar Energy Materials and Solar Cells*, 43, 09 1996.

[57] A. Badiee, I.A. Ashcroft, and R.D. Wildman. The thermo-mechanical degradation of ethylene vinyl acetate used as a solar panel adhesive and encapsulant. *International Journal of Adhesion and Adhesives*, 68:212 – 218, 2016.

[58] Dan Wu, Jiang Zhu, Thomas R. Betts, and Ralph Gottschalg. Degradation of interfacial adhesion strength within photovoltaic mini-modules during damp-heat exposure. *Progress in Photovoltaics: Research and Applications*, 22(7):796–809.

[59] M. D. Kempe, G. J. Jorgensen, K. M. Terwilliger, T. J. McMahon, C. E. Kennedy, and T. T. Borek. Ethylene-vinyl acetate potential problems for photovoltaic packaging. In *2006 IEEE 4th World Conference on Photovoltaic Energy Conference*, volume 2, pages 2160–2163, 05 2006.

[60] Peter G. Pape. 29 - adhesion promoters: Silane coupling agents. In Myer Kutz, editor, *Applied Plastics Engineering Handbook*, Plastics Design Library, pages 503 – 517. William Andrew Publishing, Oxford, 2011.

[61] Edwin P. Plueddemann. *Chemistry of Silane Coupling Agents*, pages 31–54. Springer US, Boston, MA, 1991.

[62] F. J. Pern and A. W. Czanderna. EVA degradation mechanisms simulating those in PV modules. In *American Institute of Physics Conference Series*, volume 268 of *American Institute of Physics Conference Series*, pages 445–452, December 1992.

[63] Nochang Park. The effect of encapsulant discoloration and delamination on the electrical characteristics of photovoltaic module. *Microelectronics Reliability*, 53:1818–1822, 10 2013.

[64] Series Resistance. `https://pveducation.org/pvcdrom/solar-cell-operation/series-resistance`.

[65] Matthew Boyd, Sanford A. Klein, Douglas Reindl, and Brian Dougherty. Evaluation and validation of equivalent circuit photovoltaic solar cell performance models. *Journal of Solar Energy Engineering*, 133, 05 2011.

[66] Effect of temperature. `https://pveducation.org/pvcdrom/solar-cell-operation/effect-of-temperature`.

[67] Shunt Resistance. `https://pveducation.org/pvcdrom/solar-cell-operation/shunt-resistance`.

[68] Cl. Buerhop, D. Schlegel, M. Niess, C. Vodermayer, R. Weißmann, and C.J. Brabec. Reliability of ir-imaging of pv-plants under operating conditions. *Solar Energy Materials and Solar Cells*, 107:154 – 164, 2012.

[69] Thomas Schlegl Christoph Kost. Study: Levelized cost of electricity- renewable energy technologies, 2018.

[70] Adriana Zurita, Armando Castillejo-Cuberos, Maurianny García, Carlos Mata-Torres, Yeliz Simsek, Redlich García, Fernando Antonanzas-Torres, and Rodrigo A. Escobar. State of the art and future prospects for solar pv development in chile. *Renewable and Sustainable Energy Reviews*, 92:701 – 727, 2018.

[71] A. Lay-Ekuakille, P. Vergallo, A. Arnesano, R. Morello, and C. De Capua. Effects of environmental conditions on photovoltaic module measurements. In *2013 Seventh International Conference on Sensing Technology (ICST)*, pages 933–936, 12 2013.

[72] Cass Whaley. Best practices in photovoltaic system operations and maintenance, 2nd edition, 2016.

[73] Dirk C. Jordan, Timothy J. Silverman, John H. Wohlgemuth, Sarah R. Kurtz, and Kaitlyn T. VanSant. Photovoltaic failure and degradation modes. *Progress in Photo-*

voltaics: Research and Applications, 25(4):318–326, 2017.

[74] Christian Camus, Ayodeji Adegbenro, Jakob Ermer, Vignesh Suryaprakash, Jens Hauch, and Christoph J. Brabec. Influence of pre-existing damages on the degradation behavior of crystalline silicon photovoltaic modules. *Journal of Renewable and Sustainable Energy*, 10(2):021004, 2018.

[75] Pv durability and reliabilty issues. `https://www.renewableenergyworld.com/articles/print/pvw/volume-1/issue-5/solar-energy/pv-durability-and-reliability-issues.html`.

[76] Milton Ohring and Lucian Kasprzak. Chapter 1 - an overview of electronic devices and their reliability. In Milton Ohring and Lucian Kasprzak, editors, *Reliability and Failure of Electronic Materials and Devices (Second Edition)*, pages 1 – 38. Academic Press, Boston, second edition edition, 2015.

[77] Advanced silicon solar cells: Detecting defects that reduce efficiency. `http://energy.mit.edu/news/advanced-silicon-solar-cells/`.

[78] Mismatch effects. `https://www.pveducation.org/pvcdrom/modules/mismatch-effects`.

[79] H. Field and A. M. Gabor. Cell binning method analysis to minimize mismatch losses and performance variation in si-based modules. In *Conference Record of the Twenty-Ninth IEEE Photovoltaic Specialists Conference, 2002.*, pages 418–421, 05 2002.

[80] Alessandro Massi Pavan, Adel Mellit, Davide De Pieri, and Vanni Lughi. A study on the mismatch effect due to the use of different photovoltaic modules classes in large-scale solar parks. *Progress in Photovoltaics: Research and Applications*, 22(3):332–345.

[81] Xavier F. Brun and Shreyes N. Melkote. Analysis of stresses and breakage of crystalline silicon wafers during handling and transport. solar energy materials and solar cells. pages 1238–1247, 8 2009.

[82] S. Silvestre and A. Chouder. Effects of shadowing on photovoltaic module performance. *Progress in Photovoltaics: Research and Applications*, 16(2):141–149.

[83] Ababacar Ndiaye, Abdérafi Charki, Abdessamad Kobi, Cheikh M.F. Kébé, Pape A. Ndiaye, and Vincent Sambou. Degradations of silicon photovoltaic modules: A literature review. *Solar Energy*, 96:140 – 151, 2013.

[84] Manish Kumar and Arun Kumar. Performance assessment and degradation analysis of solar photovoltaic technologies: A review. *Renewable and Sustainable Energy Reviews*, 78:554 – 587, 2017.

[85] Kholid Akhmad, Akio Kitamura, Fumio Yamamoto, Hiroaki Okamoto, Hideyuki Takakura, and Yoshihiro Hamakawa. Outdoor performance of amorphous silicon and polycrystalline silicon pv modules. *Solar Energy Materials and Solar Cells*, 46(3):209 – 218, 1997.

[86] Heman Shamachurn and Thomas Betts. Experimental study of the degradation of silicon photovoltaic devices under ultraviolet radiation exposure. *Journal of Solar Energy*, 2016:1–9, 07 2016.

[87] T. J. Trout, W. Gambogi, T. Felder, K. R. Choudhury, L. Garreau-Iles, Y. Heta, and K. Stika. Pv module durability -connecting field results, accelerated testing, and materials. In *2017 IEEE 44th Photovoltaic Specialist Conference (PVSC)*, pages 2312–2317, 06 2017.

[88] Corinne Packard. Development of a visual inspection data collection tool for evaluation of fielded pv module condition, 2012.

[89] Mallikarjun Hudedmani, Gita Joshi, R M Umayal, and Ashwini Revankar. A comparative study of dust cleaning methods for the solar pv panels. *Advanced Journal of Graduate Research*, 1:24–29, 01 2017.

[90] Ali Alshehri, Brian Parrott, Ali Outa, Ayman Amer, Fadl Abdellatif, Hassane Trigui, Pablo Carrasco, Sahejad Patel, and Ihsan Taie. Dust mitigation in the desert: Cleaning mechanisms for solar panels in arid regions. pages 1–6, 12 2014.

[91] W. Herrmann and N. Bogdanski. Outdoor weathering of pv modules — effects of various climates and comparison with accelerated laboratory testing. In *2011 37th IEEE Photovoltaic Specialists Conference*, pages 002305–002311, 06 2011.

[92] Raul Cordero, Alessandro Damiani, Jose Jorquera, Edgardo Sepulveda, Marta Caballero, S Fernandez, Sarah Feron, P Llanillo, Jorge Carrasco, David Laroze, and Fernando Labbe. Ultraviolet radiation in the atacama desert. *Antonie van Leeuwenhoek*, 111, 03 2018.

[93] M. Gagliardi and M. Paggi. Long-term eva degradation simulation: Climatic zones comparison and possible revision of accelerated tests. *Solar Energy*, 159:882 – 897, 2018.

[94] J. Herrmann, T. Lorenz, K. Slamova, E. Klimm, M. Koehl, and K. Weiss. Desert applications of pv modules. In *2014 IEEE 40th Photovoltaic Specialist Conference (PVSC)*, pages 2043–2046, 06 2014.

[95] Francisco Araya, Pablo Ferrada, Jorge Rabanal Arabach, Aitor Marzo, and Edward Fuentealba Vidal. Performance analysis of photovoltaics systems installed at different sites in the atacama desert. 06 2016.

[96] Ahmed Bouraiou, Messaoud Hamouda, Abdelkader Chaker, Mohammed Mostefaoui, Salah Lachtar, Mohammed Sadok, Nadir Boutasseta, Mourad Othmani, and Attoui Issam. Analysis and evaluation of the impact of climatic conditions on the photovoltaic modules performance in the desert environment. *Energy Conversion and Management*, 106:1345 – 1355, 2015.

[97] Karim Menoufi. Dust accumulation on the surface of photovoltaic panels: Introducing the photovoltaic soiling index (pvsi). *Sustainability*, 9:963, 06 2017.

[98] Sathyanarayana P., Rajkiran Ballal, Lakshmi Sagar P. S., and Girish Kumar 1. Effect of shading on the performance of solar pv panel. *Energy and Power*, pages 1–4, 2015.

[99] D C Jordan, J H Wohlgemuth, and S R Kurtz. Technology and climate trends in pv module degradation. pages 3118–3124, 01 2012.

[100] Raul Cordero, Alessandro Damiani, David Laroze, Shelley Macdonell, Jose Jorquera, Edgardo Sepulveda, Sarah Feron, P Llanillo, F Labbe, Jorge Carrasco, J Ferrer, and G Torres. Effects of soiling on photovoltaic (pv) modules in the atacama desert. *Scientific Reports*, 8:1–14, 09 2018.

[101] Douglas Olivares, Pablo Ferrada, Camila de Matos, Aitor Marzo, Enrique Cabrera, Carlos Portillo, and Jaime Llanos. Characterization of soiling on pv modules in the atacama desert. *Energy Procedia*, 124:547 – 553, 2017. 7th International Conference on Silicon Photovoltaics, SiliconPV 2017, 3-5 April 2017, Freiburg, Germany.

[102] B.H. Chudnovsky. *Transmission, Distribution, and Renewable Energy Generation Power Equipment: Aging and Life Extension Techniques, Second Edition*. CRC Press, 2017.

[103] Archana Sinha, O Sastry, and Rajesh Gupta. Detection and characterization of delamination in pv modules by active infrared thermography. *Nondestructive Testing And Evaluation*, 03 2015.

[104] E. L. Meyer and E. Ernest van Dyk. The effect of reduced shunt resistance and shading on photovoltaic module performance. In *Conference Record of the Thirty-first IEEE Photovoltaic Specialists Conference, 2005.*, pages 1331–1334, 01 2005.

[105] Otwin Breitenstein, Jan Bauer, Karsten Bothe, Wolfram Kwapil, Dominik Lausch, Uwe Rau, Jan Schmidt, Matthias Schneemann, Martin C. Schubert, Jan-Martin Wagner, and Wilhelm Warta. Understanding junction breakdown in multicrystalline solar cells. *Journal of Applied Physics*, 109(7):071101, 2011.

[106] W Herrmann, W Wiesner, and W Vaassen. Hot spot investigations on pv modules - new concepts for a test standard and consequences for module design with respect to bypass diodes. pages 1129 – 1132, 11 1997.

[107] Jan Bauer, Jan-Martin Wagner, Andriy Lotnyk, H Blumtritt, N Zakharov, and O Breitenstein. Physical mechanisms of electrical breakdown in silicon solar cells. *Annual report of Max Planck Institute of Microstructure Physics*, pages 44–45, 10 2009.

[108] Sagarika Kumar, Priyanka Jena, Archana Sinha, and Rajesh Gupta. Application of infrared thermography for non-destructive inspection of solar photovoltaic modules. *Journal of non-destructive testing and evaluation*, 01 2017.

[109] H. Glavas, M. Vukobratovic, M. Primorac, and D. Mustran. Infrared thermography in inspection of photovoltaic panels. In *2017 International Conference on Smart Systems and Technologies (SST)*, pages 63–68, 10 2017.

[110] A. Reinders, P. Verlinden, W. van Sark, and A. Freundlich. *Photovoltaic Solar Energy: From Fundamentals to Applications*. Wiley, 2017.

[111] S. S. Nekrashevich and V. A. Gritsenko. Electronic structure of silicon dioxide (a review). *Physics of the Solid State*, 56(2):207–222, 02 2014.

[112] Xiaofeng Fan, Weitao Zheng, Viorel Chihaia, Zexiang Shen, and Jer-Lai Kuo. Interaction between graphene and the surface of sio2. *Journal of physics. Condensed matter : an Institute of Physics journal*, 24:305004, 06 2012.

[113] I. S. Messaoudi, A. Zaoui, and M. Ferhat. Band-gap and phonon distribution in alkali halides. *physica status solidi (b)*, 252(3):490–495, 2015.

[114] J.M. Kalita and G. Wary. Estimation of band gap of muscovite mineral using thermoluminescence (tl) analysis. *Physica B: Condensed Matter*, 485:53 – 59, 2016.

[115] Raju P. Gupta. Electronic structure of crystalline and amorphous silicon dioxide. *Phys. Rev. B*, 32:8278–8292, 12 1985.

[116] Hatem A. ElBatal, Mohamed Y. Hassaan, Mona A. Fanny, and Mohamed M. Ibrahim. 'optical and ft infrared absorption spectra of soda lime silicate glasses containing nano fe2o3 and effects of gamma irradiation. *Silicon*, 9(4):511–517, Jul 2017.

[117] Michael D. Kempe, Gary J. Jorgensen, Kent M. Terwilliger, Tom J. McMahon, Cheryl E. Kennedy, and Theodore T. Borek. Acetic acid production and glass transition concerns with ethylene-vinyl acetate used in photovoltaic devices. *Solar Energy Materials and Solar Cells*, 91(4):315 – 329, 2007.

[118] Michael D. Kempe. Modeling of rates of moisture ingress into photovoltaic modules. *Solar Energy Materials and Solar Cells*, 90(16):2720 – 2738, 2006.

[119] P. Würfel and U. Würfel. *Physics of Solar Cells: From Basic Principles to Advanced Concepts*. Wiley, 2016.

[120] Aitor Marzo, Pablo Ferrada, Felipe Beiza, Pierre Besson, Joaquín Alonso-Montesinos, Jesús Ballestrín, Roberto Román, Carlos Portillo, Rodrigo Escobar, and Edward Fuentealba. Standard or local solar spectrum? implications for solar technologies studies in the atacama desert. *Renewable Energy*, 127:871 – 882, 2018.